Monitoring and Control of Wire Arc Additive Manufacturing Process using Artificial Intelligence

XXXVII - PhD in Product and Industrial Process Engineering

Supervisor:
Prof. Luigi Nele
Co-supervisor:
Dr. Alessandra Caggiano

PhD candidate:
Giulio Mattera

Università degli Studi di Napoli Federico II

DICMaPI
Dipartimento di Ingegneria Chimica, dei Materiali e della Produzione Industriale
Università degli Studi di Napoli Federico II

Declaration

I declare that I have written this thesis without the assistance of third parties and without utilizing any aids other than those specified. Any ideas or information obtained directly or indirectly from external sources have been acknowledged. This thesis has not been previously submitted in an identical or similar form to any Italian or foreign examination board. The thesis work was carried out under the supervision of Prof. Luigi Nele and Prof. Alessandra Caggiano at the University of Naples Federico II from 2021 to 2024 and Prof. Zengxi Pan during my visiting period at the University of Wollongong from February 2023 to October 2023.

Naples, September 2024

Giulio Mattera

Abstract

Wire Arc Additive Manufacturing (WAAM) is an additive manufacturing process that is attracting attention from both the research and industrial fields due to its high print rates and the ability to build mid to large-sized metal components in a cost-effective manner. While the mechanical properties of printed components and general print parameters have been extensively studied in the literature, a shifting focus towards the application of Artificial Intelligence (AI) to enhance the quality and sustainability of the printed components is emerging. AI can be employed to monitor the process in real-time, providing feedback on component quality. Moreover, advanced feedback control mechanisms can then adjust process parameters online to improve surface quality and prevent defects. Furthermore, optimisation techniques can be utilised to solve complex goal-oriented problems, determining optimal process parameters before printing the part. A comprehensive literature survey was conducted in this thesis, identified gaps in the current literature such as the employment of multi-sensor frameworks for process monitoring and the use of frequency domain analysis and unsupervised learning for developing monitoring applications. Additionally, advanced model-free control policies have been designed using a disruptive technology like Reinforcement Learning, substituting the need for complex and time-consuming Multiple Input, Multiple Output (MIMO) nonlinear controllers like Model Predictive Control (MPC), which represent the actual state of the art in this field. Finally, metaheuristic optimisation techniques are employed to fine-tune process parameters to achieve goals such as sustainable fabrication of components.

Author's overview

This thesis is the culmination of three years of research, conducted over two years at the University of Naples, under the supervision of Prof. Luigi Nele and Dr. Alessandra Caggiano, and one year at the University of Wollongong, Australia under the supervision of Prof. Zengxi Pan. The primary focus of this work is the implementation and integration of AI techniques for the monitoring and control of the Wire Arc Additive Manufacturing (WAAM) process.

Specifically, this thesis firstly addresses significant gaps in the literature related to the absence of unsupervised techniques for anomaly detection and monitoring in WAAM parts. Intending to find industrial applications for these research activities, the approach involves using these techniques for the first layer of a system monitoring module which allow for the localisation of targets for the non-destructive evaluation (NDE) of parts produced with WAAM technology. The development and utilisation of a new frequency feature extraction methodology resulting in a significant improvement in detection performance and interpretability of unsupervised learning applications. This aspect is necessary to help the integration of AI within certification procedure of the parts, opening new possibilities in WAAM data analysis in the context of little and unbalanced dataset. Another innovative contribution of this thesis is the application of Reinforcement Learning (RL) techniques for learning optimal feedback control laws to adjust online the process parameters for a nonlinear, constrained MIMO dynamic system process like WAAM. Finally, the attention is moved to the advantages introduced by AI in the process sustainability, employing Genetic Algorithm (GA) to explore combination of process parameters which allow the energy consumption to be reduced without generating defective parts, improving the performance of standard optimisation techniques.

List of publications

1. Luigi Nele, **Giulio Mattera**, and Mario Vozza. "Deep neural networks for defects detection in gas metal arc welding." *Applied Sciences* (2022).
2. **Giulio Mattera**, and Raffaele Mattera. "Shrinkage estimation with reinforcement learning of large variance matrices for portfolio selection." *Intelligent Systems with Applications* (2023).
3. Alessandra Caggiano, **Giulio Mattera**, and Luigi Nele. "Smart tool wear monitoring of CFRP/CFRP stack drilling using autoencoders and memory-based neural networks." *Applied Sciences* (2023).
4. **Giulio Mattera**, Alessandra Caggiano, and Luigi Nele. "Optimal data-driven control of manufacturing processes using reinforcement learning: an application to wire arc additive manufacturing." *Journal of Intelligent Manufacturing* (2024).
5. **Giulio Mattera**, Luigi Nele, and Davide Paolella. "Monitoring and control the Wire Arc Additive Manufacturing process using artificial intelligence techniques: a review." *Journal of Intelligent Manufacturing* (2024).
6. **Giulio Mattera**, Giulio, Alessandra Caggiano, and Luigi Nele. "Reinforcement learning as data-driven optimization technique for GMAW process." *Welding in the World* (2024).
7. **Giulio Mattera**, Polden Joseph, and Nele Luigi. "A Time-Frequency Domain Feature Extraction Approach Enhanced by Computer Vision for Wire Arc Additive Manufacturing Monitoring Using Fourier and Wavelet Transform." *Journal of Advanced Manufacturing Systems* (2024).
8. **Giulio Mattera**, Joseph Polden and Luigi Nele. "Monitoring Wire Arc Additive Manufacturing process of Inconel 718 thin-walled structure using wavelet decomposition and clustering analysis of welding signal". *Journal of Advanced Manufacturing Science and Technology* (2024).
9. **Giulio Mattera**, Alessandra Caggiano, Joseph Polden, Luigi Nele, Zengxi Pan and John Norrish. "Semi-supervised Learning for Real-Time Anomaly Detection in Pulsed Transfer Wire Arc Additive Manufacturing". *Journal of Manufacturing Processes (2024).*

10. **Giulio Mattera**, Massimiliano Giacalone, Gianfranco Piscopo, Maria Longobardi and Luigi Nele. "Improving the Interpretability of Data-Driven Models for Additive Manufacturing Processes Using Clusterwise Regression". *Mathematics (2024).*
11. Luigi Nele, **Giulio Mattera**, Mario Vozza, Emily W. Yap, and Silvestro Vespoli. "Towards the Application of Machine Learning in Digital Twin Technology : A multi-scale review". *Discover Applied Science (2024).*
12. **Giulio Mattera**, Joseph Polden and John Norrish. "Monitoring the Gas Metal Arc Additive Manufacturing process using unsupervised machine learning" *Welding in the World (2024).*
13. **Giulio Mattera**, Mario Vozza, Joseph Polden, Luigi Nele and Zengxi Pan. "Frequency Informed Convolutional Autoencoder for in situ anomaly detection in Wire Arc Additive Manufacturing" *Journal of Intelligent Manufacturing (2024).*
14. **Giulio Mattera**, Emily W. Yap, Joseph Polden, Evan Brown, Luigi Nele and Stephen Van Duin "Utilising Unsupervised Machine Learning and IoT for Cost-Effective Anomaly Detection in multi-layer Wire Arc Additive Manufacturing". *The International Journal of Advanced Manufacturing Technology.*
15. Mario Vozza, Joseph Polden, **Giulio Mattera**, Gianfranco Piscopo, Silvestro Vespoli and Luigi Nele. "Explaining the anomaly detection in Additive Manufacturing via Boosting models and Frequency Analysis". *Mathematics*

List of proceedings

1. **Giulio Mattera**, Joseph Polden, Alessandra Caggiano, Philip Commins, Luigi Nele and Zengxi Pan. "Anomaly detection of Wire Arc Additively Manufactured parts via Surface Tension Transfer through unsupervised machine learning techniques." *Procedia CIRP – ICME (2023).*
2. **Giulio Mattera**, Joseph Polden, Alessandra Caggiano, Stephen Van Duin, Luigi Nele and Zengxi Pan. "Defect monitoring in wire arc additive manufacturing using frequency domain analysis." *Materials Research Proceedings – ESAFORM (2024).*

3. Antonio D'Alterio, **Giulio Mattera**, Alessandra Caggiano, Luigi Nele, Massimo Martorelli and Davide Santoro. "Development of a vision system enhanced by deep learning to support robotic laser cleaning" *Procedia CIRP – ICME (2024). In press*
4. **Giulio Mattera**, Joseph Polden, Antonio D'Alterio, Alessandra Caggiano, Stephen Van Duin, Luigi Nele and Zengxi Pan. "Wire Arc Additive Manufacturing of INVAR36: A preliminary study into anomaly detection using signals from acoustic emission sensors." *Procedia CIRP – ICME (2024). In press*
5. Adelaide Marzano, Alessandra Caggiano, **Giulio Mattera** and Luigi Nele. "Towards a Digital Twin Framework for Human-Centric Laser Cleaning Design." *Procedia CIRP – ICME (2024). In press*
6. Silvestro Vespoli, **Giulio Mattera**, Guido Guizzi, Liberatina Carmela Santillo and Luigi Nele. "Adaptive WIP Control in Industry 4.0 Manufacturing via Deep Reinforcement Learning: A Case Study in Hybrid Control Architectures" *Frontiers in Artificial Intelligence and Applications (2024)*

List of under review works

1. **Giulio Mattera**, Joseph Polden and Luigi Nele. "An efficient data-driven dynamic model for Gas Metal Arc Additive Manufacturing using ensemble reinforcement learning". *International Journal of Modelling and Simulation.*
2. **Giulio Mattera**, Joseph Polden, Vittoria Laghi and Luigi Nele. "Towards a sustainable Gas Metal Arc Additive Manufacturing using Artificial Intelligence". *Progress in Additive Manufacturing*
3. Silvestro Vepoli, **Giulio Mattera**, Marigarzia Marchesano, Guido Guizzi and Luigi Nele. "Adaptive WIP Control in Industry 4.0 Manufacturing using Reinforcement Learning in a Semi-Heterarchical Decentralised Architectures". *Computers and Industrial Engineering*
4. **Giulio Mattera**, Raffaele Mattera, Emma Salatiello, Silvestro Vespoli. "Anomaly Detection in Manufacturing Systems with Complex Temporal Networks and Unsupervised Machine Learning". *Computers and Industrial Engineering*

List of abbreviations

AI – Artificial Intelligence

AM – Additive Manufacturing

ANN – Artificial Neural Network

ARX - AutoRegressive with Exogenous variable

BIC - Bayesian Information Criterion

CAD – Computer Aided Design

CAE - Convolutional AutoEncoder

CAM – Computer Aided Manufacturing

CMT - Cold Metal Transfer

CNC – Computer Numeric Control

CPS – Cyber Physical System

CTWD – Contact Tip to Workpiece Distance

CWT - Continuous Wavelet Transform

DDPG – Deep Deterministic Policy Gradient

DED – Direct Energy Deposition

DL – Deep Learning

DQN – Deep Q Network

DRL – Deep Reinforcement Learning

DWT - Discrete Wavelet Transform

FFT – Fast Fourier Transform

GA – Genetic Algorithm

GFR – Gas Flow Rate

GMAW - Gas Metal Arc Welding

GMM – Gaussian Mixture Model

GPR – Gaussian Process Regression

ICT - Information and Communication Technology

IoT – Internet of things

LQG - Linear Quadratic Gaussian

LQR - Linear Quadratic Regulator

MIMO - Multiple Input Multiple Output

ML - Machine learning

MPC – Model Predictive Control

NDE - Non-Destructive Evaluation

OLS - Ordinary Last Square

PPO – Proximal Policy Optimisation

RL -Reinforcement Learning

SISO - Single Input Single Output

SME – Smart Manufacturing Entity

SMS – Smart Manufacturing System

SPO- Particle Swarm Optimisation

STFT – Short Time Fourier Transform

STT - Surface Tension Transfer

TRPO – Trust Region Policy Optimisation

WAAM – Wire Arc Additive Manufacturing

WAPS - WAAM Procedure Specification

WFS – Wire Feed Spees

WS – Welding Speed

List of Figures

Table of contents

Chapter 1 : Introduction

1.1. Wire Arc Additive Manufacturing

Wire Arc Additive Manufacturing (WAAM) is a Direct Energy Deposition (DED) process which employs welding technology to build large metal size component in a layer-by-layer fashion. Its story started in the early 90s , when authors like Spencer et al. [1] and Norrish et al. [2] printed the first prototype parts with good structural integrity and mechanical properties. The first WAAM systems, shown in **Figure 1**, consist of CAM software which, starting from a CAD model of the component, generates the path for the welding torch mounted on a motion platform, generally a 6-axis robotic arm or a CNC machine. The welding parameters, selected on the welding machine during the setup process, are maintained fixed during the deposition. However, the innovations in welding technology, automation and Information and Communication Technology (ICT), are transforming this process, which now allows building more sustainable metal components with reduced number of defects and higher mechanical proprieties. [3] Thanks to recent innovations, this technology is increasingly being applied across various industries, including naval, aerospace, oil and gas, and construction, with several notable case studies, such as large propellers [4] and bridges [5].

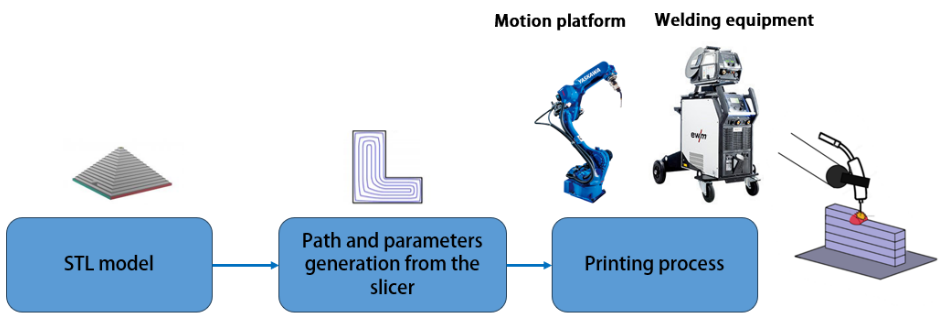

Figure 1 Standard workflow for WAAM process, from CAD model to the printing process.

As discussed by Pan et al. [6] several Arc welding processes may be employed for Additive Manufacturing (AM), however Gas Metal Arc Welding (GMAW) is the most commonly employed given its low cost and easier automation [7]. The conventional GMAW process involves applying a constant voltage V to the electrode wire, which, when in contact with the substrate or with the previous layer, draws by a current I. This current, referred as welding current or arc current, is influenced by the applied voltage (V), which depend on the arc length, function of the stick out or Contact Tip to Workpiece Distance (CTWD) and of the Wire Feed Speed (WFS). [8], [9] Furthermore, the Gas Flow Rate (GFR) and its composition influence the voltage drop and then the welding current. In this conventional GMAW process, another parameter which influence the process is the Welding Speed (WS), which - together with the welding voltage and welding current - is related to the heat input supplied to the material, therefore with the geometry of the deposited bead and residual stresses and distortion. [10] The self-adjusting nature of the natural GMAW process, shown in **Figure 2**, led to an unstable process which is susceptible by slight process parameters variations. In fact, little changes in CTWD are associated to large variations in the welding current, which could result in undesirable defects such as porosity, incomplete penetration, cracks or burn through. Additionally, the nature of the WAAM process can introduce defects such as inhomogeneous microstructure, humping, and layer geometry deviations that affect both mechanical proprieties and quality of surface, necessitating post-processing. This is the reason why this technology is often referred to as a near-net-shape process. [11]

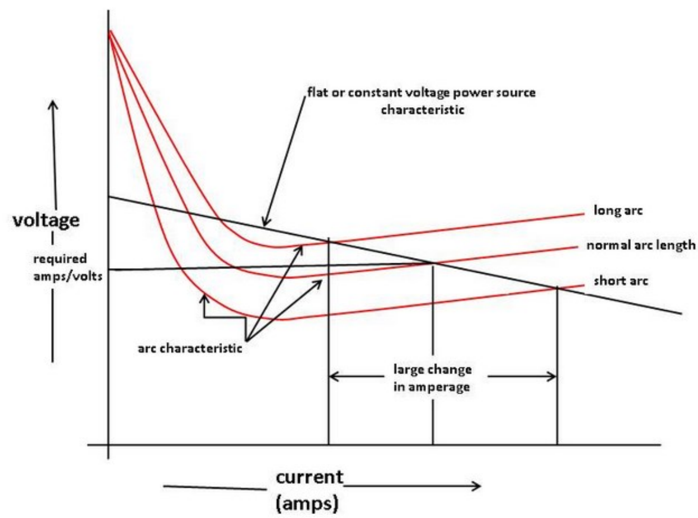

Figure 2 The current-voltage characteristic of the electric arc during a welding process which show different equilibrium points based on arc length (in red).

In relation to process stability, the selection of the process parameters affects the mode of metal transfer within the melting pool. As illustrated in **Figure 3** , three primary types are discernible: dip-transfer (or short-circuit), globular transfer, and spray transfer, which are differentiated by an increment of heat input from dip-transfer to spray transfer. [12] In the context of a WAAM process, the preferred transfer mode to employ is the dip-transfer due to its lower current and voltages, resulting in reduced heat input and, consequently, reduced residual stresses and deformations on the final component. However, the uncontrolled natural dip transfer is associated to instability and spatter during the deposition, which increases the possibility to generate defects like porosity and that reduces the surface quality of the components due to high variability of the deposited layer geometry under the same parameters condition. For this reason, the innovations in welding technologies like waveform control welding processes based on controlled dip transfer (e.g. Cold Metal Transfer by Fronius, Surface Tension Transfer by Lincoln or ColdArc by EWM) are largely employed as welding techniques in WAAM. These processes reduce the heat input supplied to the material and to control it during the deposition process, reducing the presence of defects like instability, porosity and distortion, resulting in well documented improvement in mechanical properties and better surface quality, given the consistency of the deposited layer geometry. [13], [14]

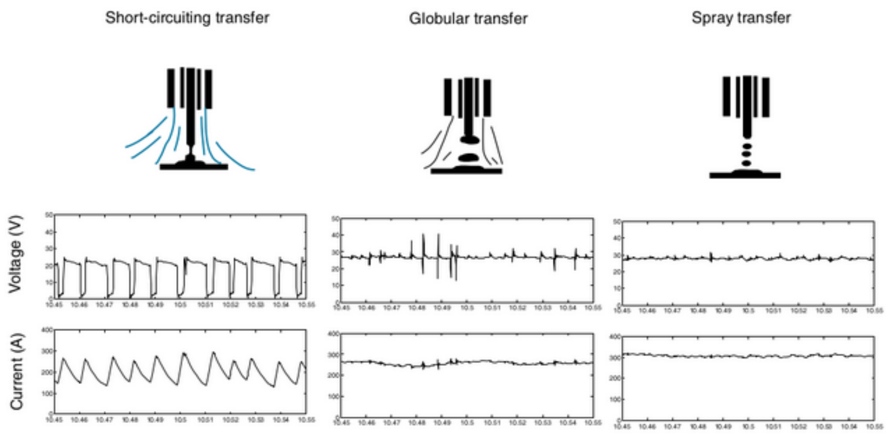

Figure 3 Metal transfer modes in standard GMAW process, inspired by Pires et al. [15].

1.2. Related challenges and research gaps

As mentioned in the previous section, innovations in automation and ICT are transforming the WAAM process. In particular, the fourth industrial revolution, driven by pivotal technologies like Artificial Intelligence (AI), Cyber Physical Systems (CPS) [16] and the Internet of Things (IoT), is changing the production paradigm, pushing the development of Smart Manufacturing Systems (SMS), composed of several Smart Manufacturing Entity (SME) at the machine level. [17] At the process level, a CPS (see **Figure 4**) consists of a physical asset, i.e. in the case of WAAM the robotic system, the welding process and the integrated sensors, and of a hardware. In the digital world a CPS uses AI-driven big data analytics, such as Machine Learning (ML), to autonomously sense and respond to the dynamics of its environment. By adopting this fabrication paradigm, manufacturing costs related to waste associated with the production of defective parts and the power consumption can be minimised, promoting a more environmentally friendly and sustainable approach to production. [18], [19]

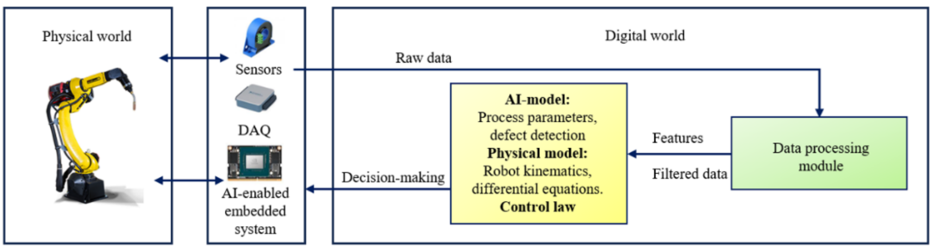

Figure 4 A Cyber Physical System consists of manufacturing physical counterpart, i.e., motion system, tools, etc., and hardware that guest the digital counterpart, which hosts real-time advanced data processing techniques.

In this relative new production context, the research in WAAM technology is moving towards the study the new possibility introduce by AI in enhancing the quality and sustainability of the WAAM process [20]. To understand where AI can most effectively enhance the performance of a WAAM system, it is essential to outline the workflow in detail.

This workflow begins with the CAD model of the component to be printed, progressing through welding parameters and path planning definition, which represent the primary sources of critical challenges encountered offline during the planning phase. However, several challenges persist during the deposition process (online), due to the need for process monitoring and feedback control.

1.2.1. Offline challenges

Once the material of the component to build is defined by previous design, a WAAM Procedure Specification (WAPS) must be defined, indicating the welding process and the process parameters to employ. It is well known in welding technology that different materials require different process parameters to be deposited, therefore experimental campaigns have to be conducted to assess the best process parameters to employ based on the different materials and wire dimensions available.

Furthermore, several physical phenomena—such as thermal conduction, the arc forces, and surface tension—affect the amount of droplet realised in the melting pool and all of them are material-dependent and influence the parameters selection, which highly impact the deposited bead geometry. Therefore, the set-up of the WAPS requiring expertise in metallurgy and welding technology, and serves as a functional specification for components in terms of quality and productivity. In fact, the employed process parameters must result into a component that provides the mechanical requirements, without generating defects.

Additionally, the parameters defined in the WAPS servs as a reference for nominal operating parameters, essential for the monitoring systems, which uses expert-defined limits to detect anomalies using statistical analysis. [21], [22], [23] Although this set-up process is well established in welding technology, the AM nature of WAAM complicate the WAPS design. In fact, once the CAD model of the component is defined, the slicer software generates the path planning for the motion platform which hold the welding torch, based on the estimation of the layer height and layer width (see **Figure 5**). As discussed by Ding et al. [24], [25], the slicer software in WAAM highly depends on the bead model, which correlates with the process parameters (input) with the bead geometry (output).

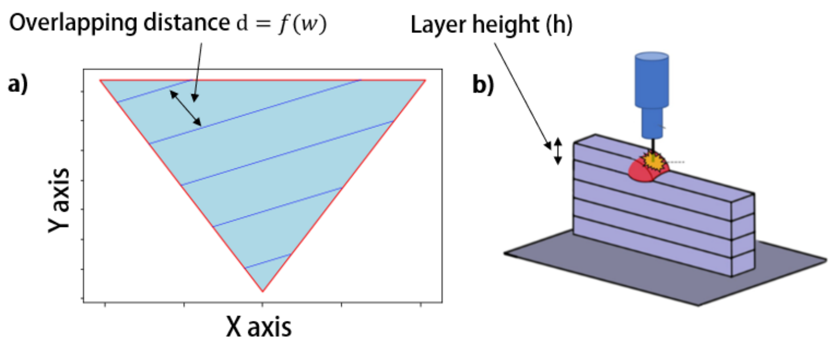

Figure 5 The slicer software depends on the employed parameters and vice-versa since the overlapping distance (function of layer width) and layer height are parameters dependent.

Consequently, after the process parameters are chosen in alignment with the WAPS, an estimation of the bead profile, encompassing dimensions such as width and height, is employed to generate the robotic path. Furthermore, as illustrated in **Figure 6**, once the layer width and height are determined, in instances where a multi-bead deposition is necessary, such as for thick structures, the slicer needs the definition of the overlapping value (denoted as "d") and the number of paths (denoted as "nd"). These values must be chosen to maintain geometrical accuracy and align with the dimensions of the layer at its boundaries.

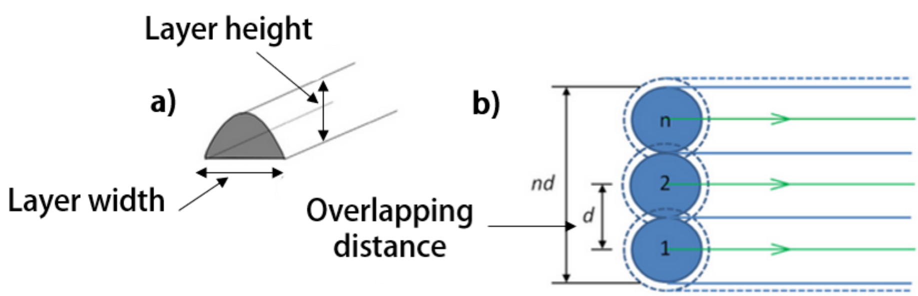

Figure 6 a) layer geometry and b) overlapping distance are important parameters for the slicer software.

The workflow from CAD model to the generation of the path program for the motion platform is shown in **Figure 7**.

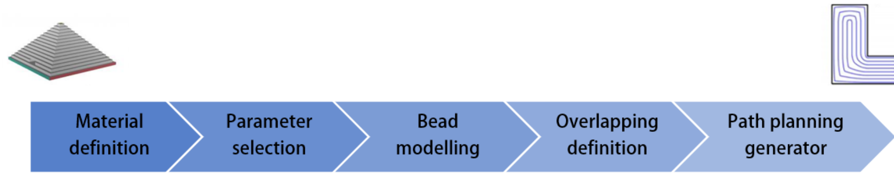

Figure 7 The workflow from CAD model to the path program.

Incorrect path planning at this stage, may results in void within the components and reduced the mechanical proprieties of the components. As shown in **Figure 8,** if the optimal overlapping strategy proposed by Ding et al. [25] is used, in which the overlapping value equal to $d = 0.738 \cdot w$, the component is full filled, and it does not presents voids once machined.

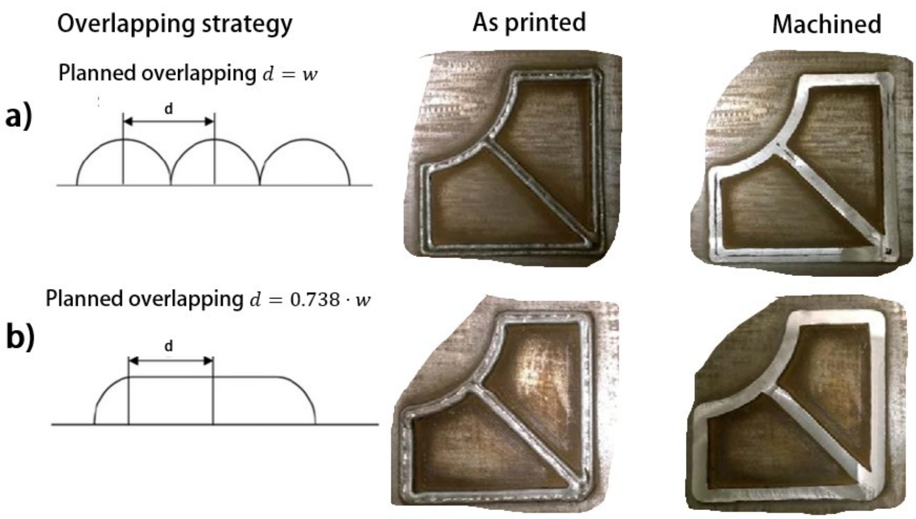

Figure 8 The results of employing different overlapping strategies in WAAM. a) overlapping distance equal to estimated layer width b) using the methods proposed by Ding et al. [25]. An incorrect selection may reduce the mechanical proprieties of the components.

Currently, these steps are performed manually by machine makers. WAAM machine manufacturers define experimental parameters (e.g., 2-3 sets) and allow the users for little variations around them. As a result, components are produced with the estimated mechanical properties and quality as stated by the WPS.

Despite this, advancements in AI can introduce several benefits, such as defining parameters outside of those found experimentally, which can still meet goal-oriented functions. Employing ML techniques for both data-driven modelling and goal-oriented data-driven optimisation, new optimal solutions can be found.

However, some challenges persist, since most of the literature studied modelling techniques for bead modelling in single bead on plate scenario, which for several reasons, like heat accumulation, are not practical for WAAM process. [26], [27] This means that during the deposition, due to neglected phenomena in the modelling activity, the layer geometry is different with respect to the planned one. An incorrect estimation of layer height and width can result in excessive or insufficient overlap compared to the planned design. This affects the subsequent layer height and can lead to unexpected changes in the CTWD. As mentioned in the previous section, such variations in CTWD can alter the welding current during the process. If not properly adjusted, this can cause defects like excessive spatter and porosity due to inadequate shielding gas coverage. These problems are illustrated in **Figure 9**.

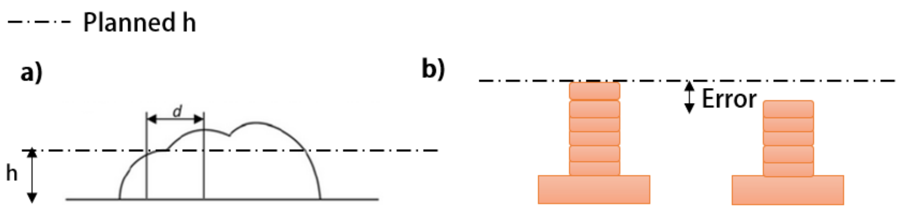

Figure 9 Example of incorrect path planning. Variation in CTWD introduced by a) excessive overlapping or b) lower layer height due to heat accumulation.

1.2.2. Online challenges: process monitoring

As mentioned above, several factors can introduce defects during the deposition. Therefore, online monitoring modules that detect instable conditions and feedback control loop that adjust the process parameters, e.g. correct online the CTWD if a deviation is detected, are required to enhance the product quality. However, in addition to complex phenomena, also simple factor like missing gas and incorrect parameter selection can introduce defects within components and detecting these simple conditions is also important. CPS enhanced by AI, allows to develop real-time monitoring of the process, analysing the data coming from different welding sensors sources, such as welding camera, infra-red camera, current and voltage signals or audio signals for different scopes [28], [29], such as:

- *Anomaly Detection and Root Cause Identification*: Real-time monitoring fundamentally involves capturing data from sensors during the production process. This serves a dual purpose: identifying anomalous conditions and/or providing feedback about the performance of the system, enabling early detection of deviations from the normal operation. This classification task becomes particularly important for developing root cause analysis systems, which seamlessly connect with decision-making modules to facilitate informed and targeted responses.
- *State Estimation or Soft Sensor*: The second aspect of real-time monitoring focuses on state estimation. In practical scenarios, not all states or critical information about a system may be directly measurable using sensors (e.g. layer penetration in the substrate). This limitation is addressed by incorporating mathematical models that describe the system's physics and other relevant aspects. State estimators or observers, such as the Kalman filter, play a pivotal role by using available sensor measurements and system dynamics to accurately estimate unmeasured or latent states. This approach bridges the gap between what is directly observable and what is necessary for a comprehensive understanding of the system's behaviour, creating feedback loops for control systems.

In the field of monitoring, due to process complexity, ML techniques have been employed to detect system states and/or detect anomalies online. [30] In **Figure 10** are shown various approaches to defect detection based on ML, namely supervised, unsupervised and semi-supervised learning. Using supervised learning models requires intentionally introducing defects into components and labelling each type of defect. Alternatively, a binary classification problem can be set up, with one label for normal cases and another for anomalies. Although the high performances of supervised approaches, these may present different problems related to overfitting [31] and data acquisition.

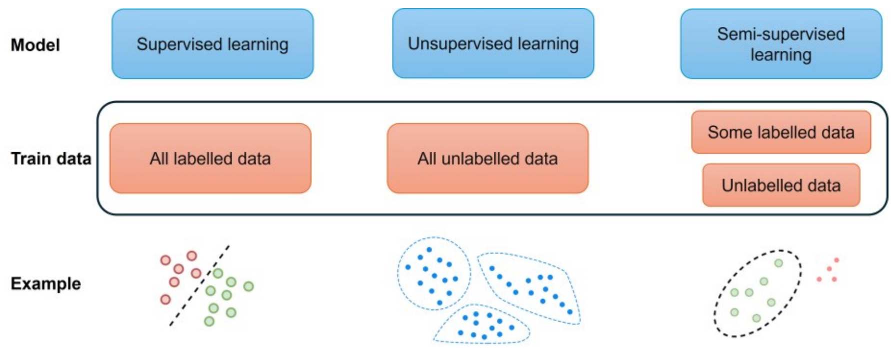

Figure 10 Machine learning approaches to develop monitoring applications.

In fact, supervised learning approaches necessitate balanced datasets comprising equal proportions of defective and normal deposition data, and experimentally acquiring and labelling such datasets proves challenging in practice.

In unsupervised learning, data is clustered based on data features. This clustering process serves in identifying patterns for both normal cases and anomalies within an unbalanced and low-dimensional training dataset. Any data that deviates significantly from the clusters representing normal cases can be identified as outliers or anomalies. Moreover, by using cluster centroids, new data points can be categorised as anomalies or normal data, and the stability degree of the system can be estimated as well. This gives the possibility to a WAMM system to use with low-intensive resources these approaches online for process monitoring also in the case of low dimensional dataset. However, while time domain features extraction possesses several problems related global representation of the data, the state-of-art methods rely into features extraction in this domain. This is because supervised learning approaches, with their tendency to overfit, can classify even little differences between data, whereas unsupervised learning methods are weaker in this regard. Therefore, the performance of the unsupervised learning algorithms in WAAM is often lower than their supervised counterparts, resulting in a lack of knowledge in the research field.

In the field of WAAM monitoring, open challenges include studying the impact of overfitting on supervised learning models, which currently represent the state of the art, with numerous studies exploring various data sources and techniques. On the other hand, unsupervised learning models remain relatively unexplored. These methods offer interesting potential for industrial applications, demanding further in-depth research to enhance their performance.

Finally, another unexplored area of research is related to multi-sensor monitoring systems, which are able to detect anomalies and classify system state and/or defects based on different data sources. In fact, some sensors are able to detect internal defects happening under the welding torch, such as porosity via welding current and welding voltage sensors, others are able to detect internal and superficial defects happening during the solidification, such as microphones and Acoustic emission sensors, while other able to detect superficial defects like humping, such as welding camera. Although this is well documented by past research, multi-sensors and sensors fusions approaches based on AI are not studied yet, therefore there is a lack of knowledge about the effective advantages of employing multi-sensor monitoring in this field.

1.2.2. Online challenges: process control

As discussed, WAAM technology involves several complex phenomena that require online feedback control to adjust process parameters and maintain stable deposition conditions. However, controlling WAAM is challenging due to its nature as a nonlinear, Multiple Input Multiple Output (MIMO) dynamic system, with hidden and not well-understood mathematical relationships between system states—like layer geometry, defect presence, instantaneous values of welding current and welding voltage—and process parameters.

AI is widely used in this field for system modelling [32], [33], enabling the prediction of future states based on current states and input process parameters. This capability supports the development of Model Predictive Control (MPC) strategies, which represent the state of the art in WAAM control systems. [34] However, MPC faces challenges such as dependency on the system model, risks of overfitting, and limitations in simulating future states that account for potential defects under certain process parameters. Furthermore, the cost function employed in this controller is mainly error with respect to the set-point dependent.

CPS enhanced by Digital Twin (DT) technology offers a promising opportunity for advancing decision-making strategies using AI solutions, in both offline optimisation and online control. For example, employing disruptive techniques like Reinforcement Learning (RL), it is possible obtain better results than traditional approaches, enabling more efficient control actions and optimisation in WAAM processes. In particular, the free and metaheuristic design of the cost function allow to generate control policy which depends on different goals, surpassing the simple error-based MPC controllers.

1.2.4. Parts certification

AM represent a transformative force in the production landscape, offering innovative possibilities. However, a considerable challenge arises in automating the certification process for AM parts, holding the promise of mitigating the costs associated with time-consuming certification procedures. Despite the introduction of supervised machine learning techniques for defect classification, a significant constraint emerges due to stringent norms that restrict the adoption of "black box" models in the certification of components. These norms explicitly call for transparency and interpretability in the certification process, underscoring the imperative to guarantee the reliability and safety of the manufactured parts. However, AI and in particular unsupervised ML approaches, represent an unexplored field that may be employed to overcome this challenge.

1.3. Objectives and contributions

As discussed, there is a growing interest in understanding how AI can enhance performance in WAAM. This thesis presents a detailed literature review in the *Chapter 2* that reveals most research in this area focuses on monitoring applications, with supervised learning being predominant. In situ process monitoring has been developed to detect defects and anomalies during deposition using welding cameras, current and voltage sensors, and audio signals for various purposes. While this is a well-established field, the review highlights a knowledge gap in the use of other machine learning techniques, such as unsupervised learning, which could be applied for similar or different objectives.

In the *Chapter 3* , this thesis highlights the main reasons for the limited use of unsupervised learning in process monitoring, specifically focusing on the challenges associated with time-domain feature extraction from time-series signals such as current and voltage sensors. To address this, *Chapter 3* proposes innovative frequency and time-frequency domain feature extraction techniques for these signals, with a detailed discussion on the physical motivation behind this approach. Additionally, a discussion about how these techniques can be integrated into the certification process for AM parts is presented. In particular, the application of unsupervised learning techniques offers the potential to precisely locate Non-Destructive Evaluation (NDE) targets within AM components, thus streamlining the certification process. By leveraging position data from the robot controller and anomaly detection outputs, this approach presents a promising solution despite its ambitious goals. In fact, it aligns with the need for a more interpretable and norm-compliant certification process in AM. Moreover, this approach represents an additional tool to develop high-performance applications also in cases of small size dataset, e.g. derived by data collection during the certification procedure.

In addition to monitoring, AI can be employed for both online feedback control and offline process optimisation. However, the literature review reveals a significant gap in contributions to this field. In response, *Chapter 4* of the thesis introduces a RL based approach for online process control of WAAM. Specifically, an innovative multi-goal-oriented reward function is proposed, along with a practical workflow for implementing this technology in manufacturing processes. An example for layer geometry control is then proposed in the field of WAAM, with comparison with other controllers such as MPC and Linear Quadratic Regulator (LQR). Finally, an evolutionary theory metaheuristic optimisation approach named Genetic Algorithm (GA), is proposed in the *Chapter 5* for offline process parameter optimisation, aiming to improve energy efficiency of the process. Employing AI-discovered process parameters, results show better performance with respect to human-selected parameters.

The main contributions of this thesis are listed below:

1. Introduction of unsupervised learning as a technology for process monitoring and anomaly detection in WAAM. *(Published in* [35]*)*
2. Develop a methodology for the features extraction in the frequency and time-frequency domain of welding signals, which demonstrates the ability to improve unsupervised learning performance, now comparable to supervised learning performance (around 90%). *(Published in* [36]*)*
3. Development of a workflow for RL integration and continuous training in manufacturing processes *(Published in* [37]*)*
4. Design of an innovative multi-objective cost function for feedback control in manufacturing processes, with an example to WAAM *(Published in* [37]*)*
5. Application of AI for offline data-driven optimisation of WAAM process based on energy-efficient cost function and GA. *(Unpublished contribution of the thesis, under review).*

1.4. Flowchart employed in the thesis

In this thesis, a flowchart for monitoring, control, and optimization of Wire Arc Additive Manufacturing (WAAM) using AI techniques is presented, as illustrated in Figure 11. Specifically, during the certification procedure, data are collected in terms of welding current and welding voltage signals. Furthermore, power consumption is computed from these signals, and layer geometry is measured. This constitutes the offline data collection procedure. The defect-free data are then filtered and utilized for monitoring purposes through an unsupervised learning paradigm, ensuring effective process state monitoring and fault detection. By comparing real-time online process data to the defect-free dataset, deviations can be observed and addressed promptly. The measured data, including power consumption and layer geometry, are subsequently used to develop a Reduced Order Model (ROM). This ROM plays a critical role in both optimization and policy design. Optimization is performed using a Genetic Algorithm, which interacts with the ROM to identify optimal process parameters, enhancing both efficiency and quality. Additionally, the ROM is employed to synthesize a control policy through simulation using Reinforcement Learning (RL). Once deployed in the real system, this policy dynamically adapts to process variations, effectively controlling layer geometry. Together, the proposed approaches ensure a highly efficient and adaptive WAAM process, representing a significant advancement compared to current commercial machines.

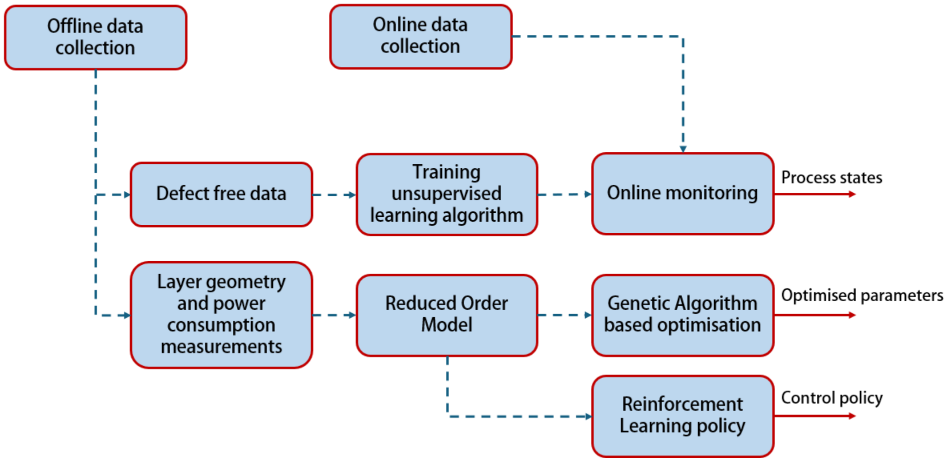

Figure 11 The flowchart employed in this thesis

Chapter 2 : Literature background

In response to increasing demands for higher quality, productivity, and flexibility imposed by Industry 4.0 paradigm, the implementation of advanced methods for online inspection of component quality and intelligent control of fabrication and production processes has become a critical aspect of developing modern production systems. To achieve this objective, diverse sensors are employed to observe and estimate process parameters, creating a feedback loop for the control system and facilitating the monitoring of system states and the identification of defects.

Typically, robotic systems utilise encoders to provide information about joint pose and velocity, while welding power sources offer information about employed process parameters. However, in the context of WAAM systems, the integration of external sensors is of paramount importance. These sensors, coupled with appropriate processing modules, contribute to online information about the process. Optical sensors such as profilometers and cameras provide geometry information, while thermal cameras or pyrometers offer insights into temperature variations and distribution. Acoustic sensors, on the other hand, provide information about metal transfer modes and the presence of defects, such as porosity and cracks. Current and voltage sensors provide information about the instantaneous values of welding current and welding voltage, related to the heat input supplied to the material.

In the analysis acquired data, AI techniques, including ML, Deep Learning (DL), and RL, stand as the state of art in various computer science domains. This chapter provides an exploration of diverse AI techniques employed in this thesis in the **Section 2.1** and **Section 2.2**. Additionally, a literature review is presented in the **Section 2.3** to highlight the current state of the art in data processing applied to both GMAW and WAAM processes, given their shared equipment and basic phenomena.

2.1. Machine learning

Supervised and unsupervised machine learning are two fundamental paradigms that play an important role in data analysis. Supervised machine learning involves training a model on a labelled dataset, where the input data is paired with corresponding output labels. On the other hand, unsupervised machine learning deals with unlabelled data, looking for find hidden patterns within the dataset. By combining both supervised and unsupervised techniques, these methods enhance the overall capability to address complex challenges in WAAM and contribute to the advancement of this field.

2.1.1. Polynomial regression

Regression analysis is a statistical modelling technique used to describe the relationship between a dependent continuous variable y (output) and one or more independent variables x (input or features) in the form of a mathematical relationship, as reported in **Equation 1**. Nowadays even more research used regression analysis for several industrial application, and different approaches can be used to estimate the parameters θ.

$$y = f_{\theta}(x) \tag{1}$$

The most common form of regression is linear regression, where the relationship between the *N* independent variables (x) and the *K* dependent variable (y) is assumed to be linear as in **Equation 2**, and dependent by a matrix *W* of dimension *KxN*.

$$y_k = W_{kn} x_n \tag{2}$$

Since the regression is a supervised learning approach, the weights (*W*) multiplied by the input factors (*x*) can be estimated using the knowledge of the desired outcome. Ordinary Last Square (OLS) estimator, Lp estimator, or gradient descent optimisation [38] can be used with this scope. Although linear regression is highly interpretable and simple to train, it is limited to capturing linear relationships between data, and it does not consider the correlation between them [39]. For these reasons, polynomial regressions or advanced regression models like Decision Trees, have been employed to handle nonlinearity and multicollinearity in regression.

Polynomial regression (see **Equation 3** for a one-dimensional problem) assumes an nth-degree polynomial model between the independent variables and the dependent variables. Unlike linear regression, which assumes a linear relationship, polynomial regression can capture non-linear patterns and provide a more flexible model for the data.

$$y = \beta_0 + \beta_1 x + \beta_2 x^2 + \cdots + \beta_n x^n + \epsilon = Bx \quad (3)$$

where y is the dependent variable, x is the independent variable, $\beta_0, \beta_1, .. \beta_n$ are the regression coefficients, n is the degree of the polynomial, and ϵ represents the error term. The degree of the polynomial determines the complexity of the relationship that can be captured. Higher-degree polynomials can fit the data more closely but may risk overfitting, especially with limited data, as reported in **Figure 12**. It is essential to reach a balance between model complexity and the risk of overfitting.

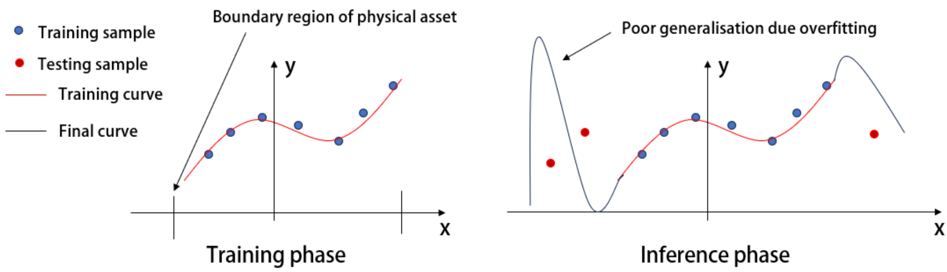

Figure 12 The poor generalisation introduced by overfitting can drastically reduce the performance of prediction of models within boundary regions.

Overfitting is often the big challenge related to data-driven models, especially within industrial field due to limited data that can be hard to collect in extreme or unsafe operating conditions. This data scarcity in this region often results in a dataset with low variance, increasing the risk of overfitting despite its volume.

As in standard linear regression, several methods can be used to estimate the parameters B. If no correlation between inputs is assumed, the most popular method is the OLS estimator. While Linear Regression analysis is typically used for regression tasks, the softmax trick can be applied at the output using the non-linear transformation defined in **Equation 4**. This enables the transformation of the K regression outputs into probabilistic values, each associated with a k-th discrete label in a classification problem. In this case, the Maximum Likelihood Estimator (MLE) is employed to estimate the parameters of matrix B.

$$p_i = \frac{e^{y_i}}{\sum_{i=0}^{k} e^{y_i}} \tag{4}$$

2.1.2. AutoRegressive Regression

An Autoregressive Regression (AR) is a statistical model used in time series analysis to model dynamic systems, in which the current state depends on previous states or observations. Mathematically, a linear AR model of order *p*, denoted as *AR(p),* can be represented as in **Equation 5.**

$$y_t = c + \phi_1 y_{t-1} + \cdots \phi_p y_{t-p} + \epsilon_t \tag{5}$$

where y_t is the value of the variable at time t, c is a constant term, ϕ_p are the autoregressive parameters representing the effects of the previous p values on the current value and ϵ_t is the error term assumed to be independent and identically distributed with mean zero and constant variance.

AR models can use both linear and polynomial regression models, and the parameters of the p lags can be found using OLS or gradient-based techniques. However, most of physical dynamic systems change their behaviour subject to external control actions or eXogenous variables, which are independent by target variable y.

Mathematically, an ARX model (AutoRegressive with eXogenous variable) can be described as in **Equation 6**, in which, β_q are the parameters representing the effects of the exogenous variables, $x_{q,t}$ on the current value.

$$\begin{aligned} y_t = c + \phi_1 y_{t-1} + \cdots \phi_p y_{t-p} + \epsilon_t + \ \beta_1 x_{1,t} + \cdots \\ + \beta_q x_{n,q} + \epsilon_t \end{aligned} \tag{6}$$

As for polynomial regression, also the auto regression requires careful consideration of polynomial degree in both input and time dimensions. To prevent overfitting and ensure good generalisation, a balance must be found between model complexity and data fit through manual tuning or specific domain knowledge.

2.1.3. Decision Trees for classification and regression

The regression tree algorithm is a straightforward method that recursively divides the input space into smaller regions, fitting a basic model, often a constant value, in each region. Each feature undergoes multiple splits based on a threshold method, determined by a splitting criterion measuring split quality. The resulting tree structure serves as the decision tree model, where leaf nodes hold predicted values for regression or the predicted class for classification. Despite its simplicity this method has been largely employed for both classification and regression tasks [40]. However, this method faces limitations such as overfitting, sensitivity to small variations, lack of smoothness in regression, and challenges in capturing simple linear relationships.

Due to the piecewise constant predictions resulting from separate regions in decision trees, they are less suitable for continuous space problems like regression. The inherent lack of smoothness hinders capturing simple linear relationships, requiring numerous splits for modelling linear aspects. Additionally, decision tree structures are better suited for handling discrete, complex, nonlinear data and revealing underlying multicollinearity. While decision trees exhibit prediction challenges, bootstrap aggregation techniques, known as bagging [41], offer a remedy by training multiple models on sub-sample datasets and averaging their outcomes. Random forests [42] extend this approach by introducing additional bootstrapping on the input vector, encouraging greater diversity among the trees composing the forest. This diversity enhances outcomes by reducing correlation in the models, ultimately improving the averaging process. Furthermore, gradient boosting methods [43] take an approach where each new predictor is fitted to the residual errors made by the preceding predictor. This iterative process aids in refining predictions over successive steps.

2.1.4. Isolation Forest

Isolation Forest (iFOREST) (see **Figure 13**) is a tree-based algorithm that isolates anomalies by randomly partitioning data points into subsets, and then recursively splitting the subsets until each point is in a separate subset. Anomalies are identified as points that require fewer splits to isolate them from the rest of the data, as they are less representative of the data distribution. The resulting anomaly scores may be used also for root cause detection.

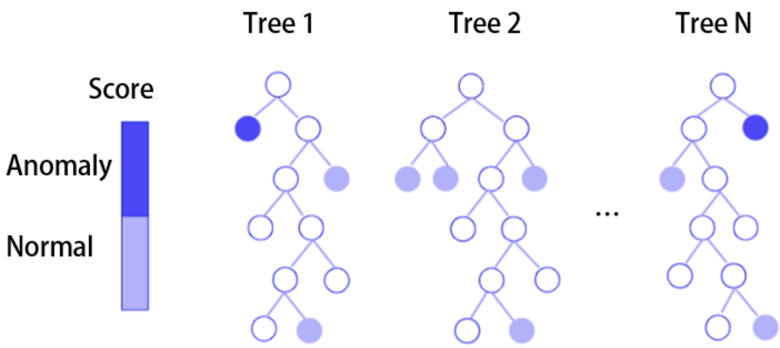

Figure 13 Schematic representation of the isolation forest algorithm.

2.1.5. One-Class Support Vector Machine

One-class SVM (OC-SVM) is a variant of the Support Vector Machine (SVM) algorithm used for anomaly detection. It is a type of unsupervised learning algorithm that aims to learn a decision boundary that separates the normal data from the anomalies in a dataset. The decision boundary is learned by maximizing the margin around the normal data, which is the distance between the boundary and the closest normal data points. After defining the hyperplane that can maximize the margin concerning the closest normal data point, the algorithm returns +1 if point X is inside the boundaries, -1 otherwise.

2.1.6. Principal Component Analysis for anomaly detection

Principal Component Analysis (PCA) is a data-processing technique typically used to reduce the dimensionality of data [44]; as a matter of fact, it transforms the data from a high-dimensional space to a lower-dimensional space while preserving most of the variance. This technique is also used for anomaly detection, since by applying an inverse transform it is possible to obtain the input high-dimensional data starting from the low-dimensional one. [45]. So, the basic idea is to identify the principal components of the data, i.e. the linear combinations of the original features that explain most of the variance in the data and use the inverse transformation to obtain the starting features from the low-dimensional projected ones. When the algorithm, with its learned weights, is used to extract the principal components and reconstruct the input signal via inverse transform, a large final reconstruction error is obtained if the input data deviates from the ones used to train it. At this point, a threshold method can be used to identify anomalies. To automatise the process, usually the threshold equal to *(1-contamination)* quantile of the errors obtained during the training is used, with the *contamination* become an hyperparameter of the algorithm.

2.1.7. Local Outlier Factor

Local Outlier Factor (LOF) is a commonly used density-based technique that identifies local outliers present in the dataset by comparing the local density of each data point with that of the neighbourhood [46]. Once defined a point O of the dataset, composed of the 12 features extracted, the k-neighbours are considered. Furthermore, the Local Reachability Distance (LRD) is evaluated as the inverse of the average distances of O concerning the neighbours, described by the Euclidean distance. The LOF is defined as the ratio between the LRD of point O and the average LRD of the neighbours. If the LOF is greater than 1, then an anomaly is found. As for all the presented algorithms, only the training dataset was used during the training phase and a k value of 5 was employed.

2.1.8. Gaussian Mixture Models

A Gaussian mixture model (GMM) is a weighted sum of M component D-variate Gaussian densities as given by the **Equation 7**, where x is a D-dimensional continuous-valued data vector (i.e., measurement or features) and the covariance matrix Σ and the mean vector μ of the M components are synthesised by parameter λ.

$$p(x|\lambda) = \sum_{i=0}^{M} w_i \cdot g(x|(\mu_i, \Sigma_i) \tag{7}$$

The covariance matrices can be full rank or constrained to be diagonal. Additionally, parameters can be shared, or tied, among the Gaussian components, such as having a common covariance matrix for all components, and they define the model configuration. Once a model is defined, GMM parameters are estimated from training data using the iterative Expectation-Maximization (EM) algorithm or Maximum a Posteriori (MAP) estimation

[47]. Gaussian Mixture Models (GMMs) can be utilised for anomaly detection by leveraging their ability to estimate the underlying probability distribution of the data. Anomalies are typically data points that deviate significantly from the normal or expected patterns in the data. By modelling the normal behaviour using a GMMs, we can identify data points that have low likelihoods under the estimated distribution, indicating potential anomalies.

2.2. Deep learning

Deep Learning (DL) consistently outperforms classical ML techniques in complex problem-solving. The hierarchical and adaptive nature of Artificial Neural Networks (ANN) allows them to capture intricate patterns and relationships within the data, avoiding the manual feature extraction activities typical of ML development.

One notable advantage of DL is its synergy with transfer learning [48]. Transfer learning leverages knowledge gained from solving one problem to tackle a different but related problem more efficiently. DL models, especially pre-trained ANNs, can be fine-tuned on specific tasks, saving valuable computational resources and time while achieving impressive results. This capability is particularly valuable in situations where labelled training data is scarce or expensive to acquire.

When it comes to time series data, traditionally processed through auto-regressive models like ARX, DL introduces a paradigm shift. Recurrent Neural Networks (RNNs), a type of deep learning architecture, excel in capturing temporal dependencies within sequential data. This makes them exceptionally well-suited for time series analysis, offering a more sophisticated alternative to conventional ARX models. The flexibility of RNNs allows them to model complex relationships in dynamic data, making them a preferred choice for tasks such as modelling time-dependent phenomena like physical systems. Moreover, deep learning's application extends seamlessly to image processing, where it overcomes the limitations of manual filtering. Rather than relying on predefined filters, deep learning models, especially Convolutional Neural Networks (CNNs), can automatically learn hierarchical representations of features directly from images. This not only eliminates the need for handcrafted filters but also enables the extraction of intricate details and patterns that might be challenging for human-designed filters to capture. As a result, deep learning has become the cornerstone of image recognition, object detection, and computer vision applications.

2.2.1. Artificial Neural Networks

The core idea of a neural network is to find the parameters θ of a function f_θ that minimize a cost, once a nonlinear combination of the inputs *g(x)* is made $y = f_\theta(g(x))$. The success of the method came from a universal approximation theorem by Cybenko [49] and from backpropagation [50]. The basic structure of a neural network is the artificial neuron, shown in **Figure 14**, a function f of the inputs $(x_1, x_2, .., x_n)$. weighted by a vector of connection weights $(w_{j,1}, \dots, w_{j,n})$ and completed by a bias $(b_1, \dots, b_n)$ and nonlinear function called activation function ϕ.

$$y_j = \phi(w_{jn}x_n + b_j) \tag{8}$$

The activation function ϕ and the initialization algorithm of the weights at the beginning of training are crucial ingredients for neural networks several functions and initialization algorithms might be used [51].

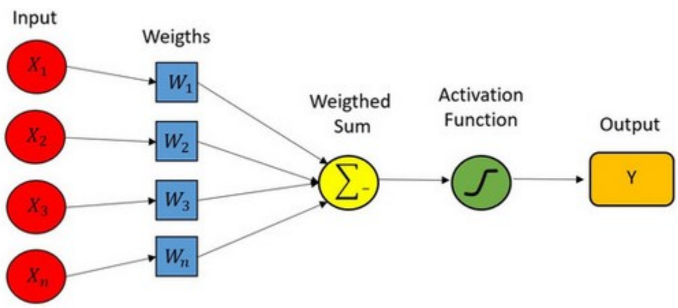

Figure 14 A neuron is a computational agent that gives in output a linear combination of the inputs passed in a non-linear activation function.

ANNs found applications in both regression and classification problems, such as system modelling and anomaly detection. [52]

2.2.2. Recurrent Neural Networks

Recurrent Neural Networks are used to infer sequential data such as text or time series, and for this purpose, a feedback loop is created into the networks' inputs as illustrated in **Figure 15**.

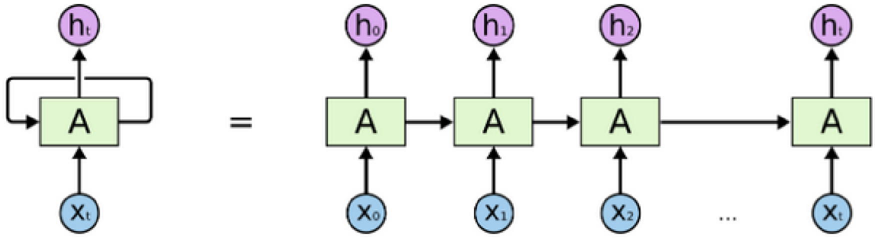

Figure 15 Unrolled representation of a Recurrent Neural Network. The hidden layer output at time t is given as additional input at the time t+1.

Respect to **Equation 8** another gate is added, with a matrix U, to compute the output at time t, as reported in **Equation 9**.

$$y_j^t = \phi(w_{jn}x_n^t + b_j + u_{jn}y_j^{t-1}) \tag{9}$$

RNN are very powerful dynamic models used to process sequential data. However, this model has problems into learn long time dependencies due to the vanishing gradient [53], which has led to the development of other architectures as Long Short-Term Memory (LSTM) [54] or Gated Recurrent Unit (GRU) [55].

Thanks to the presence of weighted input, output and forget gates an LSTM could prevent the gradient vanishing, allowing to store long term memory without losing training performance. The GRU is similar to LSTM but simpler to compute and implement. Based on LSTM the GRU combines the forget gate and input gate into the update gate and merges the hidden state with cell state, simplifying the architecture by reducing the number of weights, which corresponds to faster training, without losing performance. The comparison between the two architectures is shown in **Figure 16**.

RNNs and the derivate models, found industrial applications for both dynamical system identification and modelling [56], [57] and time series anomaly detection [58].

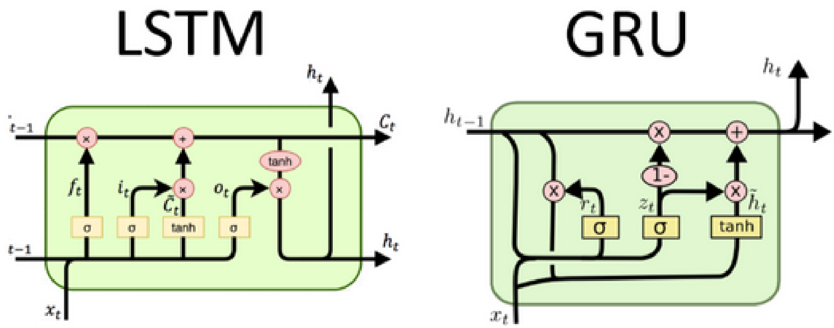

Figure 16 Comparison between LSTM and GRU architectures. The GRU architecture is computationally faster than LSTM, thanks to the presence of few gates.

2.2.3. Convolutional Neural Networks

For some data like images, in which spatial information is relevant, ANNs are not helpful since they are defined for vectors as input data. The innovations introduced by LeCun with the Convolutional Neural Networks (CNN) [59] were helpful since the development of computer vision applications passed by the "manual" extraction of features that required a lot of image processing experience to a self-learning features capability of the agent.

The CNN is composed of several layers convolutional layer (see **Figure 17**), composed by the series of Convolutional and Pooling operations, that stacked together allow the network to extract features during the learning process, and a fully connected layers that solves the defined task using the extracted features. Over the years, more complex and accurate architectures were proposed, and new hints to build a performance CNN were discovered.

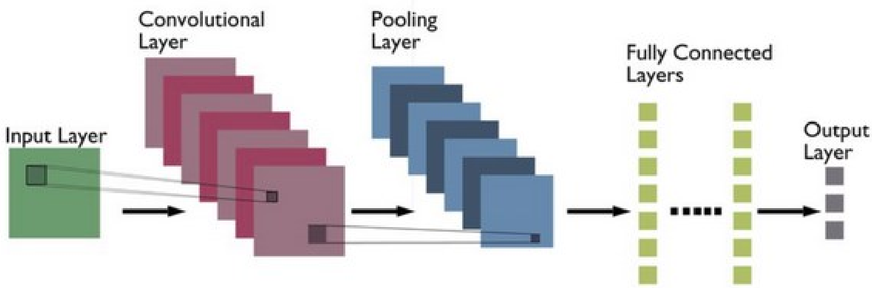

Figure 17 Naive convolutional stack composed of convolutional and pooling layers. The final layer of a convolutional stack is flattened and processed by feedforward networks.

A comprehensive benchmark of different architectures was reported by Bianco et al. in [60], and shown in the ball chart in **Figure 18**. The presented ball chart reports the accuracy with respect to computational complexity on the ImageNet-1k validation set for different convolutional neural network architectures, each one described by a ball. The ball size corresponds to the model complexity, described by the number of parameters.

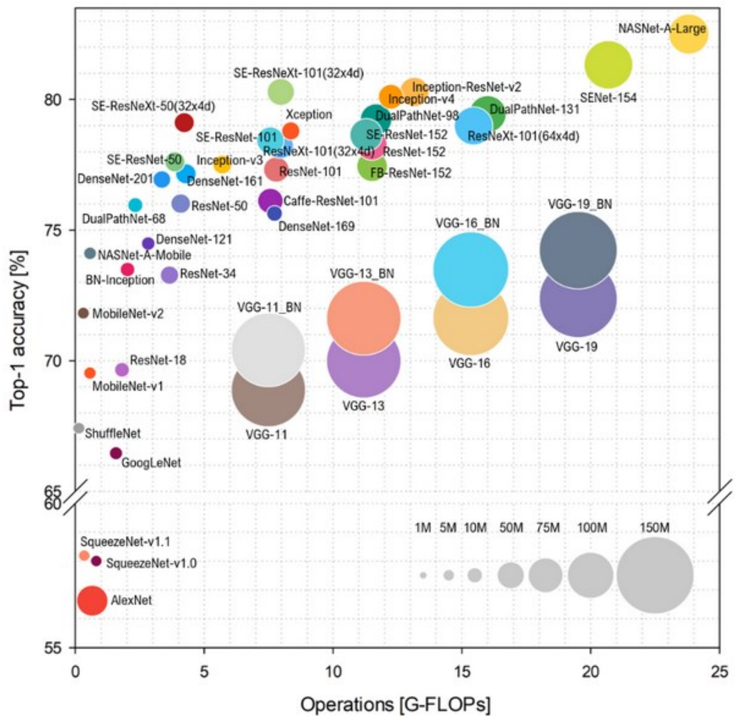

Figure 18 Accuracy vs. computational complexity of different CNN architectures by [60]

CNNs are largely employed in industry for object localisation [61], image classification [62] and process control [63].

2.3. Reinforcement learning

2.3.1. A gentle introduction

Reinforcement Learning (RL) is a field of ML originated from optimal control theory, e.g. Receding Horizon Control, and dynamic programming. The goal of the RL agent consists of optimising the input trajectory obtained from the environment via an iterative interaction (see **Figure 19**), described by the initial state, the control action and the next state, maximising the value function *V(s)*, which describes the goodness of being in a particular state, using the Bellman equation [64] in **Equation 10**.

$$V(s_t) = R_t + \gamma \sum P(s_{t+1}, u_t) \cdot V(s_{t+1}) \qquad (10)$$

Where $s_t$and s_{t+1} are the states at time *t* and *t+1*, γ is the discount factor u_t is the action vector at the time *t* and *P* is the transitional probability of arriving at the next state s_{t+1} given current state s_t and control input u_t, so the model of the system. R_t is the *reward function* obtained applying the action u_t in s_t which result into system movement to state s_{t+1}. This represent the crucial aspect of RL, since in the reward function are described all the goals and constraints of the optimisation.

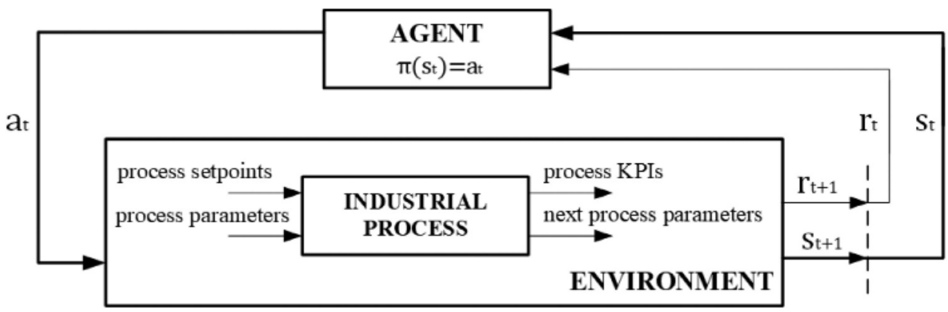

Figure 19 A scheme of RL in industrial processes, with the agent interact iteratively with an industrial process, e.g. WAAM.

Although the theoretical background of dynamic programming is elegant, this technique suffers from the curse of dimensionality, since the computational cost grows exponentially with the number of states, becoming impractical for continuous systems. Moreover, it needed a perfect model of the system to work optimally. To overcome this problem, different algorithms have been proposed to find the best action u_t to take in a given state s_t that maximises the value *V(s)*, such as: [65]

- Dynamic programming
- Monte Carlo
- Temporal difference learning

Today most RL algorithms are based on Temporal difference (TD) learning, due to its simplicity and less computational cost. TD methods combine the advantage of the possibility to learn from experience directly interacting with the systems, typically of Monte Carlo methods, with the bootstrapping, which consists of updated estimates based in part on other learned estimates, without waiting for a final outcome, typically of the dynamic programming. These characteristics allow having a model-free agent that can learn online during the interaction with the environment, without a model and without waiting for the end of an episode to evaluate the final discounted cumulative reward *G*, as reported in **Equation 11** conventionally computed for Monte Carlo methods.

$$G = \sum_{t=0}^{E} \gamma^t R_t \tag{11}$$

Where t is the t-th interaction between the agent with the environment, while E is the maximum number of episodes. If for Monte Carlo methods the value function *V(s)* at each step is computed as reported in **Equation 12**, in the case of TD learning, the update of the value is made according to **Equation 13**.

$$V(s) = V(s) + \frac{1}{N}(G - V(s)) \tag{12}$$

$$V(s) = V(s) + \alpha\delta_t \tag{13}$$

where δ_t is the TD error, defined as reported in **Equation 14**, for the case in which the agent updates its knowledge just after one interaction with the environment.

$$\delta_t = R_{t+1} + \gamma(V(s_{t+1}) - V(s_t)) \tag{14}$$

For control tasks, the *Q* value, which describes the goodness of state action pairs *Q(s,u)*, is used more than the value *V*, since it gives more information about control quality.

The most important feature distinguishing RL from other types of ML algorithms is that no prior knowledge is given to the agent regarding the best action to take (or labels), so this is what creates the need for active exploration. A crucial topic in this sense is the difference between exploration and exploitation, so in all algorithms are important to find a trade-off between the two. Generally speaking, the earlier learning step usually explores the action space using random policies, this phase is called exploration. Once learning goes on, more importance is given to exploitation, in which actions are taken directly from the optimal policy.

Originally, RL was proposed to solve discrete systems, and in this case, all the V or Q values were stored in tables. Since the industrial processes are physical continuous-based systems, both state and action space is infinitely huge, so methods based on approximation of the value function were developed [66], as reported in **Equation 15**, in which a function *f* is used to compute the value *V* using a continuous state *s*.

$$V_{\pi}(s_t) \approx f_{\theta}(s_t) \tag{15}$$

where θ are the parameters of the function *f* that approximate the Value V that come from the usage of the policy π. In this case, the perfect optimum is not guaranteed but using a differentiable and continuous approximation function it is possible to use optimisation algorithms, such as gradient-based optimisation [67] to evaluate with low-computational effort the Q or V values using the TD error for the cost function computation (C), as reported in **Equation 16** and **Equation 17**.

$$C = \frac{1}{N}\sum_{t=0}^{E} \delta_t^2 \tag{16}$$

$$\theta_{t+1} = \theta_t + \alpha \nabla C \tag{17}$$

Where E is the number of collected trajectories over the episode time with time step t, α is the learning rate, θ are the parameters of the function. In any case, the optimal control policy π^* is straightforward because the selected action is the one with highest V value, as reported in **Equation 18**.

$$\pi^* = argmax[V(s)] \tag{17}$$

To deal with continuous problems using the same foundations, simplification needed to be introduced. For example, a solution would be discretising the space of actions. However, in this way, a strong dependence on the degrees of freedom of the system exists. In fact, if we consider a joint in space with 6 degrees of freedom, trying to discretise the space of actions in the simplest way using only the lower limit, the upper limit and the central value, the action space present $3^6 = 729$ combinations. Therefore, using this methodology would provide a very large action space dimension, and this makes it very difficult for the agent to explore it all, making the training process highly inefficient.

For this reason, also the policy has to be approximated by a function, and ANNs are used in state-of-art methods for this task, leading to Deep Reinforcement Learning (DRL).

2.3.2. Deep Reinforcement Learning

In the field of DRL, three different families of algorithms can be used, value-based, gradient-based and actor-critic.

In the value-based algorithms, such as SARSA or DQN [68] , a neural network with a softmax activation function in the output layer is used to approximate the Q or V values. Unfortunately, as demonstrated by Mnih et al. [69], the adoption of these algorithms to solve real problems with huge action and state space bring to unstable training, so a number of adjustments, such as replay buffers and target networks to stabilise learning needed to be introduced [70].

Gradient-based is a family of algorithms in which the policy is directly approximated using gradient-based optimisation algorithms. An example is REINFORCE [71]. in which the gradient of the loss in **Equation 19** is used in a gradient ascent optimization algorithm.

$$J(\pi_\theta) = \sum_{t=0}^{T} R_t \nabla_\theta \log \pi_\theta(u|s) \quad (19)$$

Where π_θ is the policy approximated by the neural network with θ parameters, $\nabla_\theta \log \pi_\theta(u|s)$ is the gradient of the log probability of the distribution associated with the policy at time t, which is stochastic. This means that the action is sampled by a categorical distribution for discrete action space and diagonal Gaussian for continuous action space. In the case of continuous action the output of the network is equal to $2 \cdot size(u)$, one for the mean and another one for the variance of the gaussian distribution associated with each action.

Despite their high flexibility, gradient-based methods have a huge drawback associated with the high variance caused by the calculation of rewards each time step and training instability [72]. A common way to reduce variance is to subtract a baseline from the rewards in the gradient in **Equation 20** that does not depend on the action taken from the policy.

In this way, it does not introduce any bias to the policy gradient. This could be a random number, but a good choice is to use the Q or V values as a baseline, as reported in Equation 19, leading into an Actor-Critic DRL architecture.

$$J(\pi_\theta) = \sum_{t=0}^{T} (R_t - V(s)) \nabla_\theta \log \pi_\theta(u|s) \quad (20)$$

If the value function is approximated by a neural network, such in the case of DQN or SARSA, the structure of the agent becomes an Actor (gradient-based) plus a Critic (baseline approximation), as reported in **Figure 20**.

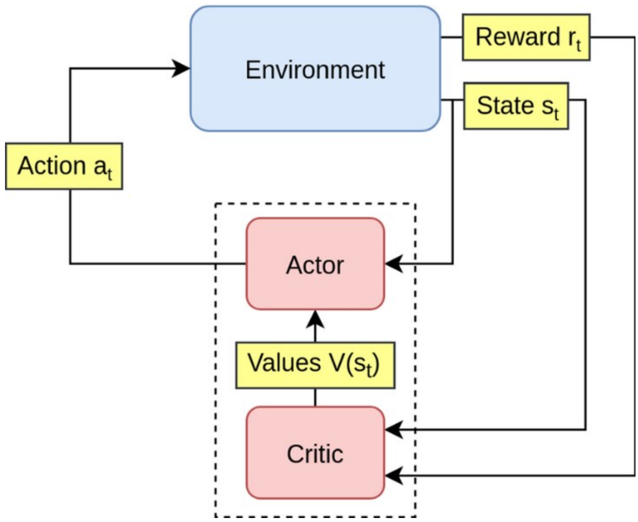

Figure 20 An high-level scheme of an Actor-Critic RL architecture.

Furthermore, the gradient ascent formula, in **Equation 21**, is used to update the policy parameters, while the TD error with a L2 loss is used to update the critic parameters, and a typical example is given by Deep Deterministic Policy Gradient (DDPG) algorithm [73].

$$\theta = \theta + \alpha \nabla J(\pi_\theta) \tag{21}$$

Although with the introduction of the baseline is possible to reduce the high variance of the returns, the problem of training instability needs additional adjustment. To overcome this problem, Trust-region learning (TRL) was proposed by Schulman et al. [74]. TRL improves the stability of the training by restricting the policy update size at each learning iteration, preserving monotonic improvement guarantees using a second-order optimisation algorithm based on the constraint reported in **Equation 22**.

$$D_{KL}\big(\pi_{\theta'}(u,s);\ \pi_\theta(u,s)\big) \leq \delta \tag{22}$$

Where θ' are the parameters of the new policy and θ of the old policy, D_{KL} refers to the Kullback–Leibler divergence between the two stochastic policies. Resolve the TRPO problems, so an optimization with hard constraint, become complicated for high space problems, so the same authors introduced the Proximal Policy Optimization [75] replacing the hard constraint with the clipping objective or DKL regularization, which reduced the mathematical and computational complexity leaving the properties of the TRPO framework untouched using a "proof by analogy". Nowadays among the presented RL algorithms the DDPG and PPO are the state-of-art in this technology, thanks to the numerous applications developed by researchers.

2.3.3. Deep Deterministic Policy Gradient

Deep Deterministic Policy Gradient (DDPG) algorithm uses an actor-critic approach to map both the action-value function and the policy [73] used to solve continuous action space problems. The DDPG uses, like the DQN, a memory buffer of predefined size, allowing it to store all the transitions given by the tuple (s_i, u_i, r_i, s_{i+1}) therefore the actor and critic weights are updated by randomly sampling from replay memory at each step, as shown in **Figure 21.** Another innovation introduced in the DDPG is the use of the target networks, namely the target critic network and target actor network, that copy the parameters of the original critic and actor networks, and whose weights are updated using a soft update through a parameter $\tau \ll 1$ as reported in **Equation 23** and **Equation 24**.

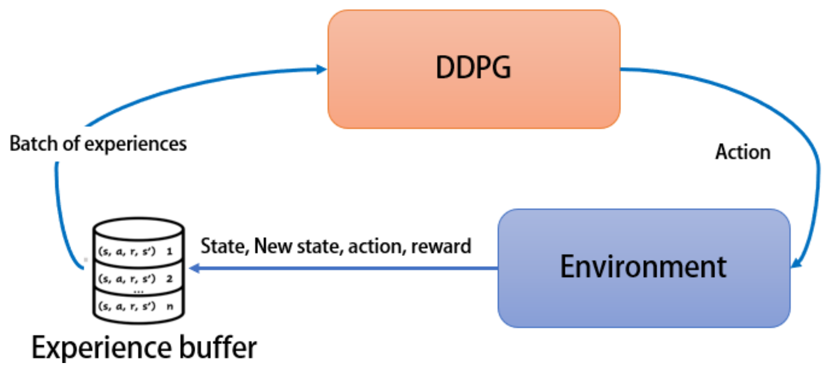

Figure 21 The RL agent parameters are updated based on random sampled batches from an experience buffer.

$$\theta_c' \leftarrow \tau \cdot \theta_c + (1 - \tau) \cdot \theta_c' \tag{23}$$

$$\theta_a' \leftarrow \tau \cdot \theta_a + (1 - \tau) \cdot \theta_a' \tag{24}$$

This avoids the divergence problem that occurs during the training phase, so using $\tau \ll 1$greatly increases the stability of the training [76]. In addition to the usage of the replay buffer and target networks, the DDPG also applies the concept of batch normalisation of deep learning, which is useful when dealing with states with different units.

2.4. Genetic Algorithm

The Genetic Algorithm (GA) [77] is a powerful metaheuristic decision-making algorithm inspired by Darwin's evolutionary theory and genetics proposed by Holland in 1992. The algorithm starts by randomly initialising a population of N potential solutions, each represented as a chromosome with genes representing different actions. The population's initialisation in the first generation is important since it is the first way for GA to explore the action space. Each chromosome in the population is associated with a score derived from a fitness function, which evaluates the quality of the solution. During the selection process, individuals with better fitness scores, indicating higher objective function values or lower cost function values, have a higher chance of survival and being chosen for the next generation. This selection bias allows the algorithm to concentrate on promising regions of the solution space. After M samples survive to form the new generation, crossover and mutation operators come into play to explore the action space and introduce diversity. Crossover combines pairs of parent individuals to create new offspring with a mix of their genes, simulating genetic recombination. Mutation introduces small random changes in the offspring, promoting exploration of the solution space. Through repeated iterations of selection, crossover, and mutation, the GA evolves the population, gradually improving the quality of solutions and it is able to find optimal or near-optimal solutions for the given problem by leveraging the principles of natural selection and genetics.

2.5. Application of AI in WAAM: Monitoring

The sensors used to monitor the WAAM process include welding cameras, thermal cameras, pyrometers, welding current and voltage sensors, and audio sensors such as acoustic emission and microphones. [78] The welding camera provides visual information on the arc length, arc stability, and solidification issues like humping, layer collapse, and porosity. However, the effectiveness of this camera depends on its mounting position, related to the scene it captures. Welding current and voltage sensors offer real-time data on these systems states, which are linked to system physics, such as electromagnetic forces influencing droplet detachment. These sensors can monitor events occurring within the torch, detect droplet detachment phenomena, and study arc stability, related to inconsistent layer geometry, as well as excessive spatter or porosity. Additionally, poor heat input, which may lead to delamination, can be identified. Audio sensors can detect both droplet detachment and porosity-related phenomena. They are also capable of identifying solidification problems like cracks, especially at high-frequency bandwidths, and phenomenon like layer collapse and humping. Finally, thermal cameras and pyrometers can detect both online issues such as porosity or lack of penetration, leading to layer delamination, and offline issues like inhomogeneous structure due to specific thermal cycles experienced by the base material.

These sensors can be used individually or combined to create multi-sensor monitoring systems, leveraging the strengths of different data sources to enhance performance. However, it is important to balance system complexity, cost, and performance. For instance, welding cameras are typically expensive, costing around 30,000 dollars, while infrared cameras can cost up to 100,000 dollars depending on factors such as frame rate and temperature range. On the other hand, audio sensors like microphones are less expensive but require additional software or hardware electronics to filter out the surrounding noise typical of an industrial setup, which can affect data acquisition. Welding current and voltage sensors offer a simpler way to capture droplet phenomena, but they provide limited information compared to audio signals.

2.5.1. Arc voltage and arc current signals

The arc current and the arc voltage signals are reliable indicators of arc stability and help to identify defects, such as layer delamination, porosity since they are associated with incorrect metal transfer mode or specific heat supplied to the material. Furthermore, since humping defect introduces changes in CTWD, also this defect can be detected using these data source, as well as porosity.

Several studies have used statistical tools to evaluate defects, principally porosity or lack of penetration, as proposed in [21], [79], [80], [81] once statistical features were extracted from signals (e.g. mean, variance, kurtosis and skewness). However, driven by democratisation of AI, several authors proposed new techniques to improve the anomaly detection performance.

Shin et al.[82] used six time-domain features extracted every 0.1 s as input of an ANN, namely the voltage standard deviation (std), voltage std during arc period, average arc time, number of short-circuiting periods, std of short-circuit time and std of instantaneous short-circuit voltage. An accuracy of 89% was reached. Similarly, Li et al. [83] proposed an SVM incremental learning approach to identify defects, using statistical features extracted by time-domain waveform of the employed GMAW process. This method can identify defects with an accuracy of 90%.

Regarding frequency domain analysis of these signals, Zhang et al. [84] employed a Continuous Wavelet Transform (CWT) to convert voltage signal to an image, called scalogram. The authors notice that the magnitudes in the time-frequency diagram of surface oxidation defects are greater than or 10 dB compared to normal weld beads. Therefore, they employed a CNN to detect this defect using a supervised learning approach.

Research gap

The conducted analysis revealed that a few relevant approaches exist, all of which utilise supervised learning techniques to address defect detection, framing it as a binary classification problem. Furthermore, despite the evident important information contained within frequency domain spectrum of these signals, few works proposed the extraction of relevant features within frequency or time-frequency domain, and no comparison between performance reached with time-domain features vs frequency or time-frequency features have been investigated. Finally, no application of unsupervised learning technique is present in the actual literature.

Addressing the identified research gaps was one of the objectives of this thesis.

2.5.2. Acoustic signals

Monitoring the audible sound emitted by the welding process is often used by expert welders since it gives good information regarding the transfer mode

[85] or pool behaviour in general. As shown by Horvat et al. [86] different sound sources appear during welding as a sound impulse, when a short arc occurs, or as a turbulent noise during spray arc mode. Furthermore, the sound is related to the arc length and welding current [87]. This means that the acoustic signal can be used to find defects during the process as current and voltage measurements, so acoustic signal analysis is widely used in feature extraction and defect recognition [88].

Pal et al. [89] showed that some features of the audio signal (e.g. kurtosis) could be used to detect burn-through during welding process. Therefore, employing statistical features extraction within time domain and ML algorithm can be effectively used as technique to identify defects. In fact, Roca et al [90] developed an ANN that predicts instabilities during the deposition using statistical features extracted by the Acoustic Emission signal. The features used in this work were the average of the peaks amplitudes in the instant of short circuit, the standard deviations of these peaks, the short circuit frequency, the time between peaks and its std, the sound pressure level in dB and RMS value of the acquired signal.

A similar approach was proposed by Rahman et al. [91] in which statistical features extracted by time domain of raw audio signal were used to cluster normal and anomaly data using K-Means algorithm, an unsupervised learning approach.

Additionally, a similar approach can be used also employing multi-sensor data. Rajesh et al. [92] in their work extracted features from both welding voltage and current signals and from audio signal collected with a microphone. In particular, they extracted the peak and variance of voltage and current signals in the time domain, the kurtosis of the time-domain audio signal, and the variance of the 3072 Hz–8192 Hz frequency band of the audio Mel spectrogram. These features were then processed using both a random forest and an ANN, with the results showing that the ANN performed better.

However, the frequency domain analysis of the audio signals remains the predominant way to process these kinds of signals, due to the high informative content and the high sample rates. For example, Yusof et al. [93] used a Hilbert Huang transform to study the frequency content of the audio signal and they show the energy information of the result could be used to detect the presence of defects.

This frequency content can be processed via both ML and DL techniques. Regarding ML approaches, Surovi et al. [94] proposed a comparison analysis in which features were extracted applying a PCA to Fast Fourier Transform (FFT) or via Mel Frequency Cepstral Coefficients from raw audio signals and then processed through different supervised ML techniques like Random Forest, k-Nearest Neighbour, SVM and ANN. The results shown that the best result was reached via FFT and PCA features processed by k-Nearest Neighbour algorithm. Alcaraz et al. [95] extracted 30 features from audio signals in both time and frequency domains. In particular Power Spectral Density is used to extract frequency features, while statistical features have been extracted in the time domain. Then these features have been processed by supervised classification algorithm to detect porosity.

However, DL approaches are the most employed thanks to generally higher performance. As mentioned in the previous section, employing time-frequency domain analysis, such as CWT or Short Time Fourier Transform (STFT), time series signals can be transformed into images called scalograms or spectrograms and then processed by CNNs. As an example, Rohe et al. [96] used a CNN to evaluate the deviation of the shielding gas from the ones defined in the WPS. Applying a STFT, they computed a spectrogram and after a normalisation they used a CNN for classification, reaching an accuracy of 94%. They showed that a flow rate below 70% of reference also produces unacceptable pores in the weld, which makes this method suitable as a defect detection module.

Research gap

The analysis revealed that both time and frequency domain feature extraction techniques can be applied to impulse ML algorithms for developing defect detection applications. Additionally, CNNs are widely used to process images generated through time-frequency analysis. Furthermore, most of the application rely on supervised learning application, but the new trend in analysing audio signals involves the use of unsupervised learning techniques. However, the application of unsupervised deep learning to analyse spectrograms obtained through time-frequency analysis is not yet explored.

Additionally, there is no known comparison of results for anomaly detection between time, frequency, or time-frequency feature extraction in the context of unsupervised learning. Finally, the literature lacks comparisons to determine whether unsupervised learning is beneficial for this task or if the performance is too low to warrant its development in industrial settings.

2.5.3. Optical signals

In addition to defects internal to the material, important defects are also those observables externally such as the humping defect, therefore also optical sensors can be used to monitor the presence of defects. Furthermore, the possibility to apply band-pass filters to the optics of the camera allow to observe the physical arc phenomena and use those images to develop several monitoring applications.

Xia et al. in [97], [98] compared the defects classification performance of different CNN architectures, showing that ResNet gave the best results with an accuracy of 97.62% in classification of humping, spatter and regular process. Similarly, Cho et al [99] used CNN for anomaly detection tasks comparing the results of several CNN architectures, showing that MobileNetV2 gives the best results in computational time (33 ms) and accuracy (95%). Lee et al. [100] used transfer learning with a VGG16 CNN architecture to develop a defect detection able to detect humping defects.

Although the proposed methodology is effective for defect detection, it requires analysis of the entire image. However, advancements in image segmentation and localisation now allow for the identification of defects within specific areas of the image. Since this new capability of vision system revealed promising in fields like pick and place or autonomous robot navigation [61], [101], the research community tried to move this technology also in the field of process monitoring. In this sense, the work of Li et al. [102] explored the possibility of using YOLOv3 architecture with modified anchors to develop a software module for item location detection and defect detection. Although the results regarding component location are excellent (100%), the same is not valid for defect detection accuracy (53%). The promising results directed numerous additional research in the field of optical process monitoring [103], [104], [105], [106], [107].

An innovative trend in monitoring of WAAM via optical sensors is given by unsupervised machine learning method. In particular Song et al. [108] proposed a Convolutional AutoEncoder (CAE) architecture to learn hidden pattern of normality from defect-free images and then detect anomaly based on reconstruction error, with an F-score of 86.3%.

Research gap

This study demonstrates that using image processing techniques with CNNs for both classification and anomaly detection is well documented. Both supervised and unsupervised learning techniques can be applied effectively, making their implementation in industrial settings feasible. Additionally, the performance of both online and offline defect localisation within components is well addressed by literature.

2.5.4.Thermal signals

WAAM is a complex thermal process with different and rapid thermal exchanges. In analogy to welding processes, the thermal history is a crucial parameter that influences the mechanical properties due to its strong correlation with microstructures. [109], [110], [111], [112]

Since the temperature is a significant parameter to monitor, infrared thermography is widely used since it provides fast responses, broad detection ranges and non-contact in both welding and WAAM applications. Alfaro et al. [113] found that defect-free welds have a temperature distribution that varies smoothly in the weld pool, while welds with defects, such as humping, present abrupt changes in the distribution of temperatures; this means that temperature could be used to estimate the presence of defects. Similar considerations are still valid for the WAAM process.

Also in this case, AI plays a crucial role for the elaboration of the data collected by thermal signals. As in the case of welding camera images, CNN are employed. For example, Chen et al. [114] proposed an AlexNet CNN architecture to classify the profile of deposited layers, such as normal, deviation or humping.

Given the significant influence of thermal history on defect generation, several studies have explored the potential of combining RNNs with CNNs to analyse images and detect defects, or to process temperature time series signals using RNNs. For instance, Mojtaba et al. [115] demonstrated that GRU could predict thermal behaviour during a WAAM process using temperature signals. Similarly, Fernandez et al. [116] employed a CNN-LSTM network to identify defects by analysing thermal camera images during a CMT welding process, achieving 97% accuracy. According to the authors, this network architecture leverages the complex temporal dynamics of the process, thereby improving classification accuracy compared to a standard CNN (95% on the same dataset), which only uses spatial information without incorporating temporal data.

2.6. Application of AI in WAAM: System modelling

Process parameters are related to the final bead geometry. In particular, several studies demonstrated that the geometry of the layers depends principally on the wire feed speed and welding speed ratio [117], [118]. Specifically, the layer width and height increased with an increase in wire feed speed, and the bead width decreased for higher welding speed. However, the other process parameters influence the layer geometry, given their relationship with heat input and the transfer mode [119], [120]. Several studies have been conducted about the possibility to establish a correlation between process parameters and layer geometry or mechanical proprieties and quality [121], [122], especially enhanced by ML [123]. Furthermore, these models can be employed as Digital Twin for parameter optimisation [124], [125]. Despite this several challenges persist, since for offline optimisation most of the developed models neglect the effect of interpass temperature, heat accumulation and layer distortion, leading to sub-optimal results in both process planning and surface finishing.

While the applications of system modelling based on process parameters are useful for slicer developments and offline optimisation, additional important applications can be found for both feedback control and monitoring. In fact, in addition to static model, also dynamic model can be employed aiming to develop soft-sensors or state estimators.

2.6.1. Arc voltage and arc current signals

In the field of state estimation and soft-sensor development, Chen et al. [126] developed a neural network to estimate the backside geometry of the weld pool during a GTAW process using process parameters such as arc current and voltage, welding speed and CTWD at sample time t and the same parameters acquired with two times delay. Similarly, Yin et al. [127] used the actual and previous values of the welding current to estimate the weld penetration, bead width and weld height or reinforcement for a single pass CMT welding through a simple neural network with an accuracy of 97%. Jin et al. [128] used time-frequency information of the current signal to estimate the back-bead geometry. In particular, they employed a Morlet wavelet transform and processed the scalogram in a CNN, reaching an accuracy of 93,5%. According to the literature, this approach might also be used to estimate the welding penetration.

2.6.2. Acoustic signals

Audio signals can be used also to predict the level of penetration since, as presented above, it is related to arc power. Lv et al. [129] extracted 39 features from both the time and frequency domains and trained an ANN to classify the state of penetration in 3 different states. In particular, they extracted features from time domain as energy and mean, and other features from Discrete Cosine Transform, as the energy of different frequency bands. Subsequently, they developed a controller for the penetration level. In particular, they increase the heat input to achieve more penetration, otherwise, they reduced it, increasing or decreasing the arc current of a pre-defined value, using an expert system.

Furthermore, Chabot et al. [130] demonstrated that certain frequencies within the FFT spectrum are linked to the CTWD, which varies depending on the material used. Specifically, the authors employed linear regression to correlate a particular frequency in the CMT process for stainless steel with the CTWD, enabling an indirect measurement of this process variable and creating a feedback loop for the process controller.

2.6.3. Optical signals

As presented above, it is possible to estimate geometrical parameters of the weld pool with secondary sensors, such as current sensors or encoders, and AI tools can create soft-sensors for indirect measurements. Optical sensors are used also to create labels. For example, Chen et al. [131] in their work used a vision system to extract geometrical information of a weld pool from images, generating the labels needed to train a neural network that estimates the geometrical parameters of the pool based on time-delayed process parameters. However, their use increases measurement uncertainty, making developing truly robust control systems challenging.

For these reasons, optical sensors are used to create direct feedback to the control system or to create labels for AI algorithms that allow the creation of soft sensors. Due to the intense light noise induced by the arc, high-speed laser sensors or cameras with appropriate 660 or 850 nm band-filters have to be used. Pinto et al. [132] used a welding camera to compute the pool geometry in real-time through computer vision algorithms. In other examples, Xia et al [133] extracted geometrical information from the welding camera by using computer vision techniques as Canny algorithm.

2.6.4.Thermal signals

As for welding cameras, thermography may be used to estimate the pool geometry [134]. Chokkanilgham et al. [135] used a thermal camera to extract eight features from the pool geometry such as peak temperature, the mean and standard deviation of the Gaussian temperature profile, thermal area, and others. Then, they employed an ANN to estimate the depth of penetration in a GTAW process. Furthermore, Ghanty et al. [136] used a Radius Based Function Network to estimate the bead width and the depth of penetration using features extracted from a thermal camera during a GTAW process. Moreover, Yu et al. [137] extracted features such as the first moment, second moment and Hu invariant moments from thermal images ROI for a CMT welding process. These features were used in an ANN to classify the state of penetration such as full-penetration, no-penetration and excessive penetration, with an accuracy of 99% for each class.

The dynamic nature and importance of the industry have prompted researchers to use RNN approaches for estimating pool geometry. In fact, Wang et al. [138] discovered that the image of the molten pool in the next frame would be affected by the previous one due to heat accumulation, which suggests that a correlation between frames exists. With this assumption, they used a PredNet to predict the molten pool geometry after 140 ms in the long term; this improved the control margin since rapid solidification dynamics introduced some uncertainties in the pool geometry control.

In addition to layer geometry, thermal images have been employed to estimate other proprieties of the final components. For example, Caio et al. [139] used neural networks to predict microstructure properties, using as label thermographic parameters obtained from a thermal camera and the process parameters. The Fusion Zone and four parameters that explain Heat Affected Zone (namely CGHAZ, FGHAZ, IHAZ, and SHAZ) were predicted with an error of 12%. These two last examples demonstrate the potential use of thermal data in constructing more complex system models. These models potentially enable the development of optimisation algorithms that aim to maximise the properties of final components by employing optimal process parameters.

2.7. Application of AI in WAAM: Optimisation and feedback control

As discussed above, several sensors can be integrated in a WAAM system with different aims, like identifying potential defects in real-time and/or create feedback loop for control systems via soft-sensor applications. Moreover, the same sensors can be used to create DT of the process useful for offline optimisation.

2.7.1 Feedback control

Addressing the feedback control of the welding process poses a complex challenge, primarily attributed to the non-linear, highly coupled dynamics of the system. Classical control systems like PIDs, designed with the assumption of linear system dynamics, are not optimally applicable in this context. Consequently, the research community has introduced innovative control techniques, including those grounded in AI.

An example of AI application can be found Cruz et al. [140] for GMAW process. The authors utilised an ANN to develop a model with bead width as the input and process parameters—WS, WFS, and V—as the outputs. A standard camera was employed to measure bead width online, allowing for error evaluation with respect to a setpoint reference. A Fuzzy Logic controller was then designed to the fuzzification of the error based on its magnitude, assigning to the different fuzzy classes different strategies for adjusting the welding speed. In the field of GTAW, other authors applied DL for process control. Chen et al. [141] used a welding camera to extract melting pool geometry information, such as the one described by Goldak [142], from a Pulsed-GTAW process. Then they employed an auto regressive ANN to correlate the peak current and the pulse duty ratio parameters at time t, t-1 and t-2 and the pool geometry information at time t-1 and t-2 with the pool geometry at time t. Once a non-linear dynamic model was established, they proposed a data-driven SISO controller, named self-neuron PSD, to control the bead width based on peak current value. In particular, the authors proposed a linear regression trained via gradient descent to correlate the error, the derivate of the error and its integral along the time with the control variable employing the developed model for both the training and as soft-sensor once deployed. Another application to GTAW welding is proposed by Kershaw et al. [143]. The authors used a CNN and an ANN to estimate the bead and back-side bead width based on WS, welding time and images collected by welding camera. Once the error between reference and predicted width has computed, WS is adjusted using gradient descent, aiming to reduce the bead width variation to zero.

In the field of WAAM, other approaches have been proposed. Xia et al. [144] used a welding camera to measure the layer width and they correlated via ARX model the relationship between layer width and WFS. Based on this data-driven linear model, they developed a SISO MPC and tested the performance in simulation, comparing the results reached with a PID controller. In the following works, the same research group introduced a MIMO MPC controller, considering as additional input variable the WS and as additional output variable the layer height, demonstrating on a real component how MPC outperforms a PID controller. [34]

Although the use of DL and data-driven techniques is well-explored in both welding and WAAM feedback control, several challenges remain. As mentioned earlier, bead geometry is influenced by more than just WS and WFS; other parameters like CTWD, interpass temperature, and voltage also need to be controlled to avoid suboptimal outcomes. Additionally, most proposed controllers have only been tested on multi-layer single bead deposition, so further research is needed to account for the effects of overlapping distance. Furthermore, in WAAM, only ARX models and MPC controllers have been suggested for process control, indicating the need to evaluate alternative techniques, such as those proposed in studies on GTAW.

In this context, given the promising achievements of RL in fields such as automation and robotics [145], [146] , RL presents a viable alternative for producing more sustainable parts with improved surface quality, reduced buy-to-fly ratios, and higher energy efficiency. In process control, RL can be employed to estimate the optimal gains for an adaptive PID controller [147] or to derive an optimal control policy through an ANN. For example, Ogoke et al. [148] utilised an Actor-Critic RL agent to optimally control laser velocity and power feed, reducing overheating in Selective Laser Melting Additive Manufacturing. A notable application in the GMAW process was demonstrated by Jin et al. [149], who used an Actor-Critic agent to control the bead width via welding current. They trained the agent using a SISO regression model, with welding current in input and bead width in output.

Despite the encouraging results achieved, few approaches of RL have been explored in both GMAW and WAAM, and those that have been proposed often involve simple scenarios with SISO systems. These systems could technically be controlled using other, less complex techniques, making the studied scenarios overcomplicated. However, RL shows promise, especially in the context of controlling MIMO nonlinear systems, an area that remains largely unexplored in WAAM process control. Therefore, the current focus on SISO and linear system models should be reconsidered, and the potential of MIMO controllers, particularly those utilising RL, needs to be further investigated.

Research gap

WAAM process control faces several open challenges. Bead geometry is influenced by more than just WS and WFS; additional parameters like CTWD, interpass temperature, and voltage also play crucial roles and need to be considered in WAAM modelling to avoid suboptimal results in control. Moreover, most current controllers have only been tested in simpler scenarios, such as multi-layer single bead deposition, which fails to consider the impact of overlapping distances, highlighting the need for more comprehensive research. Additionally, existing control techniques in WAAM are largely limited to ARX models and MPC controller, indicating the necessity of exploring alternative approaches, such as those based on DL and RL. In particular, although RL has shown promise, its application in WAAM and

GMAW is still underexplored and typically limited to simple SISO systems, which could be controlled with less complex methods. This suggests an overcomplication of studied scenarios, and the need to shift focus toward more complex MIMO nonlinear systems, where RL could offer significant potential for advanced process control.

2.7.2. Offline optimisation

For offline optimisation of process parameters, researchers have employed various methods, including GA [150] and Particle Swarm Optimisation (SPO) [151] in welding processes. Most methods rely on a data-driven model integrated with a metaheuristic optimisation algorithm, and similar approaches have been applied to the WAAM process.

Kumar et al. [152] used a polynomial regression to model the bead geometry and a GA to minimise the sum of void and post-processing material volume subject to the parameter constraints. Gulia et al. [153] employed a system of polynomial regression to model the current, voltage and the width-to-height ratio, and used a PSO algorithm to maximise the width-to-height ratio subject to constraint for the positive effect to surface roughness. The metaheuristic optimisation nature of evolutionary algorithms like PSO and GA eliminates the need for complex gradient-based optimisation methods, enabling the generation of optimised, defect-free components.

Research gap

Although system modelling and data-driven metaheuristic optimisation are well-established approaches for process optimisation, several challenges remain in the field of WAAM. Firstly, the data driven models neglect the effects of multi-layer and multi-bead deposition on layer geometry, resulting in suboptimal outcomes from optimisation procedure. Additionally, while applying process parameter constraints during optimisation can help the algorithm identify parameters to produce defect-free and optimal components, it also limits the search space of the algorithm, suggesting that alternative optimisation techniques should be explored. Furthermore, despite the importance of achieving high-performance parts, existing methods do not optimise process parameters for mechanical properties such as hardness, corrosion resistance, or tensile strength. Finally, although sustainability is increasingly crucial in manufacturing, current research does not consider these factors comprehensively, nor does it focus on the energy efficiency of the process.

2.8. Identified research gap and thesis contribution

2.8.1. Monitoring

The literature review identified key research gaps in process monitoring. While most studies focus on supervised learning, there is a growing interest in unsupervised learning, which remains largely unexplored in this context. In the field of welding current and voltage signal processing, there is a lack of exploration into frequency and time-frequency domain feature extraction methodology, as well as comparisons with time-domain techniques. Similar gap has observed for audio signals processing. Addressing these gaps was a focus of this thesis and ongoing research efforts.

2.8.2. System modelling

Although system modelling has been extensively addressed in the literature, several challenges persist.

Many offline optimisation models overlook the effects of interpass temperature, heat accumulation, and layer distortion, resulting in suboptimal outcomes in both process planning and surface finishing.

Sensor like welding current, voltage and audio can be utilised in WAAM to estimated layer geometry in real-time, providing a feedback loop to the control system. While this approach has shown promise in welding technology, the complex thermal transformations and the unique AM characteristics of WAAM need further study to fully understand the capabilities of AI methods in this context.

Despite this open issue, this thesis utilises state-of-art results for the development of innovations in process control and optimisation. However, the highlighted challenges are interesting ongoing research.

2.8.3. Process control and optimisation

The optimisation and control of the WAAM process present several challenges. Firstly, data-driven models frequently neglect the impact of multi-layer and multi-bead deposition on layer geometry, resulting in suboptimal outcomes. This issue complicates both process optimisation and the development of model-based control systems. Additionally, the optimisation process is often constrained by strict process parameters, limiting the search space of the algorithm and highlighting the need for alternative optimisation techniques. Current approaches also fall short in optimising crucial mechanical properties like hardness, corrosion resistance, and tensile strength. Moreover, sustainability and energy efficiency, which are becoming increasingly important in manufacturing, are often overlooked in existing research. Finally, regarding process control, most methods rely on linear modelling of WAAM dynamics and the use of traditional SISO control laws, such as MPC. This approach leaves unexplored the application of state-of-the-art and disruptive technologies, like RL, for MIMO nonlinear dynamic systems.

In this thesis a new technique for optimising WAAM process from an energy consumption perspective is proposed, utilising complex models rather than parameters constraint for defect-free results generation. Furthermore, the first MIMO controller for a nonlinear WAAM process based on RL is proposed, with attention to reward function design. The results of ongoing research are planned to be followed by innovative research also in the field of process optimisation and control to overcome the remains challenges.

Chapter 3 : Unsupervised learning for process monitoring

Monitoring applications are of primary importance in AM, since they give to manufacturing systems cognitive capability to automatically identify its state and take following action according to it. Furthermore, anomaly and defects can be detected, with anomaly defined as outlier states of the system that potentially lead to presence of defects. Defects are defined as condition of the system which result into not-compliant or low-quality parts.

As highlighted in the background section of this thesis, supervised learning approaches have been largely employed to solve monitoring applications, in which images from melting pool, welding current, welding voltage and audio signals can be processed to map the raw data or the extracted features with the system states labelled by humans. As illustrated in **Figure 22**, once data are collected from sensors, real-time monitoring applications allow to extract insight for decision making module.

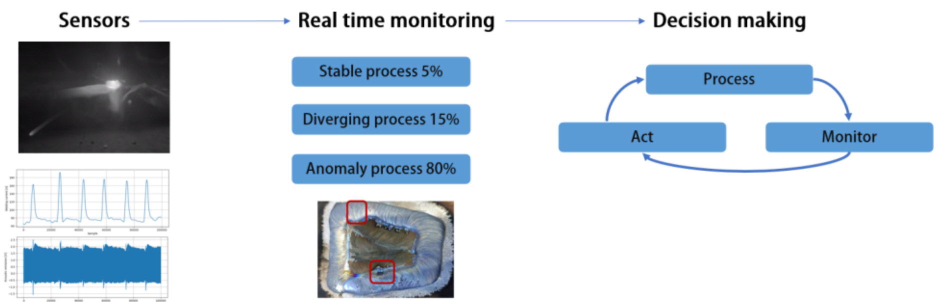

Figure 22 Once data are collected from the WAAM process, real-time monitoring allows to extract insight for the decision-making module.

Although this approach represents a well-known and effective way to monitor the process, several challenges are related to supervised approaches, such as:

- Needing to introduce defects within components to obtain labels.
- Strongly dependency by labels.

- Overfitting can affect negatively the results, especially in the case of unbalancing dataset. This is a common problem in the industrial field, since the defects are few for definition with respect to normal cases.
- Poor performance in small dataset scenarios.
- Low interpretability.

Despite this, another ML approach can be utilised to develop monitoring applications, namely unsupervised learning, which solve most of the presented problems related to supervised learning applications. However, the biggest problem in this case is the poor performance in similar task compared to supervised learning applications, which limited the study around this topic.

Pang et al. [52] discussed the main problem related to poor performance in anomaly detection reached by unsupervised learning algorithms. Anomaly detection algorithms are designed to identify outlier behaviour in data by comparing input features of a normal process with a new set of features. These algorithms often rely on distance-based methods, such as Euclidean distance, to compute differences. However, when the features are similar, the algorithms struggle to capture slight differences, leading to poor performance. To enhance the effectiveness of these algorithms, it is crucial to extract local features from the data. Global features may reduce the distinction between stable and unstable conditions, reducing detection accuracy. Without extracting more descriptive local features, anomaly detection algorithms can only identify rare and extreme events.

The problem of local features extraction is important for both images and time series data, and it is significant also in other application of unsupervised learning, such as clustering. Clustering groups similar data together, and the centroids of these clusters can define different regions in the feature space, corresponding to different system states. This makes clustering a valuable tool for classifying data from new processes. This approach is particularly advantageous in industrial settings, as it does not require balanced or large datasets, making it suitable for developing monitoring and anomaly detection applications even with small and unbalanced datasets.

In the case of WAAM, the welding current and the welding voltage signals are often collected during the qualification procedure (e.g. following the ISO

15614) [154] to assess the quality of the employed process parameters in producing defect-free components (e.g. following NI662 guidelines or the recent ISO 52943-2:2024) [155], [156] for a given material. This means that it is always possible to collect defect-free data, which results into one-class dataset. Although this is true, nowadays no techniques to make values from this small dataset are available for WAAM. However, the unsupervised learning techniques offer an alternative manner to develop specific anomaly detection application for WAAM using this kind of dataset. Furthermore, during the qualification procedure, illustrated in **Figure 23**, also some data related to the presence of defects can be obtained, but it is rare to have balanced dataset, and it is not unusual to have 70-30% dataset with 70% of defect-free data and 30% associated to some defects such as instability, porosity, humping, etc. Again, the unsupervised learning techniques offer a solution to develop monitoring application based on the clustering approach.

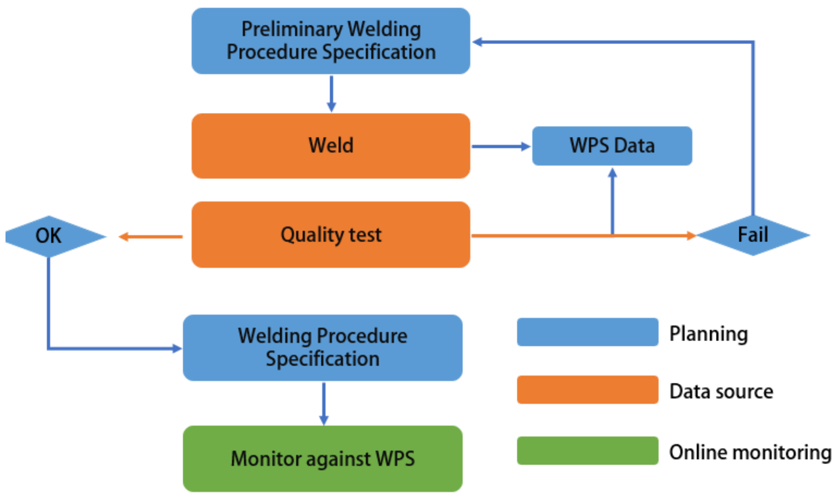

Figure 23 Workflow for defining the Welding Procedure Specification during the qualification process.

The scheme illustrated in **Figure 24** shows a potential cognitive software module based on unsupervised learning for process monitoring in WAAM. Once the data are collected and local features are extracted, a monitoring application based on clustering can identify system states and anomaly. In parallel, an anomaly detection module works to discover online anomaly with respect to the normal behaviour defined during procedure qualification. The output of these 2 systems is voted to assess the effective presence of an anomaly. If an anomaly is detected, thanks to pose of robotic motion platform a NDE target can be localised for successive inspection. This approach offers the potential to improve certification procedures for components, moving beyond the current standard of random inspections. Furthermore, a second step based on supervised learning algorithm can be used to classify the defects, giving more information about the system states to the following decision-making module. On other hand, if an anomaly is not detected, the information about system states directly flows to the decision-making module.

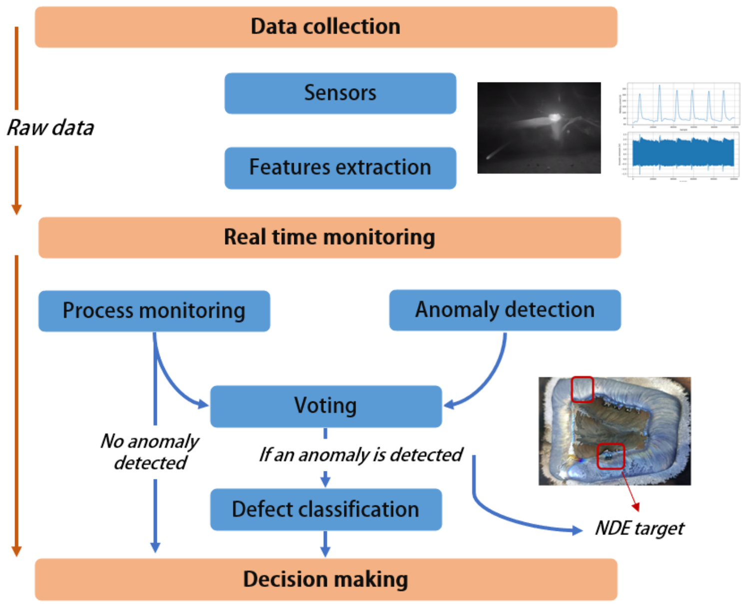

Figure 24 Cognitive multi-step monitoring module for WAAM process based on unsupervised learning.

This chapter explores the use of unsupervised learning techniques for monitoring WAAM processes through welding current and voltage data. These data sources are chosen for their low cost, ease of non-intrusive installation, and resilience to noise, while providing highly informative insights into the underlying physical phenomena. Moreover, these welding data sources must be collected during the qualification procedure as outlined by ISO standards. The experimental setup is initially presented, followed by a discussion on feature extraction techniques in both the time and frequency domains. The advantages of using frequency domain analysis to extract local features from time series data are highlighted. A comparison with time-domain feature extraction is then provided, demonstrating the improvements achieved in both process monitoring and anomaly detection.

3.1. Experimental setup

In this thesis, the experimental campaigns were carried out using a 9-axis robotic station that includes a Yaskawa MA2010 robot integrated with a PowerWave S500 welding machine supplied by Lincoln. Welding voltage and current data were recorded at a sampling frequency of 5 kHz, adhering to welding standards, using a NI-6009 DAQ. The monitoring software, hosted on an AI-enabled computer, communicates with the Yaskawa DX200 robot via TCP/IP. This setup allows the system to command process stops or adjust parameters in real-time, thanks to additional software running on a parallel thread using MotoPlus functionality. The experimental setup is illustrated in **Figure 25**.

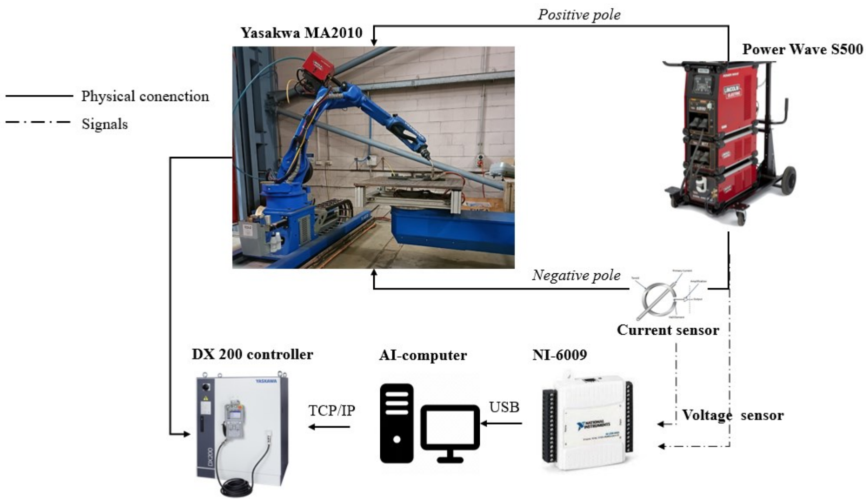

Figure 25 The 9-axis Yaskawa welding robot cell with Power Wave 500 power source is used for this experiment. For software integration an AI-computer is used to acquire and manipulate data, communicating trough TCP/IP with robot controller DX200

3.2. Time-domain vs frequency domain features extraction

3.2.1. Time-domain features extraction

Online process monitoring necessitates the real-time processing of data as it is generated by the process. In traditional welding procedures, assessments are typically conducted after the welding is completed. This approach works for welding because if an anomaly or a defect is detected, the weld can be repaired or reworked. However, in AM, particularly in WAAM where large components are built, post-process assessments can be costly and inefficient. Detecting defects only after deposition can result in significant material waste, with hours of work and several kilograms of metal potentially lost. Therefore, real-time monitoring becomes crucial in AM processes to minimise waste and ensure the quality of the build as it progresses.

The application of windowing technique for welding monitoring was proposed by Absi Alfaro et al. [157], in which the weld was monitored online analysing window of fixed length. The analysis consists of evaluating mean values for welding current and welding voltage and compare those with upper and lower limits defined by experimental evidence and human knowledge. In addition to mean values, other metrics such as standard deviation, kurtosis and skewness of the windows values can be extracted to assess online the quality. Despite this, it is possible incrementing the number of features to process from 2 to 8 make complex the definition of simple threshold method, and this is the reason why ML is coming out as a disruptive technology for online process monitoring.

In addition to statistics, other features can be extracted from time series data, such as ones related to waveform shapes of both welding current and welding voltage data, such the mean of time between pulse, peak and minimum values, etc, as illustrated in **Figure 26**. In this sense, the work of Li et al. [158] represent the state of the art of ML application for anomaly detection, in which the extracted features in the time domain were processed by a SVM algorithm.

Although this method is simple, the slight variations in global features representation of time domain features can reduce the performance in anomaly detection of unsupervised learning models.

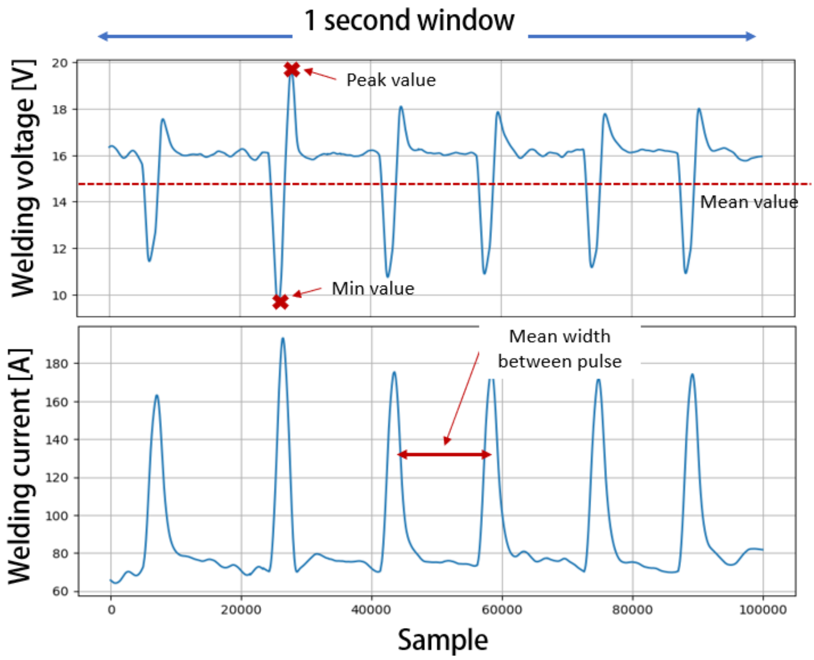

Figure 26 Example of time-domain features extracted by welding voltage and welding current windows for online process monitoring application.

To overcome the problem of global features representation, frequency and time-frequency features extraction techniques can be used.

3.2.2. Frequency-domain features extraction

Frequency domain analysis of signals is a valuable tool when the signal displays repetitive waveform content, as seen with welding current and voltage. In this context, the repetitive patterns are associated with droplet formation in the welding process, which is particularly evident during dip transfer or controlled dip transfer processes. Fourier Transform and Wavelet Transform are effective when the temporal content of the signal is not crucial. However, for frequency analysis over time, Short Time Fourier Transform (STFT) and Continuous Wavelet Transform (CWT) are more suitable, though they require processing larger data volumes.

Wavelet analysis [159] is generally more adaptable than Fourier analysis in the frequency domain, offering flexibility for analysing signals with complex frequency content. By using various wavelet functions like Gaussian or Morlet, wavelet analysis allows examination at different scales, making it ideal for handling intricate frequency characteristics, like the uncontrolled natural dip transfer processes.

Fourier analysis

Fast Fourier Transform (FFT) is a powerful tool for signal analysis, enabling us to extract the magnitude spectrum of a signal. This spectrum, as reported in **Figure 27** for a welding current signal, reveals the amplitudes of the sinusoidal components at various frequencies within the signal. When these magnitudes associated to good deposition are learned by an intelligent agent and the new data exhibit variations, it can indicate the presence of anomalies or defects.

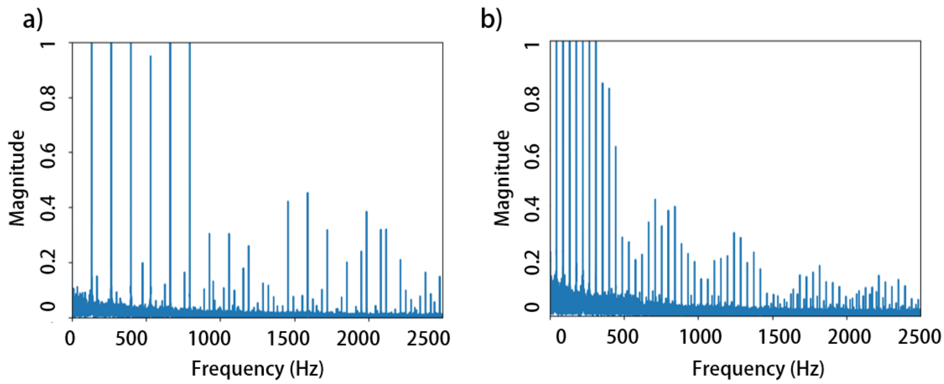

Figure 27 The output of a FFT on a welding current signal for a normal deposition (a) and a deposition with anomalies (b) of a pulsed-GMAW process.

Analysing the FFT spectrum allows for the extraction of features related to the spectrum energy, entropy, frequency peak, and amplitude at the frequency peak. Additional features can be statistically extracted from the spectrum and can be used to separate a normal behaviour from an anomalous one.

Wavelet analysis

Although FFT is a valuable tool for extracting frequency features from data, when the signals show complex shape, wavelet analysis is more suitable. With wavelet analysis, the signal is decomposed using wavelets of varying shapes and scales more able to capture complexity in signals. The Discrete Wavelet Transform (DWT), results in predefined levels of decomposition, where the sum of all these levels reconstructs the entire signal. Each level of decomposition can then be used to extract valuable insights, like the approach used in FFT.

As showed in **Figure 28**, applying a DWT with a pre-defined wavelet shape, details and approximations coefficients of each decomposition may be obtained, describing the frequency content of the signal in different bandwidths. Features can be derived from all the bandwidths, or some bandwidths of interest based on process knowledge, such as the standard deviation and energy of different decomposition levels.

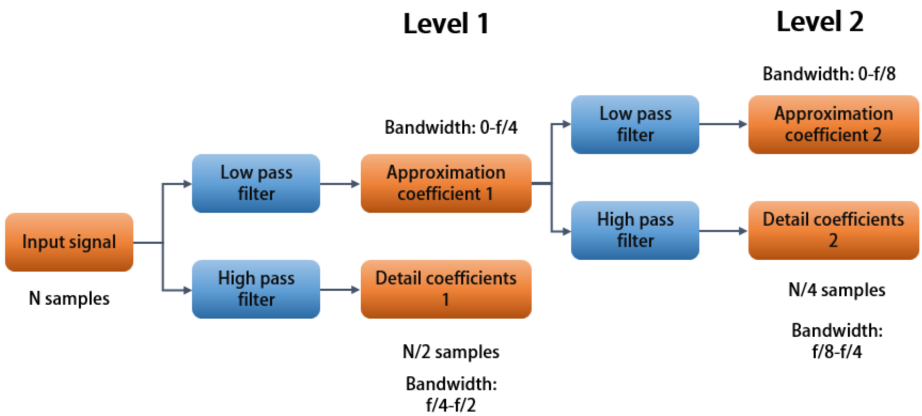

Figure 28 Applying a DWT the input signal may be decomposed in several detail coefficients which, as for the results of a FFT, may be used to identify anomalous behaviour.

3.2.3. Time-Frequency domain analysis via spectrograms

In addition to time domain and frequency domain analysis of time series signals, another technique known as time-frequency analysis can be employed. As shown in **Figure 29** for the STFT, this method involves selecting a fixed window length of the time series signal and applying an FFT to it. Overlapping between windows can also be considered, resulting in a 2D representation where the FFT results (a vector) are stacked multiple times, depending on the time length and overlap used. This approach in online monitoring allow to obtain images from time series, considering both time and frequency content, which can be processed by traditional image processing techniques, such as texture analysis [160], [161], or DL approaches like CNNs.

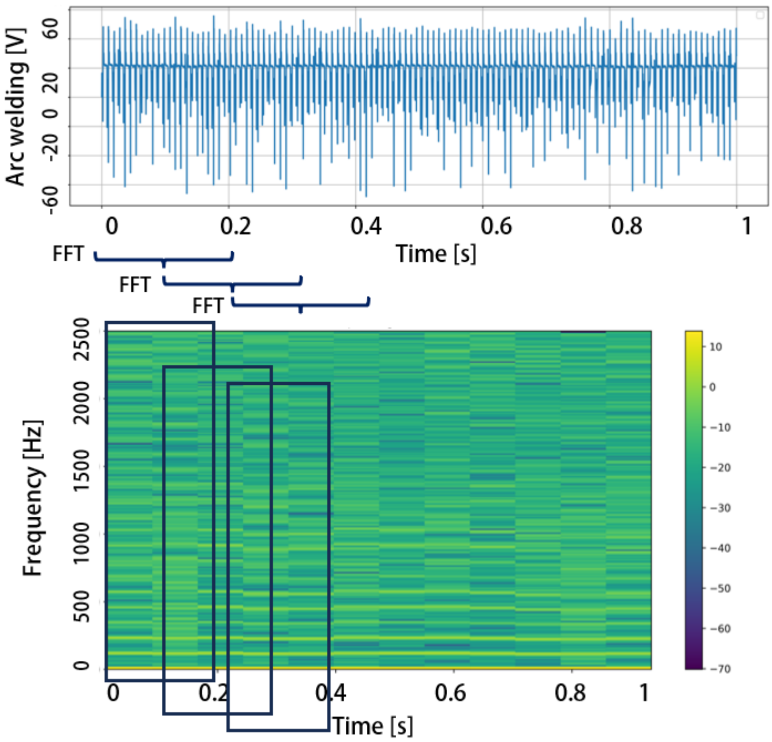

Figure 29 The output of a STFT on a welding voltage signal. Defined a window length, an FFT is applied and the results of frequency domain during the time are stored in an image called spectrogram.

In the case of CWT, various scales of the same wavelet are applied to the raw time series data. This process enables the creation of a 2D representation known as a scalogram. The scalogram provides a visual depiction of how the frequency content of the signal changes across different scales, offering a detailed analysis of the temporal and frequency characteristics of the signal. By examining the signal at multiple scales, the scalogram captures both broad trends and fine details, making it an effective tool for analysing signals with complex or varying frequency components over time, such as the welding signals, especially the natural dip transfer processes, characterised by a varying frequency content within time.

3.3. Process monitoring

The aim of this section is to demonstrate the capability in process monitoring of unsupervised machine learning algorithms. Therefore, an experimental campaign has been conducted simulating the qualification procedure of previous well-established process parameters in Inconel 718 components printing via Pulsed-GMAW based WAAM process. Inspired by ISO standards such as ISO 15614 and ISO 52943, data in terms of welding current and welding voltage were collected at the sample rate of 5kHz using the equipment described in the **Section 3.1**.

Specifically, a wall structure composed of 25 layers, each 100 mm in length, was deposited while maintaining a consistent interpass temperature of 30 °C. The parameters used were based on those previously established for industrial projects involving 1.2 mm wire Inconel 718 deposition. These parameters included a WFS of 8.5 m/min, a WS of 600 mm/min, and a CTWD of 15 mm, using a synergic line developed by Lincoln. This setup resulted in a deposition that was free of spatter and defects.

To induce anomalies within the dataset aiming to validate the methodology, another wall was deposited with the same parameters, this time without adjusting the CTWD before each deposition. This new layer contains both defect-free and anomalous layers. The introduction of disturbances in the CTWD resulted in anomalies such as spatter generation and porosity, which simulate real-world scenario due to factors such as incorrect path planning, heat accumulation and absence of a closed-feedback controller. Furthermore, the uncontrolled interpass temperature result in layer collapse, due to a too hot substrate. The experimental set up is summarised in **Table 3-1**.

After collecting the data from the two deposited walls, the Morlet transform is employed to visualise the spectrograms associated with the time series data. This step aims to identify the frequency bandwidths of interest within the dataset. Subsequently, DWT is used to extract statistical features from the specific bandwidths that have been identified. Finally, a Gaussian Mixture Model ML is used to cluster similar data. Each cluster is then labelled by analysing the cluster medoid in the time domain, as well as considering surface appearance and audio feedback from an expert welder

Experiment	Thin-walled structure printed without defects	Thin-walled structure printed with anomalies
Note	Process parameters have been controlled during the deposition with WFS 8.5 m/min, WS 600 mm/min and CTWD 15 mm at Interpass T of 30°.	Using the same parameters of good deposition experiments, the CTWD and the interpass temperature have been not controlled properly during the building process.
Anomalies	Not present	Excessive spatter Arc suppression Layer collapse

Table 3-1 Summary of conducted experiments

3.3.1. Time-frequency offline analysis

The Morlet wavelet is widely used in wavelet analysis and is characterised by its oscillatory behaviour, resembling a sinusoidal wave modulated by a Gaussian envelope. This combination allows it to effectively capture both high-frequency oscillations and transient features within a signal [162], making it especially suitable for analysing welding data in this context.

To generate scalograms of welding signals, the collected signals have been segmented into 1-second-long windows, each comprising 5000 samples, for a total of 614 samples in the dataset under study. This segmentation is crucial for developing an online approach to online monitoring welding processes. To compute the scalogram and for the further frequency analysis of welding signals, the mean value of the time window is removed to remove the contribute of the constant components. Morlet transform is then applied using 256 wavelets across different scales.

The analysis of the scalograms, illustrated in **Figure 30**, shows that the high-frequency content of the signal indicates the presence of anomalous conditions. In fact. the scalogram of the normal deposition process demonstrates a consistent frequency band cantered around 500 Hz, while in the high frequency bands a different and higher contribution can be founded when an anomaly occurs, e.g. layer collapse.

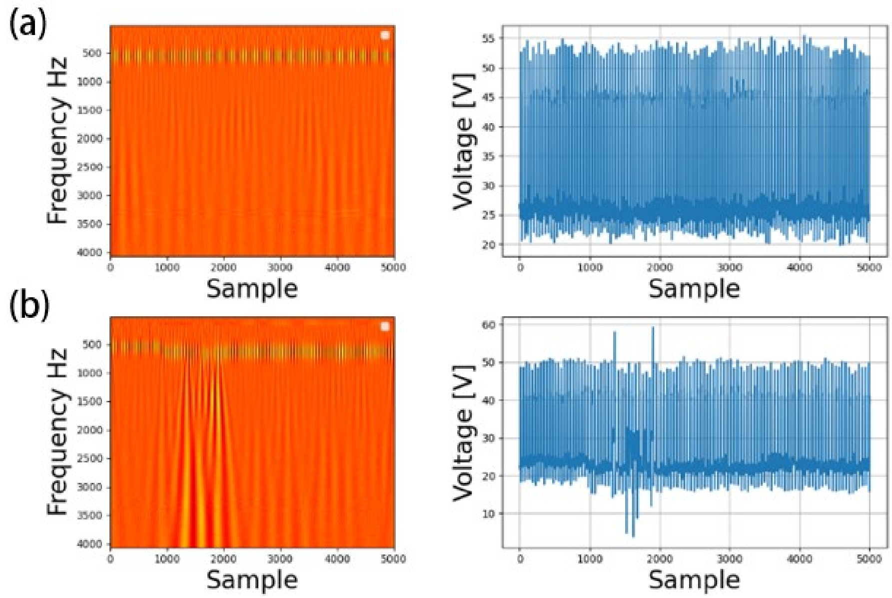

Figure 30 Scalograms obtained using the Morlet wavelet transform applied to the time series of welding voltage for (a) normal deposition and (b) deposition with anomalies.

3.3.2. Features extraction and visualisation

To extract online time-frequency domain features from the data, a DWT using a 2-level 2nd order Daubechies wavelet is employed. The signals were decomposed into 3 levels, capturing the frequency content in the bandwidths of 0-625 Hz, 625-1250 Hz, and 1250-2500 Hz. For the welding voltage signals, energy, variance, skewness, kurtosis, and the difference between the peak and minimum values (referred to as delta) of the coefficient amplitudes were extracted from the 0-625 Hz and 625-1250 Hz bandwidths, resulting in a total of 10 features per sample.

The extracted features of the training dataset, composed by the defect-free deposition, are then normalised in the range of 0-1 to assure that all the features are in the same interval and that the scale of the features do not influence the results of clustering. Obtained the minimum and maximum values on the training dataset, the features of the test dataset are scaled accordingly. Furthermore, a PCA has been conducted. In particular, the PCA has been trained on training data, associated with defect-free deposition, and the same transformation is then applied to test dataset. In this way, if new data come from a different process, e.g. an anomalous one, the applied transformation emphasises the difference between the features, increasing the anomaly detection capabilities of the proposed unsupervised learning algorithm. **Figure 31** presents a Pareto diagram of the explained variance, indicating that 90% of the variance is accounted for by using 4 components. The samples collected during the experimental campaign are visualised in **Figure 32**, which highlight the presence of anomalous deposition that can be detected by a ML algorithm, once meaningful features are extracted and reduced to 4 components.

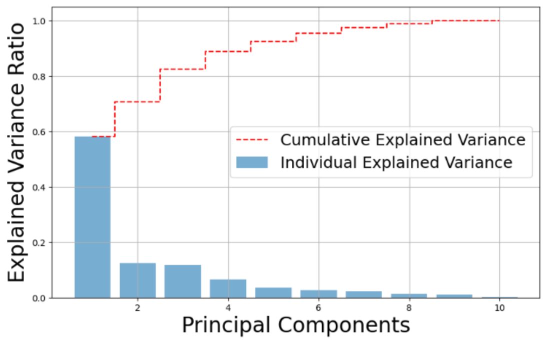

Figure 31 Pareto diagram of conducted PCA showing that 4 components explain 90% of the data variance.

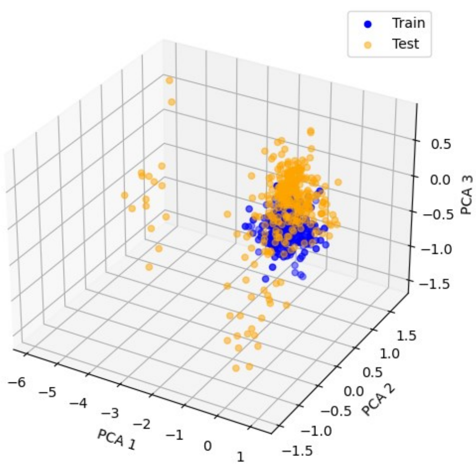

Figure 32 Principal Components that allow to visualise in the feature space the features extracted in the time-frequency domain.

3.3.3. Proposed methodology

In ML, clustering techniques group data points into subsets, or clusters, where points within each subset share similarities based on various criteria such as distance metrics, density, or distribution patterns. Algorithms like KMeans, Density-Based Spatial Clustering of Applications with Noise (DBSCAN), and Gaussian Mixture Models (GMM) are commonly used for this purpose. While clustering is primarily employed for organising datasets and extracting labels, it can also be used for online monitoring alongside supervised learning application.

An effective approach for this is the centroid and distance-based method, which assigns class labels to data points based on their proximity to cluster centroids. After identifying clusters offline, labels are assigned by examining the data within each cluster. If a new sample closely matches an anomalous cluster, it can be classified as an anomaly, otherwise other labels can be assigned to the data-point. The proposed methodology is illustrated in **Figure 33** and involves four distinct steps.

1. *Cluster Formation*: Initially, the dataset undergoes clustering and k clusters can be identified based data features.
2. *Cluster meaning evaluation*: Once the clusters have been identified, a label is assigned to each cluster following a clustered-data exploration in which engineering knowledge is used.
3. *Centroid Calculation*: Once clusters are formed and labelled, the centroid of each cluster is computed as the mean of all data points within the cluster.
4. *Monitoring application*: Once a new data come from the WAAM process, the distance with respect to identified clusters is computed and it is assigned the label of the closest centroid.

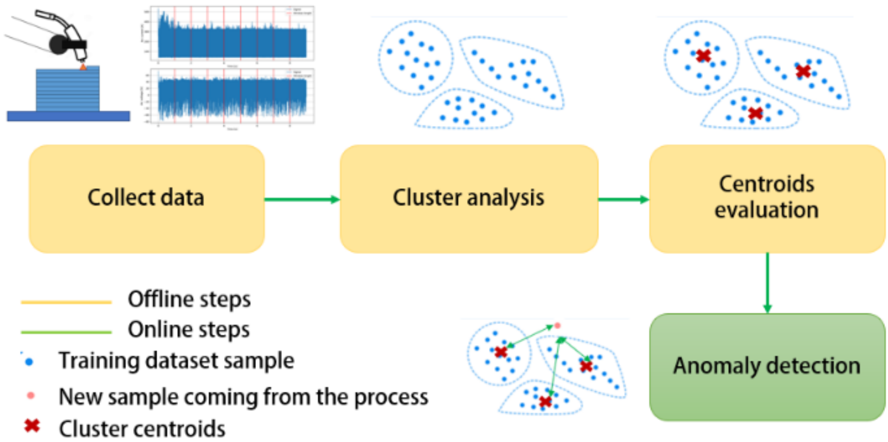

Figure 33 Proposed methodology for anomaly detection based on clustering analysis and centroid-distance methods.

Once features have been extracted, several ML techniques can be employed. In this case is shown an application which employ a GMM algorithm to cluster the datapoints collected during the experimental campaign, thanks to its ability to deal with intricate and non-linear data structures [163]. Unlike other techniques like KMeans, GMM represents clusters as probability distributions, allowing for soft assignments of data points to clusters based on the likelihood of belonging to each cluster.

Although GMM allows for capturing complex data distributions, determining the appropriate number of clusters in a GMM remains a challenging task. The Bayesian Information Criterion (BIC) offers an approach to address this challenge by balancing model complexity and goodness of fit. By penalising models with more parameters, it promotes simpler models capable of capturing the underlying data structure without overfitting. Therefore, the ideal number of clusters among the 614 samples contained in the training dataset, denoted as k, is determined by minimising the BIC score across various k values and it is equal to 4, as shown in **Figure 34**.

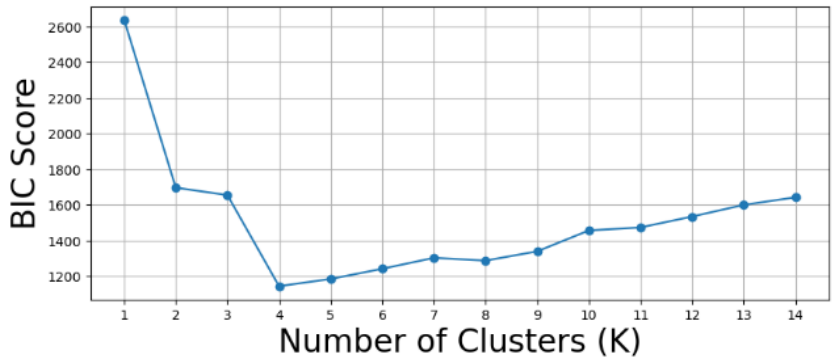

Figure 34 BIC score used to determine the optimal number of clusters.

However, the proposed approach requires modification, as a cluster is always assigned to the incoming process data. To address this, before inputting data into the GMM, the squared sum of the input vector is evaluated. If this value deviates by 10% or more from the minimum or maximum values observed in the training dataset, the data is labelled as an anomaly, thus preventing misassignment. This step is crucial because failing to implement it may cause the algorithm to incorrectly assign a sample to a cluster, even if the sample is significantly different. Such misassignments can occur when new, previously unseen anomalies arise that differ from those in the test dataset.

3.3.4. Results and discussion

Using the proposed approach, four clusters were obtained, with the centroids shown in **Figure 35**.

A medoid is defined as the point within a cluster that has the minimum average distance to all other points in that cluster. Therefore, the medoid can be used to visually represent a characteristic sample of a cluster. In the following section, the medoids of each cluster are analysed with the aim of assigning a label to each cluster.

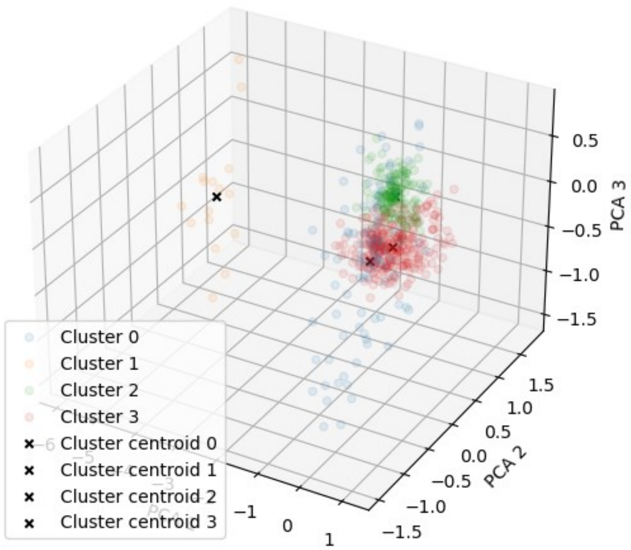

Figure 35 Results obtained using GMM clustering and centroids used for the anomaly detection task.

Analysis of cluster 0

The medoid of the cluster 0, which is contained in the training dataset, is shown in **Figure 36**. The constant droplet releasement is characteristic of the synergic pulse welding for the selected material. In this cluster follow the 54% of the samples part of this study, which is associated to a normal deposition.

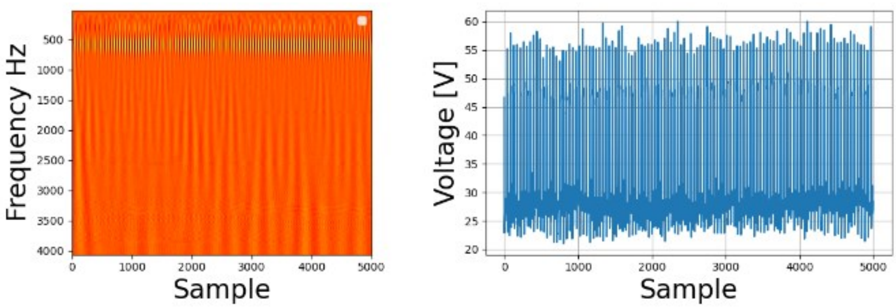

Figure 36 Scalogram and time series welding voltage signal of cluster 0 medoid.

Analysis of cluster 1

The medoid of the cluster 1 is shown in **Figure 37**, in which an anomaly associated to the unexpected arc start process can be found in a sample contained in the test dataset. More specifically, in this case is possible to notice a change in transfer mode to uncontrolled short circuit and undesired arc ignition associated to low quality deposition. In this cluster follow only the 2% of samples part of this study.

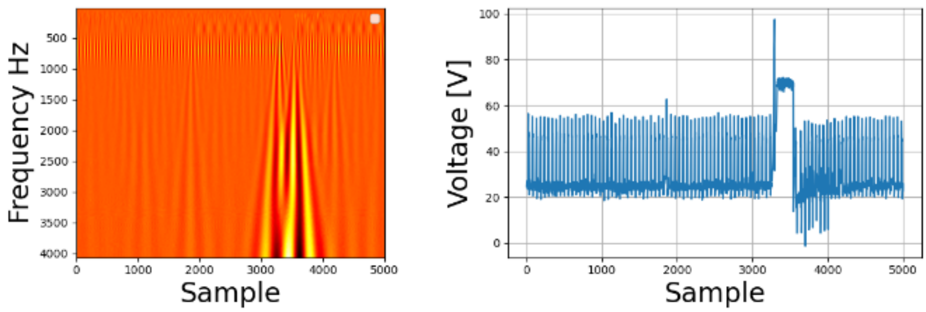

Figure 37 Spectrogram and time series welding voltage signal of cluster 1 medoid, associated to a deposition under undesired condition.

Analysis of cluster 2

The medoid of the cluster 2, contained in the training dataset, is shown in **Figure 38**, in which the deposition process is still stable, and no undesired short circuit can be founded. The slight difference in the frequency content is associated to the building process, which due to heat accumulation introduce acceptable uncertainties during the deposition. In particular, the 33% of the samples of this study follow in this cluster that represent normal deposition with the cluster 0.

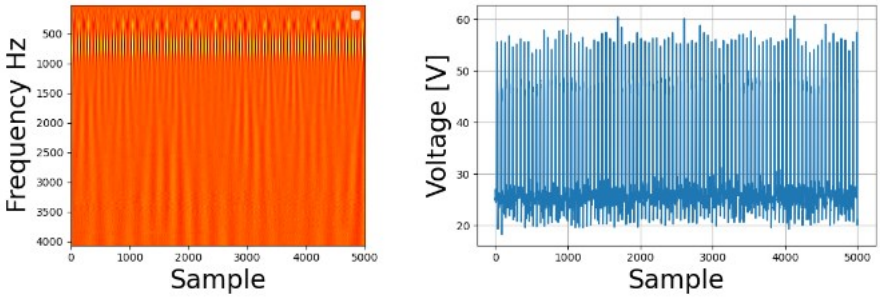

Figure 38 Spectrogram and time series welding voltage signal of cluster 2 medoid.

Analysis of cluster 3

Finally in **Figure 39** is shown the medoid of cluster 3, contained in the test dataset, in which a process that is diverging from the optimal, although a stable deposition is observed. In this particular case few undesired short circuits can be detected, which suggest a slight unstable deposition, which should alarm the operator. The 11% of the samples of this study follow inside this cluster. However, additional anomaly, such as layer collapse or humping can be detected.

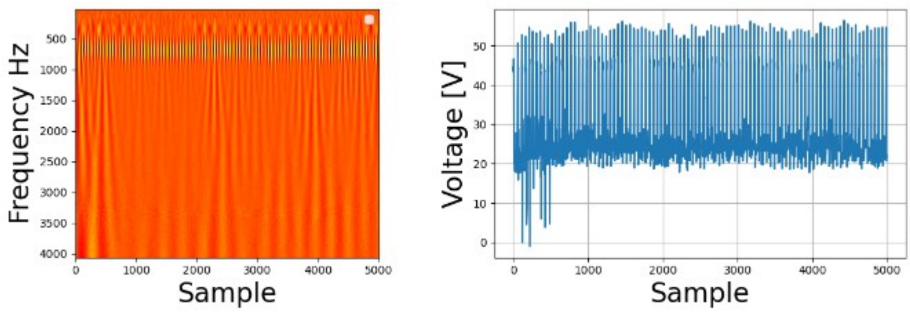

Figure 39 Spectrogram and time series welding voltage signal of cluster 3 medoid.

3.3.5. Centroid approach to monitoring

Using the proposed centroid approach, once the clusters are identified and labelled, the process can be monitored online at a sample frequency of 1 Hz. If the samples fall within clusters 0 or 2, no alarm is triggered. If the samples correspond to the distribution of cluster 3, an alert is issued to the user, indicating some instability, though it is not severe enough to cause defects in the parts. However, if the samples are close to the distribution of cluster 1 or are identified as outliers—where the squared sum of the input feature vector deviates by more than 10% from the training dataset—an anomaly is detected.

It is important to highlight that, once deployed, the proposed monitoring application consist of features extraction, features normalisation and PCA dimensionality reduction, then the distance of PCs is compared with those defined by the centroids of cluster previously identified. No ML algorithms are used during the inference, saving time and reducing the black-box nature of the proposed methodology.

The system equipped with the proposed software module is able to self-diagnosis about its state and can generate alerts the operator based on the outputs or stop the process if an anomaly is detected. The thin-walled structure utilised to develop the proposed application are shown in **Figure 40**, in which is possible to observe the difference in surface appearance of a good quality and low-quality deposition.

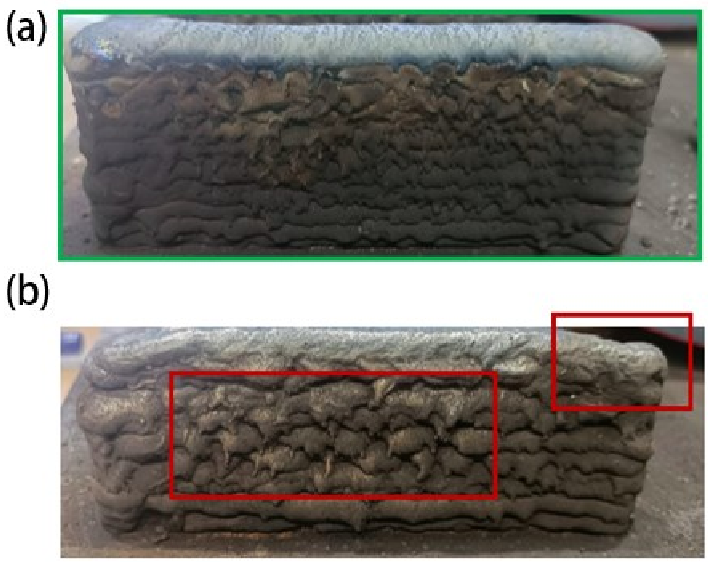

Figure 40 Thin-walled structures utilised in this work to collect and process data to develop the unsupervised machine learning methodology used to monitor the WAAM process of Inconel 718 parts. (a) defect-free wall (b) wall with anomalies

To demonstrate the performance in process monitoring, the algorithm is tested on the last layer of test wall. The results of the proposed clustering method, shown in **Figure 41**, demonstrated the ability of the proposed approach to monitor the WAAM process. In particular, the arc instability at the beginning of the deposition has been correctly individuated (as cluster 1) and the operator alerted. Furthermore, a layer height variation at the beginning of the deposition (as cluster 3, observable in **Figure 40**) has been individuated and the operator has been informed about an instability during the deposition process. Finally, **Figure 42** displays the results obtained from extracting statistical features in the time domain, including mean, variance, kurtosis, and skewness, from 1-second length welding data. PCA was also applied to emphasise the presence of anomalies. However, due to the discussed global feature representation, the system fails to identify the arc ignition as an anomaly, as well as the layer height error at the beginning of last layer of wall 2.

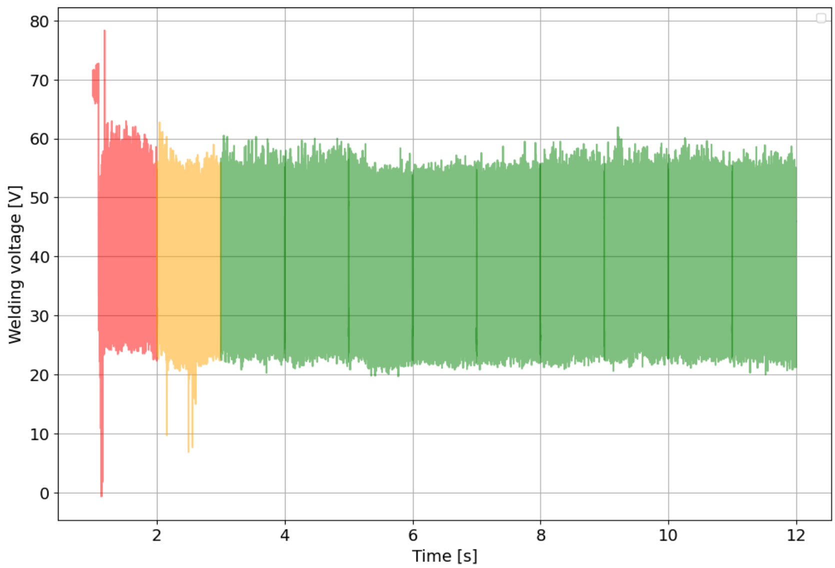

Figure 41 Results of the proposed monitoring methodology based on clustering and unsupervised machine learning in detecting the WAAM states during the deposition and in identifying anomalies.

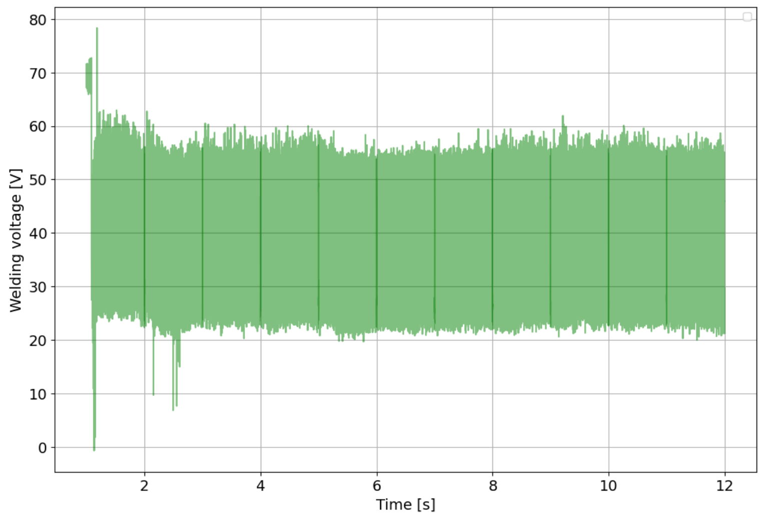

Figure 42 Results obtained employing time-domain features extraction which show the poor capability in detect anomaly behaviour due to global features representation.

3.3.6. Summary of unsupervised learning for process monitoring

This section demonstrates how time-frequency analysis can improve process monitoring in WAAM for Inconel 718 components. Specifically, DWT was used to extract features within the 0-625 Hz and 625-1250 Hz bandwidths of a P-GMAW deposition process. The monitoring results obtained with this method were compared to those from standard time-domain feature extraction. The comparison highlights the limitations of time-domain feature extraction for WAAM monitoring, as its global feature representation fails to detect anomalies such as arc ignition and layer height errors. Employing the proposed methodology together with standard time domain analysis of welding signals can improve the monitoring performance of unsupervised ML algorithms and potentially be used to develop control strategy for the following decision-making layer of a SMS. For example, if an alert is generated as in the case of cluster 3, the root cause analysis of both time-frequency and time domain features can suggest the improvement of feeding rate or the reduction of WS to solve the layer height control problem in the next layer in that point of the geometry. Despite this possibility, this topic represents a potential path for future research.

3.4. Anomaly detection

In the previous section, a monitoring application for Inconel 718 produced via P-GMAW was presented, showcasing the potential of developing such applications using a small dataset and unsupervised ML. Additionally, incorporating time-frequency domain analysis enhanced performance compared to using time-domain feature extraction, enabling the online detection of various states. However, despite its effectiveness, the algorithm was not specifically designed for anomaly detection due to its reliance on a simple centroid-based rule, making it more suitable for use in DSS rather than for NDE target localisation.

For this specific task, more advanced strategies specifically designed for anomaly detection should be employed. The experimental campaign of this study involved the deposition of 90 beads using the STT process with a 1.2 mm ER70S-6 wire, with a systematic variation in process parameters as outlined in **Table 3-2**. In particular, the experimental campaign involved varying WS, GFR, and CTWD while keeping the waveform parameters of STT process, namely the background current and peak current, and WFS constant to the values of 120 A, 320 A and 4.5 mm/min respectively. As discussed in the previous section, welding current and voltage data were collected at a sampling frequency of 5 kHz using the WAAM system described in **Section 3.1**.

With the parameters of Layers 73, 77, 83 and 86, eight walls, each consisting of 10 layers, were printed using different deposition strategies. Walls 1 through 4 were printed with the same starting point each time, while Walls 5 through 8 were printed with a varying deposition direction for each layer. This approach was used to study the impact of heat accumulation within the components, which had caused defects due to incorrect layer geometry in the Walls 1 and 3. The process is summarised in **Figure 43**. While the defect-free data related to printing process of single beads deposit and of the defect free data related to printing of Walls 1 through 7 have been employed for training, the Wall 8 data are used for algorithm testing and for the metrics evaluation.

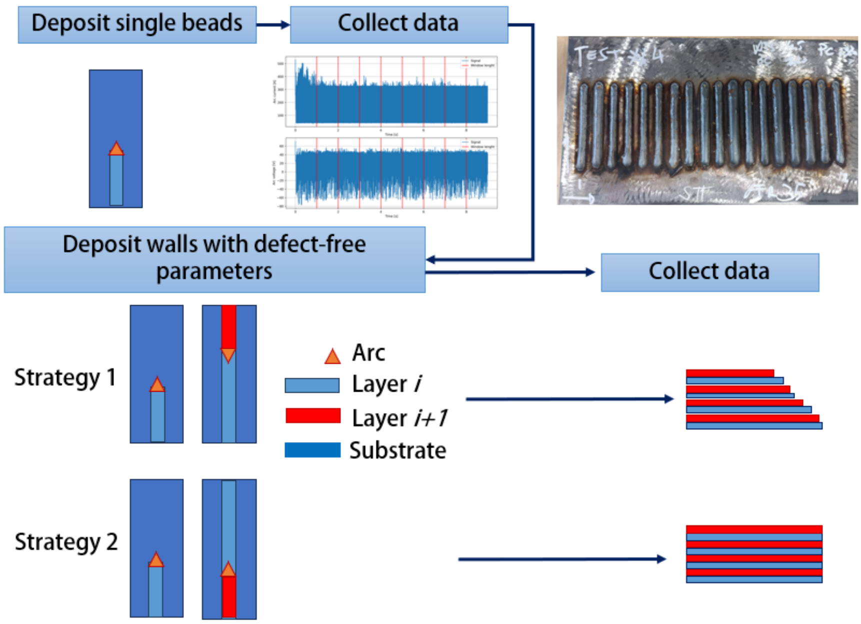

Figure 43 Proposed experimental campaign which employ the deposition of 83 single beads and 4 walls with 2 different strategies, for a total of 8 walls. Only the data coming defect-free deposition were employed for process training.

Audio signal analysis and visual inspection were conducted with the assistance of expert welders to classify the deposited layers as either anomalous or normal. Only defect-free layers, labelled with an Anomaly label of 0, were then used to train unsupervised learning models to identify patterns of normality within the data. Inspired by ISO 15614 and ISO 52943, this complex hidden pattern of normality is used to identify anomaly to label as potential site of defects such as humping, porosity and geometry deviation. By integrating output of the anomaly detector with the robot pose information coming from the robot controller, NDE targets can be accurately localised for future inspection procedures.

Layer No.	Gas Flow Rate [L/min]	Contact Tip to Workpiece Distance [mm]	Weldin Speed [mm/min]	Anomaly
1	20	15	552	0
2	20	10	348	0
3	20	18	700	1
4	20	20	700	1
5	20	22	700	1

6	20	25	600	1
7	20	30	450	1
8	20	10	600	1
9	20	10	450	0
10	20	18	552	0
11	20	18	252	0
12	20	20	552	0
13	20	20	600	0
14	20	20	252	0
15	20	20	348	0
16	20	22	348	0
17	20	25	450	1
18	20	30	700	1
19	30	15	552	0
20	30	10	348	0
21	30	18	700	0
22	30	20	700	1
23	30	22	700	1
24	30	25	600	1
25	30	30	450	1
26	30	10	600	1
27	30	10	450	1
28	30	18	552	0
29	30	18	252	0
30	30	20	552	0
31	30	20	600	0
32	30	20	252	0
33	30	20	348	0
34	30	22	348	0
35	30	25	450	1
36	30	30	700	1
37	10	15	552	0
38	10	10	348	0
39	10	18	700	0
40	10	20	700	1
41	10	22	700	1
42	10	25	600	1

43	10	30	450	1
44	10	10	600	0
45	10	10	450	1
46	10	18	552	0
47	10	18	252	0
48	10	20	552	0
49	10	20	600	0
50	10	20	252	1
51	10	20	348	0
52	10	22	348	1
53	10	25	450	1
54	10	30	700	1
55	35	15	552	0
56	35	10	348	0
57	35	18	700	0
58	35	20	700	1
59	35	22	700	1
60	35	25	600	1
61	35	30	450	1
62	35	10	600	0
63	35	10	450	0
64	35	18	552	0
65	35	18	252	0
66	35	20	552	0
67	35	20	600	0
68	35	20	252	1
69	35	20	348	0
70	35	22	348	0
71	35	25	450	1
72	35	30	700	1
73	25	15	252	0
74	25	15	348	0
75	25	15	450	0
76	25	15	552	0
77	25	15	600	0
78	25	15	700	1
79	25	15	252	1

80	25	30	348	1
81	25	30	450	1
82	25	30	552	1
83	25	30	600	1
84	25	30	700	1
85	25	10	252	1
86	25	10	348	0
87	25	10	450	1
88	25	10	552	0
89	25	10	600	0
90	25	10	700	0

Table 3-2 Results obtained employing time-domain features extraction which show the poor capability in detect anomaly behaviour due to global features representation.

3.4.1. Surface Tension Transfer

Surface Tension Transfer (STT) waveform welding technology (see **Figure 44**) was employed to control the deposition process, with the goal of minimising heat input into the material. This technology manages the surface tension of the filler droplet adhering to the weld pool by employing a high-speed inverter to adjust the output current waveform during the shorting phase, depending on the material of the wire.

Starting from a background current, the current decreases to prevent premature droplet separation. Subsequently, it increases to enhance the electromagnetic force regulating the bridge size formed during the short circuit. To prevent spattering, the current is set below the background level. An increment to peak current is then maintained for a peak time, establishing a new droplet. To prevent undesired droplet realignment, a tail-out phase reduces the current to the background level, facilitating cycle restart.

This controlled dip transfer process, with its reduced heat input, proves advantageous for WAAM by minimising distortion and spatter, consequently reducing the requirements for surface finishing and the presence of defects. The controlled current waveform is achieved by adjusting the welding voltage. Consequently, the frequency content of both the welding current and voltage signals can be linked to process stability. This is because the shape of both the current waveform (such as the pulse shape in P-GMAW) and the voltage waveform are indicators of process stability. Specifically, the welding voltage reflects the behaviour of the controller, providing insights into its performance and process control, while the current shape which deviate from the planned suggest instable process condition.

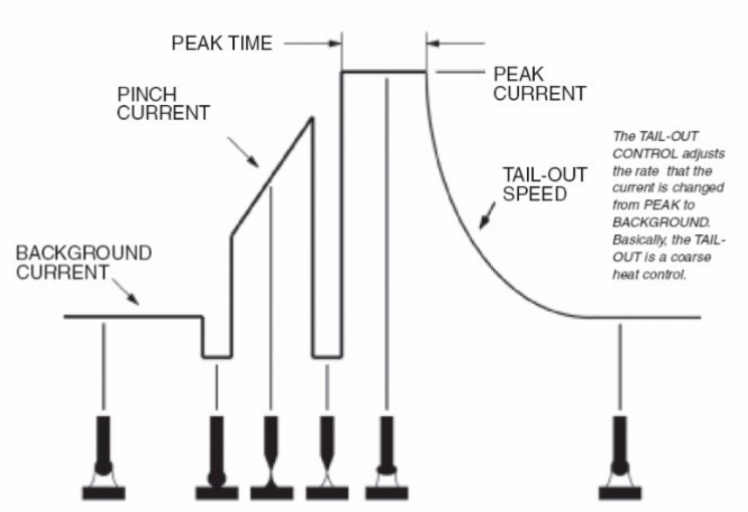

Figure 44 Typical STT waveform defined by parameters such as peak and background current, wire feed speed, tail out, wire dimensions and material.

3.4.2. Features extraction methodologies

Once the data from a defect-free deposition have been collected, training and validation data were obtained using a random split in which 90% of the samples (257 samples) were used for training, while the 10% of the samples (26 samples) were used for validation. Then feature extraction in both the time domain and time-frequency domain is performed on both training and validation data. These features are then normalised in the range 0-1 with respect to training data before being used as input for the ML algorithm, as outlined in the scheme shown in **Figure 45**. Once trained, the unsupervised learning algorithm provides feedback about the presence of anomaly to the robot controller with a frequency of 1Hz.

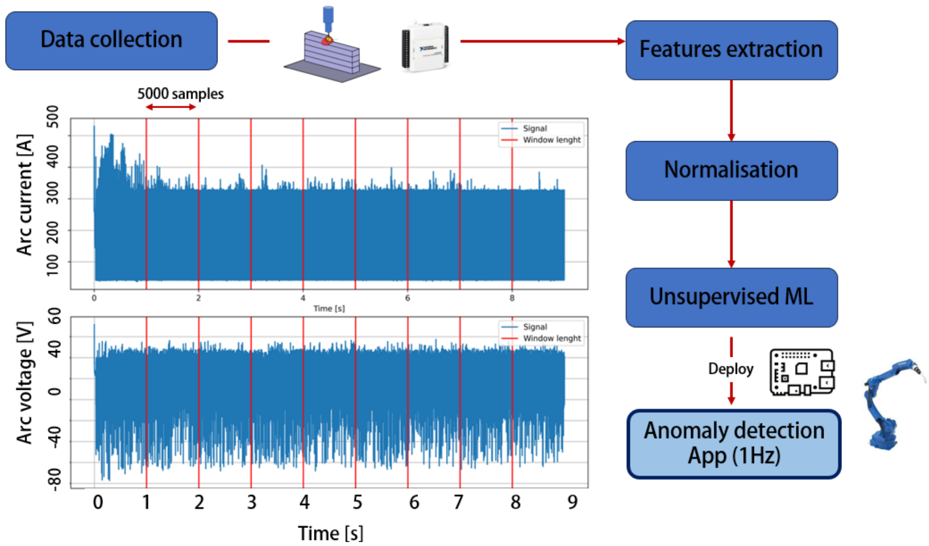

Figure 45 General scheme of the presented methodology. Once the data have been collected using a window approach, features are extracted from both buffers of welding current and voltage which contain 5000 samples each. The extracted features are used in an unsupervised machine learning algorithm that produces feedback to the Yaskawa cell every second.

Time domain features

Statistical and process-based features were derived from the welding current and voltage signals, specifically mean, standard deviation, skewness and kurtosis, which were extracted from both welding current and voltage signals.

To capture the characteristics of the waveform in the STT process, which should have a maximum value equal to the peak current and a minimum value equal to the background current, two additional process-based features were extracted from the buffer containing the current signals. These features represent the sum of the time during which the current value exceeds the peak value and falls below the background value, expressed in **Equation 25** and **Equation 26**.

$$\sum\nolimits_{on\ window} I > I_{mean} \tag{25}$$

$$\sum_{on\ window} V > V_{mean} \tag{26}$$

An elevated value, occurring too frequently, suggests a higher heat input to the material, potentially increasing the likelihood of defects such as porosity. On the other hand, a value consistently lower than the background can lead to issues like delamination, lack of fusion, and spatter during the welding process. At the end of the feature extraction activity, 10 features associated with each buffer have been extracted.

Time-frequency domain features

To extract features from one-second-long signals composed of 5000 samples of welding current and welding voltage signals, frequency features derived from FFT analysis and DWT were obtained. To perform the FFT analysis and decompose the signal using DWT, the influence of DC content on the signal was minimised by eliminating the mean value, as reported in **Equation 27.**

$$\tilde{I} = I - I_{mean}; \tilde{V} = V - V_{mean} \tag{27}$$

Subsequently, the $\tilde{I}$ and $\tilde{V}$ data were utilised to extract features such as Peak Frequency (PF), the corresponding Peak Amplitude (PA) and the Energy of the spectrum (E) from the FFT, resulting in a total of 6 features coming from FFT.

Then a four-level decomposition using a 4th order Daubechies wavelet, features were extracted from the four detail coefficients and the last approximation coefficient. Specifically, two features were derived from each decomposition level: the Standard Deviation per Level, offering insights into the distribution of wavelet coefficients across various decompositions, and Average Energy of each level, providing a measure of the overall importance of that component in the signal. A total of 20 features were extracted by welding voltage and welding current signals via DWT.

In total, 26 features were extracted, collecting information about the general frequency response through FFT and details in the frequency bands of 2500-

1250 Hz (level 1), 1250-625 Hz (level 2), 625-312.5 Hz (level 3), 312.5-126.5 Hz, and 0-126.5 Hz (level 4) using a 4th order Daubechies wavelet. To compare the results obtained using frequency domain analysis, the same algorithms used with time domain features have been used with the same hyperparameters. In particular, the same training, validation, and testing datasets are used for the metrics evaluation.

3.4.3. Metrics for anomaly detection in unbalanced dataset

When dealing with unbalanced datasets, it is crucial to avoid in relying solely on accuracy as a performance metric. This is particularly important in anomaly detection scenarios, where anomalies are a minority compared to normal cases.

In such cases, it is essential to consider additional parameters like specificity, precision, and recall. In particular, specificity Sp, in **Equation 28** measures the performance of the model in identifying normal cases. Precision P in **Equation 29** calculates the ratio of anomalies detected by the model that are true anomalies. Recall R in **Equation 30**, instead quantifies the proportion of normal cases identified by the normal as normal cases. A high precision value indicates that the model has a low rate of false positives, which is important in scenarios where minimising false alarms is critical. A high recall value signifies that the model has a low rate of false negatives, reducing the likelihood of missing anomalies. In practice, precision and recall often have an inverse relationship.

$$Sp = \frac{TN}{TN + FP} \tag{28}$$

$$P = \frac{TP}{TP + FP} \tag{29}$$

$$R = \frac{TP}{TP + FN} \tag{30}$$

Evaluating the performance of an algorithm from the metrics is complex, especially in anomaly detection. Defining a "good" system is not straightforward, as it depends on the trade-off between precision and recall, alongside context.

While an approach may favour high precision and low recall, when false positives are costly, the opposite can be favoured when is more costly missing an anomaly. In the context of anomaly detection in AM, it is often preferable to detect more anomalies, even if they do not all translate into actual defects. This approach is justified for several reasons.

Firstly, as described in the introduction, additional and more sophisticated software modules can be employed as a secondary check to validate the anomalies detected. These modules can provide a more in-depth analysis to distinguish between actual defects and false positives. Secondly, considering the potential consequences of a defect in AM, such as a loss of mechanical properties in the components, the cost of false alarms (detecting anomalies that are not defects) is generally lower than the cost of missing genuine defects. Therefore, developing a monitoring system which is more sensitive to anomalies, even if some turn out to be false alarms, aligns with the goal of minimising the risk and potential waste of time and materials associated with undetected defects.

In line with this concept, the performance of the algorithms are assessed by comparing two key metrics: specificity and the F2-score. The F2-score, in **Equation 31** with $\beta = 2$ is a comprehensive metric that considers both recall and precision, with a particular emphasis on recall, aligning with the objectives in AM of avoiding missing anomaly.

$$F2 = \frac{(1+\beta^2) \cdot P \cdot R}{\beta^2 \cdot P + R} = \frac{5 \cdot P \cdot R}{4 \cdot P + R} \tag{31}$$

3.4.4. Results and comparison among different unsupervised ML techniques

The features extracted in both time and time-frequency domain are then used to train and validate several ML algorithm, namely Isolation Forest, One-Class Support Vector Machine (OCSVM), and Local Outlier Factor (LOF). Specifically, the Isolation Forest was constructed with 20 trees utilizing three random features to split the normal data, with each tree using 75% of the training data and 75% of the total features to mitigate overfitting. A contamination rate of 1% was applied. For the LOF algorithm, a contamination rate of 1% and consideration of 10 neighbours for score evaluation was employed. The OCSVM utilized a radial basis function kernel and a ν factor, with an upper limit on the fraction of training errors and a lower limit of the fraction of support vectors set to 0.01.

Results in time domain

The performance metrics described in the previous section for the proposed unsupervised ML models are reported for the time-domain features extraction case in **Table 3-3**. The standout performer is the Isolation Forest showcasing a robust validation accuracy of 100%. With a precision score of 0.922, it correctly labels normal instances most of the time. The recall, standing at 0.76, and an F2 score of 0.784 underscore its effectiveness in detecting anomalies. The LOF algorithm possesses the same validation accuracy and a higher precision of 0.94. However, its lower recall of 0.69 and an F2 score of 0.735 suggest slight lower performances in detecting the anomalies. The test accuracy is higher, but in unbalanced dataset problems, it cannot be used as comparative metrics, since it is more influenced by the precision, due to the highest number of normal depositions with respect to anomalies. In the case of the One-Class SVM, it achieves the lowest validation accuracy of 88.4%. Its precision of 0.9 indicates a good ability to correctly classify normal instances. However, the lower recall of 0.47 and an F2 score of 0.503 reveal strong limitations in identifying abnormal instances, potentially leading to false negatives.

Algorithm	Validation accuracy	Precision	Recall	F2 score	Test accuracy
Isolation Forest	1.0	0.923	0.759	**0.784**	0.733
Local Outlier Factor	1.0	0.942	0.698	0.735	0.801
One Class SVM	0.884	0.901	0.475	0.503	0.801

Table 3-3 Summary of results of the proposed methodology based on time domain features

Results in time-frequency domain

The introduction of frequency-based feature extraction significantly improves the performance of all the algorithms presented. Indeed, each algorithm present a high precision value, with Isolation Forest and LOF achieving 0.89

and OCSVM reaching 0.96. The slightly lower precision is offset by a substantial increase in recall. Specifically, Isolation Forest, LOF, and OCSVM exhibit increments of 10%, 17%, and 30%, respectively, in recall. Notably, LOF shows the highest improvement in F2-score, with a 14% increase. Nevertheless, Isolation Forest remains the top-performing algorithm, with an F2-score of 0.85, with an increment of 8% with respect to 0.784 reached using time domain features.

Algorithm	Validation accuracy	Precision	Recall	F2 score	Test accuracy
Isolation Forest	1.0	0.892	0.841	**0.850**	0.733
Local Outlier Factor	1.0	0.894	0.810	0.829	0.867
One Class SVM	0.961	0.961	0.615	0.647	0.733

Table 3-4 Summary of results of the proposed methodology based on time-frequency domain features

3.4.4. Results and comparison with CNN

Utilising FFT and DWT enables the extraction of a general frequency response from welding signals. While DWT provides more detailed information than FFT, the analysis remains general due to the extracted statistical measures such as energy and mean values. Consequently, small and rapid events within the window, such as those related to defects during deposition, may be overshadowed by more dominant normal characteristics.

To address this issue, time-frequency analysis techniques such as spectrogram analysis obtained via STFT, combined with advanced image processing methods like CNNs, can be utilised. The self-learning capability of CNNs is particularly beneficial for extracting local features from the image data, in that way eliminating the need for manual feature extraction techniques.

In the context of DL Autoencoder (AE) architectures, illustrated in **Figure 46**, are commonly employed [164], [165], [166]. These models use an Encoder to compress the input vector into a latent space and a Decoder to reconstruct the input from the latent space features. These features contained in the latent space are automatically extracted employing backpropagation with a Mean Squared Reconstruction Error (MSRE) Loss.

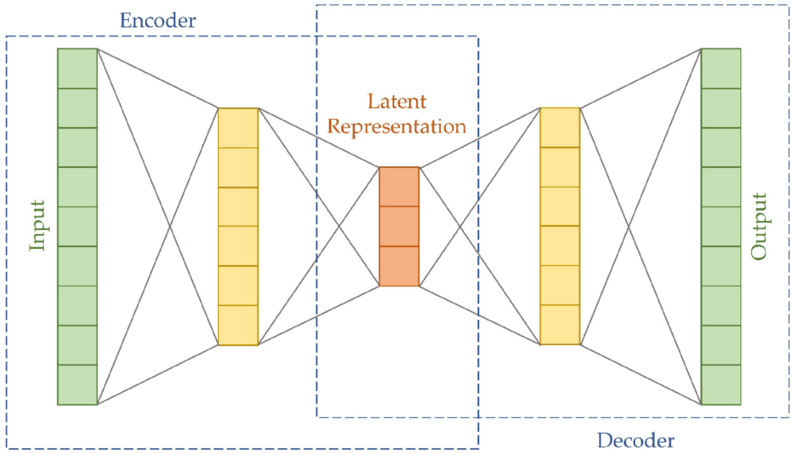

Figure 46 A typical Autoencoder architecture. The input is compressed in a latent space using a non linear transformation and another non linear transformation is used to reconstruct the input aiming to minimize the reconstruction error

The AE architecture can be designed using any type of DL model and in the case of anomaly detection of images, Convolutional AutoEncoder (CAE) are used, with convolutional layer responsible of extracting local features from images. The usage of CAE architecture to anomaly detection is simple and it is based on MSRE obtained in the training phase employing normal images as input. The idea is that any deviation from what the algorithm learned during reconstruction indicate the presence of defects.

The proposed additional methodology based on CAE architecture is illustrated in **Figure 47**. Once data has been collected every 1 second, the spectrograms have been obtained using the STFT method performing FFTs on a window of 128 samples with an overlap of 64 samples, resulting in an output spectrum of dimensions 77 by 65.

The two obtained images, corresponding to the spectrograms of welding voltage and of the welding current, are then resized to a consistent shape of (64,64) using a bicubic interpolation and concatenated into two channels.

A 2D-Convolutional AutoEncoder (2D-CAE) is employed to process the images, featuring a symmetrical architecture composed of three hidden convolutional layers. Each layer consists of two stacks of n filters, each with a size of (3x3), applied consecutively. The three layers in the encoding part are configured with filters in the sequence (8, 8, 16, 16, 64, 64). After each repetition, a stride of 2 is utilized to halve the input image dimensions. The decoding part mirrors this structure in reverse order.

To train the network Adam algorithm is used with a learning rate of 0.001 and a batch size of 16 samples for 2000 epochs. During the inference phase, the reconstruction error, namely the MSRE, is used to detect anomalies. The threshold THR is selected considering the 99.9 quantiles of the errors obtained at the end of the training phase.

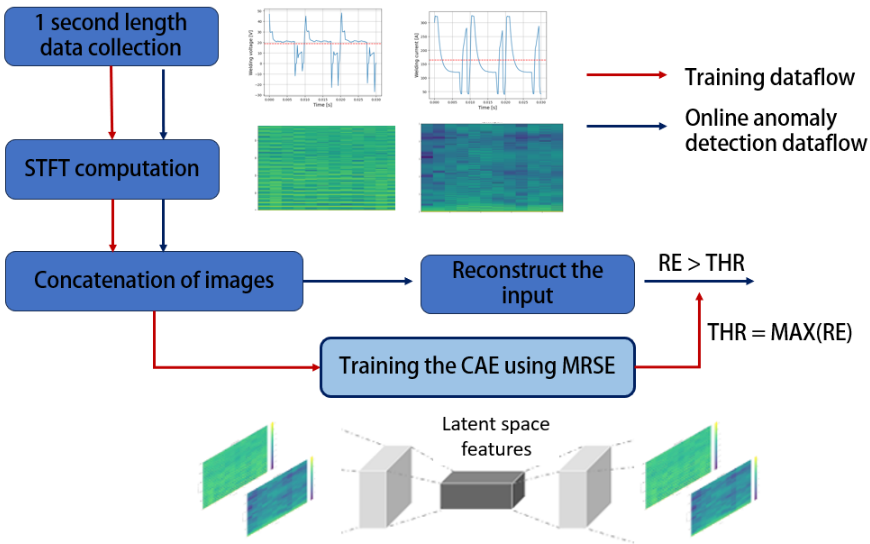

Figure 47 The proposed methodology consists of training a 2D-CAE aiming to reconstruct the spectrograms associated with good deposition. After the training phase the threshold (THR) is chosen as the 99.9 quantiles of the reconstruction error (RE) obtained at the end of the training phase.

The final results in terms of validation accuracy, precision, recall and F2-score of the proposed algorithm based on CAE are then compared with the best results obtained with the other methodologies in **Table 3-5**.

The time domain Isolation Forest demonstrates robust performance in detecting normal cases, indicating a higher overfitting on normal data. However, when leveraging frequency domain features, it excels particularly in recall and F2-score, but a lower precision is obtained. This suggests its effectiveness in detecting all defects but also indicates a tendency to generate more false alarms. On the other hand, the CAE presents a well-balanced performance, showcasing high precision and recall, respectively of 0.966 and 0.88, higher than 4 % with respect to best results.

While it may not identify all anomalies, it generates a reasonable number of false alarms, with an F2-score comparable to accuracy metrics reached by supervised learning methods in the literature and higher of then 5% with respect to the best case of frequency domain Isolation Forest. In general, also the test accuracy is higher than 12% with respect to time-domain ML method.

Algorithm	**Validation accuracy**	**Precision**	**Recall**	**F2 score**	**Test accuracy**
Time domain Isolation Forest	1.0	0.923	0.759	0.784	0.733
Frequency domain Isolation Forest	1.0	0.892	0.841	0.850	0.733
Convolutional AE	1.0	0.966	0.881	**0.895**	0.867

Table 3-5 Summary of the best results obtained with the same STT-WAAM dataset with the proposed methodologies

3.4.4. Conclusion and future developments

The task of anomaly detection is crucial for the future of additive manufacturing (AM) systems. While supervised learning algorithms have been widely employed to address this challenge, unsupervised approaches offer several advantages. These include eliminating the need for balanced datasets containing equal amounts of normal deposition and depositions with various types of defects, and enabling the development of applications even when only one-class or small-volume datasets are available. Although this methodology shows promise, particularly in industrial environments where cost reduction and efficient defect localisation are essential, unsupervised machine learning algorithms struggle to identify anomalies that closely resemble normal deposition, as evidenced by a time-domain case with an F2-score of 0.78. This difficulty arises because these algorithms are primarily designed to detect rare events. To enhance anomaly detection performance, this chapter of the thesis demonstrates how frequency analysis of welding signals, such as current and voltage, can be advantageous. Specifically, the F2-score improves to 0.85 when global time-frequency features are used as input to machine learning algorithms, and further increases to 0.895 when local features are automatically extracted from spectrograms. These results are comparable to those of supervised learning algorithms, which typically achieve around 90% accuracy, demonstrating the practical applicability of the proposed methodology in real industrial systems.

In the field of process monitoring, multi-sensor systems could be integrated into the proposed methodology to assess the potential improvements achieved by incorporating additional time-series signals, such as Acoustic Emission or audio signals. While this area is not extensively studied in the literature, exploring the use of multiple sensor sources holds promise for further enhancing performance. Different sensors can capture various aspects of the process—for example, Acoustic Emission sensors can monitor events during the solidification phase. The proposed architecture is adaptable for processing multi-sensor data using the same methodology. For instance, a spectrogram of Acoustic Emission could be added as a third channel in the input vector of the proposed CAE, representing one of the ongoing research directions.

3.5. Summary of process monitoring investigation

Process monitoring is the area where most AI applications in the field of WAAM are concentrated. Despite this, the majority of applications in both process monitoring and anomaly detection rely on supervised learning algorithms, which pose challenges, particularly in scenarios with limited or imbalanced datasets. In this chapter of the thesis, unsupervised learning approaches to both process monitoring and anomaly detection are presented, offering innovative contributions through data processing enhanced by frequency analysis of welding current and voltage signals. Additionally, the chapter discusses the application and integration of these methodologies within certification processes.

Two experimental campaigns were conducted on Inconel 718, printed via the P-GMAW process, and ER70S-6, printed via the STT process, demonstrating the effectiveness of the proposed methodology in state-of-the-art waveform welding technologies. By incorporating techniques such as FFT and DWT to extract features across specific frequency bandwidths, this approach overcomes the limitations of traditional time-domain feature extraction methods, addressing significant research gaps in the literature.

However, to further enhance monitoring performance, the integration of multi-sensor systems requires more extensive research, highlighting a knowledge gap that persists in both supervised and unsupervised learning applications for WAAM, particularly in process monitoring and anomaly detection. Despite this, the proposed CAE architecture based on spectrogram analysis demonstrates adaptability in processing multi-sensor data, such as Acoustic Emission signals, as spectrograms can also be computed for other time-series signals. This approach offers a promising avenue for ongoing and future research, with the potential to significantly advance process monitoring and control in WAAM.

Chapter 4 : Reinforcement learning for process control

Manufacturing processes pose significant control challenges due to their nonlinear or time-varying dynamics, constraints on control and state variables, and complex multivariable interactions. Despite this, these processes are typically managed using linear system design tools, favoured for their rigorous stability and performance guarantees, as well as their relative simplicity in system modelling and simulation. However, the linear tools fail to address the inherent nonlinearity and constraints within process control and they often leads to suboptimal outcomes, limiting the effectiveness of the controller to few degrees of control.

From a general control perspective, a nonlinear MIMO dynamic system can be approached in different ways. The first approach is to decouple a MIMO system into several SISO systems and then an adaptive controller can be developed to deal with the single non-linearities [167]. For example, the adaptive controllers can use an active linearisation around operating points (e.g. Taylor series expansion or derivative tools) and then apply linear control tools, such as PID or pole placement. Additionally, the controller can employ a gain scheduling techniques to deal with time-varying nature of the systems [168], which can be modelled as different linear models based on operating point. In both cases, different linear controllers are switched during the time due to changes in the external condition of the system. For example, in the case of the WAAM process, traditional controllers result in bead height being dependent solely on WFS and bead width only on WS, decoupling system dynamics. However, this approach is impractical because it fails to decouple the effects of process parameters on both system states, leading most developed controllers to manage only one state at a time, leaving the other uncontrolled.

Furthermore, an industrial process is usually a MIMO system in which uncertainties are present, so we can define it as a stochastic process. To overcome the uncertainties problems, robust controllers were proposed, such as H infinity [169], Linear Quadratic Gaussian (LQG) [170] control or

Internal Model Control [171], since standard tools like PID or Linear Quadratic Regulator (LQR) controllers do not deal with systems uncertainty.

Using these controllers, the MIMO nature and uncertainties of the system can be effectively managed, provided that models for both the system dynamics and the uncertainties are available. However, feedback controllers are not the only solutions to process control; feedforward controllers are also utilised, as shown in **Figure 48**.

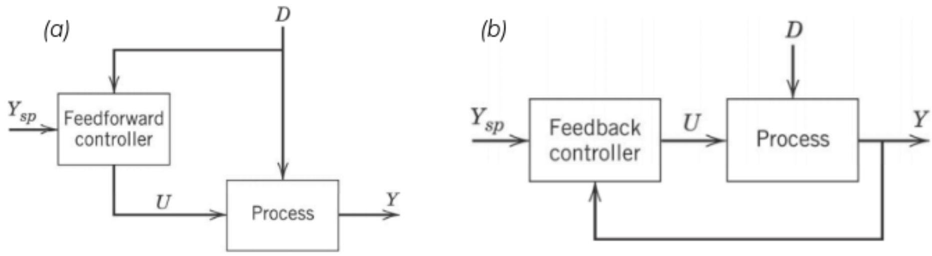

Figure 48 (a) feedforward controller. A control variable is selected based on a reference and external disturbances. (b) in a feedback controller, or closed loop, sensors are used to measure the states and adjust the control variables with the aim to reduce the error.

These families of controllers are based on evaluating the actions inverting the system dynamics, and it is demonstrated that these controllers can completely eliminate the impact caused by measured disturbances on the process output and model uncertainties [172]. This family of controllers is more suited for non-linear MIMO systems, but their development and performance strongly depend on the validity of the model, which can be described by both traditional physics models (e.g. transfer function and differential equations) and AI models (regression, ANN, etc.).

Although some industrial applications are developed using the presented families of controllers, the problems of state and control variables constraints are not managed with these methods. This means that, without carefully design the controller, actions that may drive the process in unstable conditions or potential breakage can be applied. To overcome this problem an evolution of LQG control is proposed in a new family of controllers named Receding horizon control also known as Model Predictive Control (MPC). The basic idea of MPC, shown in **Figure 49**, is to use a model to predict the future behaviour of the controlled system over a finite time horizon, and then compute an optimal control input that minimises, each time step, a quadratic function subject to constraints on the system states and actions.

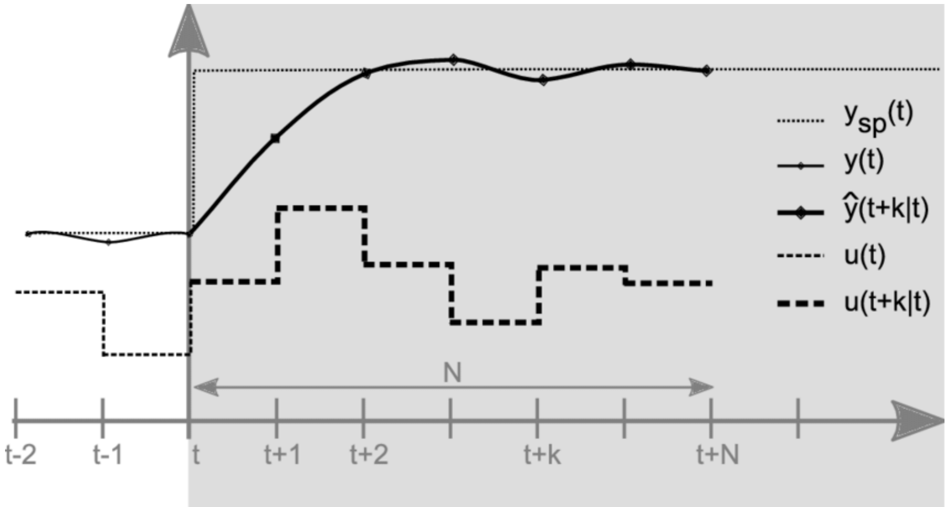

Figure 49 Illustration of the receding horizon control concept [173]. For a finite time horizon N, a series of control actions are taken on the system and his dynamic evolution is computed by a model with the aim to reduce a loss function. At the end of the simulation and optimisation process only the action at time t+1 is taken, and the process is repeated for the next time step.

The main disadvantage of MPC is that a quadratic optimisation problem must be solved at each step, making this control algorithm useful for systems with slow sampling [174]. In all presented cases, a perfect knowledge of the optimal process references is needed to develop the controller.

Although an industrial process often comprises multiple subsystems whose complex interactions can lead to the desired outcomes, once the optimal process variables are identified, control can usually be achieved by managing individual devices, such as electric motors for motion or orifice-valves, which can be treated as linear SISO systems. In these cases, after establishing a complex and non-linear model for the entire process, a high-level controller must be developed to optimise performance by setting optimal reference points that minimise errors. This high-level controller is responsible to the generation of the set-points for the following single low-level controllers, as shown in **Figure 50**.

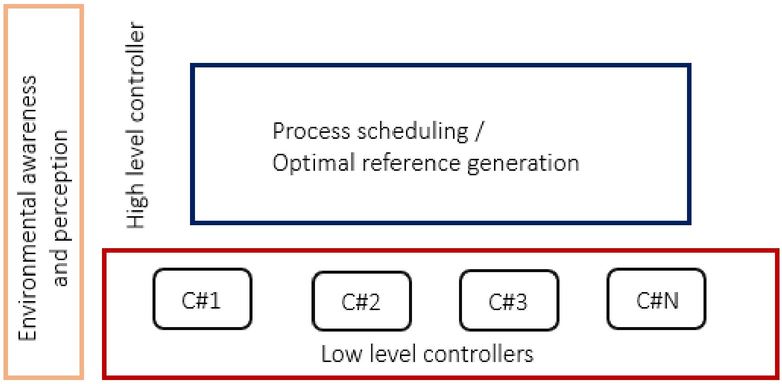

Figure 50 A generic hierarchal scheme of industrial process control structure.

MPC is particularly useful for this purpose, as it solves quadratic optimisation problems to find optimal control variables while considering state and control constraints to maintain process quality, such as ensuring a maximum value of a state beyond which the final component becomes non-compliant. However, the problem of this kind of controller is not only connected to the necessity of finding a realistic model for the system, otherwise, the optimisation work is wasted, but the major drawback is related to the need for high-performance hardware to satisfy the time constraint of a digital control system. In this complex scenario, for the development of new intelligent manufacturing systems, is important to find a way to optimise the process with less effort from a computational perspective and at the same time increase the level of automation in terms of self-adjustment and learning of the production systems.

For this section of the thesis an innovative branch of ML, named RL, is proposed for the optimisation and optimal control of WAAM process, representing an innovation in the field. The general framework applicable to general fabrication process is presented in the **Section 4.1** and then in the **Section 4.2** is presented the application of the framework for WAAM process. In the **Section 4.3** the main conclusion is discussed.

4.1. A general framework for industrial processes

The fundamental components in establishing a RL framework for industrial process control are mainly related to the data-driven modelling of the target process. The primary goal is to synthesize, through simulation, an initial policy that closely resembles the optimal policy for the real system. Additionally, a crucial aspect involves the design of the reward function, which can be fine-tuned using the developed model. The reward plays a pivotal role since selecting it correctly can help prevent undesirable consequences, such as instability or the breakage of system equipment. Therefore, although RL is known as model-free controller, the model of the system represents a crucial aspect for the training of the agent.

To highlight the importance of the reward shaping activity, a comparison with the State-of-the-Art reward for process control is proposed in the following sections. Several other aspects of RL, particularly relevant from a control perspective, are also discussed. These include active exploration, exploitation, and considerations related to the design and scaling of the output layer. These elements contribute to the robustness and effectiveness of the RL framework in the context of industrial process control.

The proposed framework and workflow are illustrated in **Figure 51**. After collecting real-world data, physics-based simulations can be parameterised to generate synthetic data. Both synthetic and real-world data are then used to develop a ROM using data-driven techniques. This ROM helps in tuning the hyperparameters of both the RL agent (e.g. architecture of ANN used for policy approximation) and the reward function. Once the policy is optimised in simulation, a fine-tuning process on the real system can be conducted.

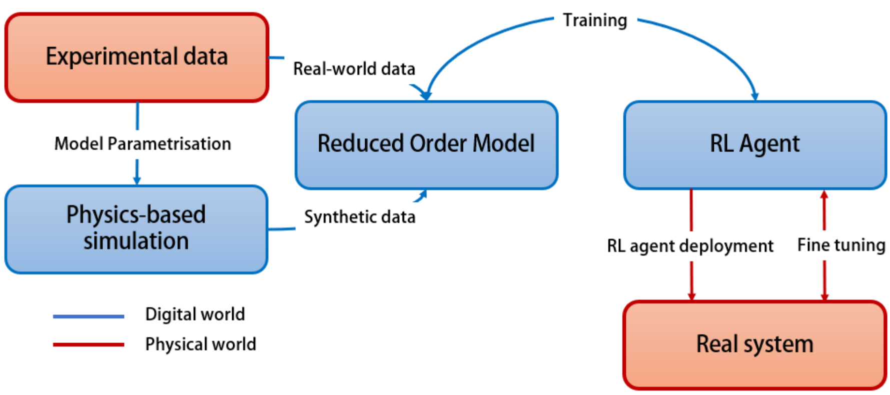

Figure 51 The proposed framework and workflow for RL deployment in industrial process

4.1.1. Reduced Order Modelling

A model is a mathematical representation of the dynamic or static behaviour of a system. Different approaches to extracting models exist, but in the industrial field one of the most used is the physical-based modelling, which provides accurate input-to-output mapping of the process.

However, since physical-based dynamics processes can be studied through non-linear differential equations, many problems occur in the development of controllers based on these models, as reported in the previous section. Furthermore, the computational time of physics-bases solution limit their application to control task.

The problem of model reduction or Reduced Order Modelling (ROM) consists in replacing a given mathematical model with a new "smaller" that approximately gives the same results of the complex model. In this area there are generally two types of methodologies. One is the black-box approach, which generates surrogate models using data-driven techniques, such as the one proposed in the **Section 2.5** of this thesis or transfer function parameterisation [175]. The other is the physics-based approach, which manipulates the structure and equations of the "bigger" model to find a lower dimensional approximation.

Due to the huge amount of produced data in an industrial environment and the improvements of simulation software, data-driven techniques are even more used, and a combined approach, named grey-box approaches, can be used to extract models from processes leveraging both data collected from experimental campaign and data generated by complex physical models. For example, experiments can be made with the aim to parametrise a numerical simulation, which allows the extraction of synthetic data. This data allows exploring new system configurations and operational points, difficult to obtain in a real industrial environment. Once real and synthetic data are collected, different data-driven modelling techniques can be used to extract a model from data, and an example of this approach can be found in the work of Xiao et al. [33] for composite drilling modelling.

Once a ROM is obtained, it can be used by both model-based controllers, e.g. MPC, and model-free controllers, such as RL. In the case of RL, the ROM is treated as the real system, so the agent policy (the controller) is firstly designed in simulation, making it interact directly with the ROM. Using this approach, the reward function can be carefully shaped, as well as the policy architecture. Furthermore, if the ROM closely approximates the behaviour of the real system, a near-optimal policy can be derived through simulation. This approach minimizes the need for extensive interaction with the real system during optimisation and avoids potentially dangerous actions, as exploratory random actions which are tested on the simulated model rather than the real system.

4.1.2. Reward function shaping for fabrication processes

The reward function is a crucial element in a RL algorithm because it defines the desired outcome of the task. In control systems, the primary objective is to ensure that certain variables track specified trajectories or setpoints. When designing or shaping the reward function, it is important to follow specific guidelines to improve performance, particularly in terms of the rate of convergence to the optimal solution and successful achievement of the goal.

From a mathematical perspective, although in RL the optimisation procedure follows a sort of metaheuristic approach, since no gradients of the reward are computed for the backpropagation, generally a reward function is more successful if the agent has a gradient to work with. In fact, the presence of a gradient allows it to better understand when it gets closer or further from the target. Regarding state-of-art reward function for setpoint control problems, Matignon and Spielberg proposed some methodology for reward shaping.

Matignon et al. [176] proposed a Gaussian-based function, reported in **Equation 32**. The reward R is uniform for some states s far from the goal s_g to avoid unlearning problems, and on the other hand, there is a reward gradient in a zone around the goal. Specifically, β adjusts the amplitude of the function and σ, the standard deviation, so the reward gradient influence area. For setpoint problems, such as the control one, the goal s_g is the setpoint.

$$R(s, a, s') = \beta e^{-\frac{d(s,s_g)^2}{2\sigma}} \tag{32}$$

Spielberg et al. [177] proposed a sparse reward function , which works better for the process control problems, described by **Equation 33**.

$$R(s,a,s') = \begin{cases} c, & \sum_{i=0}^{N} s_g^i - s^i < \epsilon \\ -\sum_{i=0}^{N} s_g^i - s^i\,, & othwrwise \end{cases} \tag{33}$$

When the process output is closer to the set-point by the error tolerance defined by ϵ, the agent receives the highest possible reward c, otherwise it receives the negative reward whose magnitude is the deviation from the set-point.

Incorporating negative rewards is important for the learning process. When certain areas of the state space primarily yield negative rewards, the agent may strive to terminate its episode quickly to avoid accumulating excessive penalties. Adding negative values to the reward function can thus speed up the learning phase. However, the magnitude of these negative rewards must be carefully chosen, as excessively negative rewards can lead to issues like poor exploration.

Although the continuous and sparse reward functions proposed by Matignon and Spielberg effectively address setpoint control problems in RL, the potential of RL to solve more complex problems is limited by these rewards. Beyond achieving setpoint goals, other objectives like power consumption and the quality of the fabrication process also need to be considered. Therefore, in this thesis, we introduce a new reward function designed to account for these additional factors.

In new reward design proposal, several factors are considered. Firstly, incorporating negative values in the reward computation can accelerate the learning process, therefore in the proposed reward negative values are proportional to both errors and process power consumption. In fact, achieving the goal in the most sustainable way is crucial in modern fabrication processes. Therefore, the reward function needs to account for not only the setpoint accuracy but also factors like power consumption (P_c) and product quality (Q), as expressed in **Equation 34**.

$$R \propto -(s_g - s);\ R \propto -P_c; R \propto Q \tag{34}$$

Moreover, it is also crucial for the reward function to have a gradient that indicates how far the current trajectory is from the optimal path. Nevertheless, to prevent unlearning, the reward function should be bounded above and below by predefined values *m* and *M*, as expressed in **Equation 35**.

$$m \leq R \leq M \tag{35}$$

Based on these considerations, the proposal of this thesis is a polynomial reward function, reported in **Equation 36**, where $\Delta_1 < \Delta_2$ represent the reward bounds, $\delta = |\sum s_g - s|$ denotes the absolute error with respect to the set-point, and ϵ is the error threshold parameter.

$$R(s, a, s') = \begin{cases} \Delta_2 \xi, & \delta < \epsilon \\ -(\delta^2 + k\delta + \Delta_1)\xi, & otherwise \end{cases} \tag{36}$$

The values of Δ_1 and Δ_2 are hyper parameters to tune according to simulation performance. The hyperparameter ξ varies the range $0 \leq \xi \leq 1$ according to power consumption or final component quality. For example, if the final component is not quality compliant, the value $\xi = 0$, otherwise $\xi = 1$. For what concern the power consumption, ξ may depend by to the ratio between the instantaneous power consumption P_c and the maximum power allowable P_{max} or in formula $\xi = 1 - \frac{P_c}{P_{max}}$.

The value of k is determined by resolving the **Equation 37** for $x = \epsilon$ and $y = \Delta_1$, as reported in **Equation 38**. In this way when the error threshold is reached, the reward is equal to the lower bound value.

$$y = x^2 + kx + \Delta_2 \tag{36}$$

$$k = \frac{\Delta_2 - \Delta_2 - \epsilon^2}{\epsilon} \tag{37}$$

4.1.3. Design of the architecture of the agent

The background analysis in **Section 2.3** highlights that state-of-the-art RL methods like DDPG use ANNs as approximators for both policy and value functions to address continuous state-action space problems. While general ANNs can be employed for this purpose, the specific characteristics of industrial process control must be considered when designing the network architecture for optimal performance. This section provides guidance on constructing policy approximators.

The initial insight is that, due to constraints on the action space in industrial processes, the activation function of the actor's output layer needs to be bounded. Although they face challenges with vanishing gradients—since their derivatives approach zero for large inputs—the hyperbolic tangent *(tanh)* and *sigmoid* functions are two suitable S-shaped bounded curves for the activation function in the output layer of an ANN designed to approximate the optimal control policy.

tanh function is symmetric about the origin, therefore the learning convergence is usually faster if the average of each input variable over the training set is close to zero [178]. This is obtained normalising the input, therefore the best choice to speed up the learning process is to use a normalisation layer followed by a hyperbolic tangent to describe the bounded output layer of a policy approximator function. However, the output of hyperbolic tangent is contained between -1 and +1. Therefore, an additional scale operation is needed to transform the maximum value of the network output, namely *+1,* into upper bounds of control action, and at the same to transform the minimum value, namely *-1*, into lower bounds, as reported in **Equation 39**.

$$u = \frac{\phi(s) - 1}{2}\Delta u + u_{max} \tag{39}$$

Given $\phi(s)$ the output of the policy approximator -which have the *tanh* as output layer - and $\Delta u = u_{max} - u_{min}$ the upper and lower bounds of the process parameters.

Some additional suggestions for the first-tentative architecture construction are:

1. Avoid using to deep architecture for the actor, with the aim to reduce the vanishing gradient problem.
2. If the critic is used, use two different branches for its inputs when Q-value is estimated, namely one branch for the states and one for the action.
3. In Actor-Critic architecture, the state branch can be constructed similar to the policy network (actor architecture). Then a concatenation layer can be used to merge the two branches (state and action branches).
4. Since the suggestion is to use hyperbolic tangent activation function for the actor and ReLU for the critic:
    a. Xavier uniform weights-initialisation is suggested for the actor
    b. He normal random initialisation is suggested for the critic.
    c. Starting with low values to avoid rapidly saturation
5. Generally, also clip the gradient amplitude during the training process can help to avoid to saturation of the activation during the training.

4.1.4. Exploration vs exploitation

Another crucial topic regards the exploration and the exploitation of the control policy during the learning process, and it is important to find a trade-off between the two.

In DQN algorithms the *ε-greedy* exploration technique is used, in which a uniformly random action with probability ε is taken to explore the whole action space in order to obtain a non-biased view of the problem. The value of ε is reduced with defined strategies during the training, in order to explore more at beginning of the learning process and use only the greedy policy at end of the training. For algorithms used for continuous action space problems, such as DPPG, a similar myopic approach is used. While myopic exploration is known to have exponential sample complexity in the worst case [179], it still remains a popular choice in practice. This is because myopic exploration is easy to implement and works well in realistic scenario [180].

In the DDPG an undirected exploration is applied adding noise sampled from a noise process N_{OU} as described in **Equation 40**.

$$\pi(s) = \pi_\theta(s) + N_{OU} \tag{40}$$

Where θ are the parameters of the policy network, N_{OU} is an Ornstein-Uhlenbeck correlated noise process. In the Twin Delayed Deep Deterministic policy gradient algorithm (TD3) paper [181] the authors proposed to use an uncorrelated noise for exploration as they found that the originally proposed noise process offered no performance benefits.

Therefore, also a white gaussian noise N described by zero mean and a variance σ can added to give the agent exploration capability during the training, as described in **Equation 41**.

$$\pi(s) = \pi_\theta(s) + N \sim (0, \sigma) \tag{41}$$

With $\sigma < 1$ that reduce with the number of episodes. For a MIMO control problem also a multivariate diagonal gaussian process with zero-mean and variable standard deviation may be used. After the training, so during the validation, and then the deploy, the exploration noise needed to be neglected.

For the described policy, this means add a random white noise to the *tanh* output, which then must be clipped between the range -1 and +1. It is important to remark that the scaling layer output is to use only as the action to the system, while for the training purposes the original *tanh* output must be used.

4.2. An application to WAAM layer geometry control

The literature review in **Section 2** revealed that the geometry of the deposited layer is heavily influenced by the selection of process parameters. Additionally, it was discussed that using constant process parameters during the building process fails to achieve the desired layer geometry, as factors like heat accumulation components with affect the outcome. This highlights the need for closed-loop control in the WAAM process to produce the highest possible quality.

However, the WAAM process presents several challenging issues from a control perspective due to its MIMO and non-linear stochastic behaviour. Additionally, the process requires a controller capable of managing constraints on both control variables (the process parameters) and state variables, such as layer geometry, to prevent defects in the components. This challenge is related to the physics of the process, as only a limited number of operating points in the electrical characteristics of the arc ensure stable and effective layer deposition. In this thesis a simple set point controller is developed for a natural GMAW based WAAM process using RL, showing the application of the proposed methodology in a simulation environment, representing a starting point for the studies in this field.

4.2.1. Experimental set-up

Using a 3 axes cartesian motion platform equipped with a SELCO Quasar 400 MSE welding machine, 18 walls have been deposited using a copper-plated solid wire AWS ER 70S-6 of 1 mm of diameter under the protection of CO2 shielding gas. For the 18 walls deposited, different process parameters have been employed, such as the welding voltage (V), the Wire Feed Speed (WFS), the Welding Speed (WS), the Contact Tip to Workpiece Distance (CTWD), Interpass temperature and Gas Flow Rate (GFR). In particular, the experimental data were conducted using four welding voltage values (18, 20, 22 and 24 V), five WFS values (2.5, 3.5, 4.5, 6 and 7 m/s), two values for the CTWD (12 and 20 mm), two values of GFR (18 and 20 L/min) and three WS values (280, 487 and 561 mm/min), depositing the raw material of the wire on top of a substrate plate. During the deposition, all process parameters were maintained constant. Then the layer width and height steady-state values were measured using an optical microscope Leica flexacam C1, as shown in **Figure 52**.

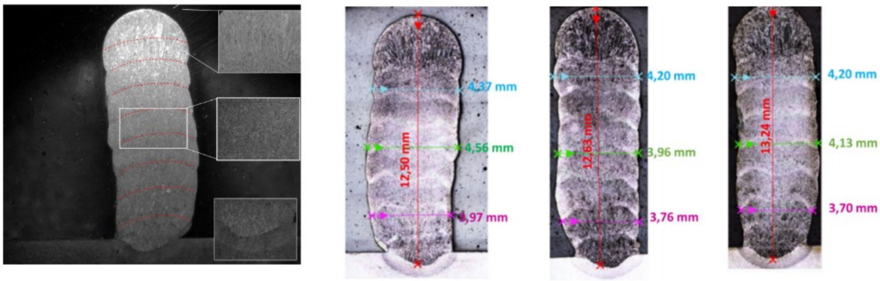

Figure 52 Manufactured specimens observed under an optical microscope. The procedure allowed the geometry of the layers to be determined.

4.2.2. ROM development

As reported by Li et al. [182], the layer-forming process possesses a dynamic characteristic. Since the WAAM process is based on arc welding, Goldak's double ellipsoid heat source model can be used to approximate this dynamic system with a lumped model. Observing **Figure 53**, when the welding torch is in point *g1*, the geometry obtained *g1* depends on the previous value, namely *g0*, and on the process parameters used to arrive at point *g2*. Following the same statement, the layer at point *g2* depends on the previous value and process parameters used to arrive at point *g3* and so forth, according to heat model of Goldak.

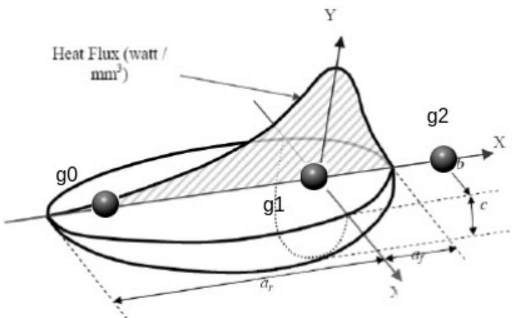

Figure 53 Goldak's double ellipsoid heat source model.

Using this assumption is possible to obtain a data-driven lumped dynamic model for the system which simulates the bead formation back to the welding torch. Experimentally was observed that when the parameters used to arrive at point *g1* were not changed we can assume the same value of the bead geometry at the point *g0*, otherwise when parameters used to arrive in *g1* from *g0* are changed the variation in the bead formation process takes around 0.5 seconds to be completed for the used materials and process parameters, so a time constant of $\tau = 0.1s$ can be assumed for that system. In this application, first-order dynamics is assumed for both the width and height formation process, so once the steady-state value x_{ss} is determined starting from the used process parameters, this value is passed in input to a space state model, in **Equation 42**, generating the final fist-order dynamic ROM of WAAM process.

$$\begin{cases} \dot{x} = -5 \cdot x + x_{ss} \\ \quad y = 5 \cdot x \end{cases} \tag{42}$$

For a simulation purpose, the system is discretised with a sample time of $T_s = \frac{\tau}{10}$ and solved with a Euler forward method. A neural network is used to approximate the steady-state value for both width and height, once the process parameters were given in input. The proposed network is a shallow network with:

- 6 normalised inputs, namely the V, WS, WFS, CTWD, interpass temperature and gas flow rate.
- 15 neurons in the hidden layer passed in a hyperbolic tangent activation function.
- 2 neurons in the output layer passed in a rectified linear unit activation function.

The network was trained with a Root Mean Square propagation algorithm with a learning rate $\alpha = 10^{-4}$, momentum $\mu = 0.1$ and a discount factor $\rho = 0.9$ for 2000 epochs using a training dataset which consist of 80% of the data. The final Mean Squared Error obtained was of 0.0018 on test dataset, testing the good capability of generalisation of the proposed ANN. The simulator employed in this study is then integrated within a robotics simulation environment named RoboDK and is illustrated in **Figure 54**.

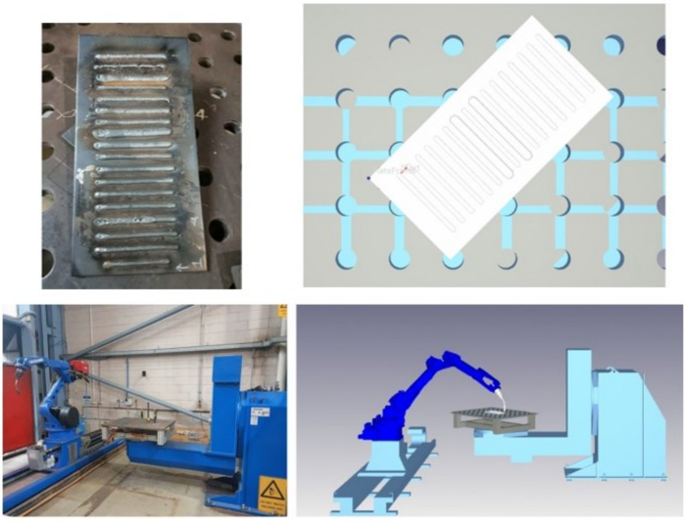

Figure 54 The integrated simulation environment of WAAM process consist of robotic kinematic simulator integrated within process modelling enabled by an ANN.

4.2.3. Policy training in simulation via DDPG agent

In a control problem, actions are traditionally determined based on computed errors relative to reference values. However, an optimal policy can extend beyond this by considering the previous history of the system. Consequently, the input vector for the proposed controller comprises the actions taken on the system at time step t-1, the current state, and the reference values. This not only implicitly provides feedback on errors but also offers additional information about current state of the system and the previous action. Therefore, the inputs are:

- The system state: layer heigh and layer width at time step t.
- The reference values for both layer heigh and layer width.
- The action taken at the time step t-1.

The simulation environment, shown in **Figure 55**, integrates the dynamic model of the WAAM process and the DDPG controller. This simulation environment was implemented in Python using the NumPy, RoboDK and TensorFlow libraries.

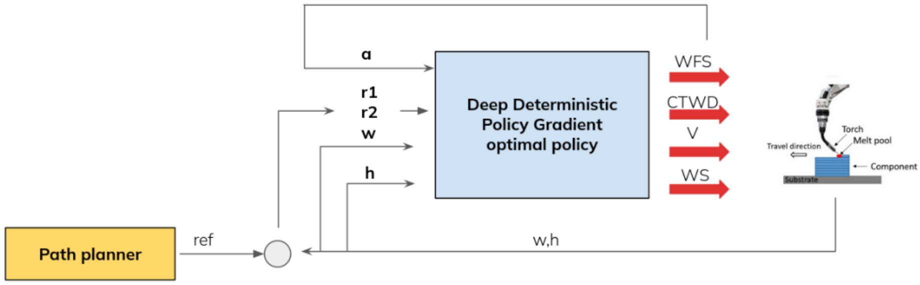

Figure 55 The proposed framework is composed of a Deep Deterministic Policy Gradient optimal controller that interact with a data-driven reduced order model of the Wire Arc Additive Manufacturing neural network-based. A path planner give in input to the controller the path references, the other input to the controller are the measured width and height and the actions used at previous time step.

In this example the goal of the controller is to change the process parameters to reduce the error for both layer width and height, once the width and height references to produce the layer in **Figure 56** are known. The error used to compute the reward is the mean average of the width and height errors.

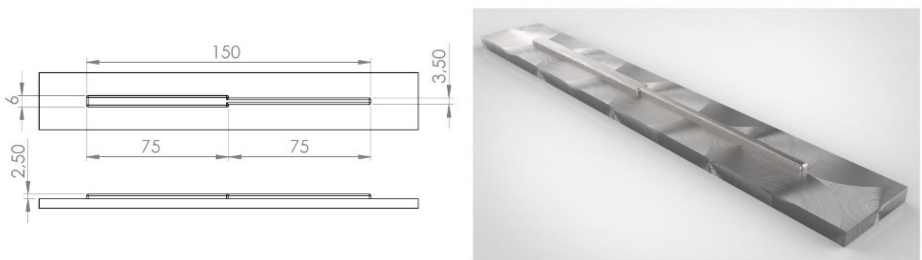

Figure 56 The layer to be made is 150 mm long. After 75 mm, the width changes from 6 mm to 3.5 mm, while the layer height is fixed at 2.5 mm.

The actor-network is composed of 2 hidden layers with 64 neurons and ReLU activation function. The output layer is composed of 5 neurons, the number of process parameters, with a hyperbolic tangent activation function and a random uniform distribution weight initialisation.

In this simulation, the interpass temperature and GFR were fixed at 25°C and 20 l/min, respectively. As these parameters remain constant, they are not included as inputs to the control policy. Consequently, the input layer of the actor network consists of 8 elements: the measured variables, such as layer width and height (2), the reference values (2), and the scaled actions from the previous time step—normalised with respect to their maximum values (4).

The critic-network has 2 different branches for actions and states. The state branch, similar to the policy network, has 64 neurons in one hidden layer, while the action branch has 32 neurons, since the action space size is near to the half of actions space. After a concatenation layer, two layers with 128 neurons are used to approximate the Q-value. All hidden layers of the critic-network used ReLU activation function, while no activation function for the output layer, in which the Q-value is estimated.

The used training options are summarised in **Table 4-1.**

Training setting	**Value**
Optimiser	Adam
First momentum (β_1)	0.90
Second momentum (β_2)	0.98
Actor leaning rate (α_{actor})	$1 \cdot 10^{-4}$
Critic learning rate (α_{critic})	$2 \cdot 10^{-4}$
Discount factor (γ)	0.97
Soft update (τ)	0.01
Initial variance action noise ($\Sigma = \sigma \cdot I$)	0.5
Episodes *(e)*	50
Batch size	64
Buffer size	5000
Reward (Δ_1)	0.1
Reward (Δ_2)	1
Error threshold (ϵ)	0.1
Quality factor (ξ)	1

Table 4-1. Training settings and hyperparameters

4.2.3. Results and future works

The reward computation in this study involves the mean of width and height errors, since the quality factor ξ is maintained equal to 1. **Figure 57** illustrates the progression of average episodic rewards over episodes, indicating a positive trend after 30 episodes and nearing the maximum value after 40 episodes, signifying successful problem resolution with the proposed reward. In **Figure 58** results comparing the proposed reward (a) and Spielberg reward (b) for the synthetise control policy are presented. The outcomes highlight superior performance with the reward function proposed in this study.

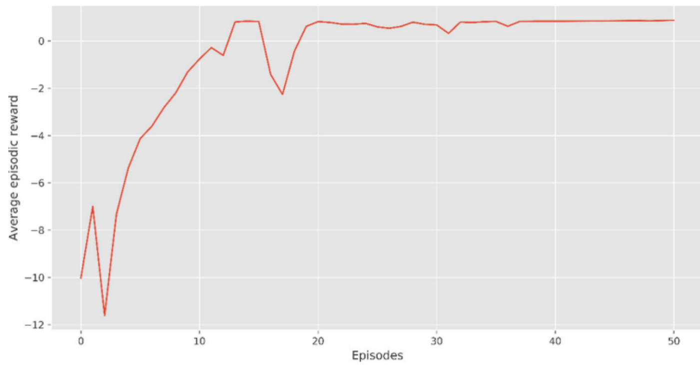

Figure 57 Average episodic reward trend.

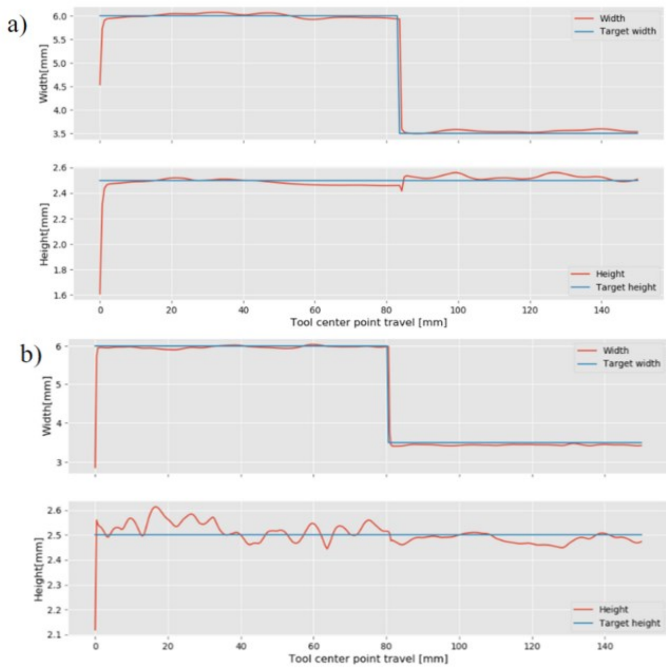

Figure 58 a) Output responses for width and layer control using the trained DDPG controller with the proposed reward computation (b) Output responses for width and layer control using the trained DDPG controller with reward computed as suggested by Spielberg with c = 1

The training to solve the presented task involved 50 episodes, each lasting 22 minutes. For control action inference time, relying on input from a buffer with references, current layer geometry, and previous control actions, it took only 23 ms. This inference time is significantly lower than control logic based on MPC, which requires simulating the entire welding process for optimal action determination. Finally, in **Figure 59**, are shown the results in simulation of the trained controller.

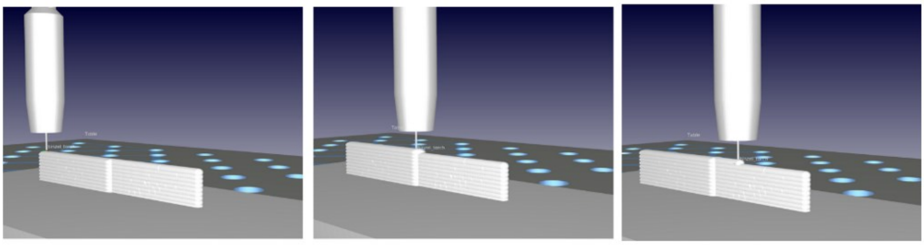

Figure 59 Results of using optimal control law in the WAAM simulator developed in this work

4.3. Comparison with alternative methods

As discussed in this chapter, designing a MIMO controller for the WAAM process is challenging without introducing simplifications in the model.

One approach is to fix all parameters and develop separated SISO models, e.g. with layer width depends only by WS and layer height by WFS. However, this method overlooks the influence of these variables on other states (WFS on layer width and vice-versa), becoming impractical. An alternative approach is to create a linear model of the process and apply linear MIMO controllers such as LQR, as suggested by [34], [144].

Therefore, using the same dataset, a linear model for WAAM process was found using a linear regression. The linear WAAM representation is then expressed by the equation in **Equation 43.**

$$\begin{cases} h_{ss} = 0.97 \cdot WFS - 0.006 \cdot WS + 0.017 \cdot CTWD - 0.005 \cdot V \\ w_{ss} = 0.15 \cdot WFS - 0.005 \cdot WS - 0.038 \cdot CTWD + 0.29 \cdot V \end{cases} \tag{43}$$

As for the previous established ROM, a first order dynamic is assigned to the system, which can be described in the state space by **Equation 44**, with A and B matrix described in **Equation 45 and Equation 46** and the state x defined as layer height and layer width $x = [h, w]$.

$$\dot{x} = Ax + Bx_{ss} \tag{44}$$

$$A = \begin{bmatrix} -5 & 0 \\ 0 & -5 \end{bmatrix} \tag{45}$$

$$B = 5 * \begin{bmatrix} 0.97 & -0.006 & 0.017 & -0.005 \\ 0.15 & -0.005 & -0.038 & 0.29 \end{bmatrix} \tag{46}$$

The results obtained in simulation are illustrated in **Figure 60**, showing poor performance in step response obtained employing $Q = I_{2x2}$ and $R = 0.1I_{4x4}$, which are used to solve the algebraic Riccati equation .

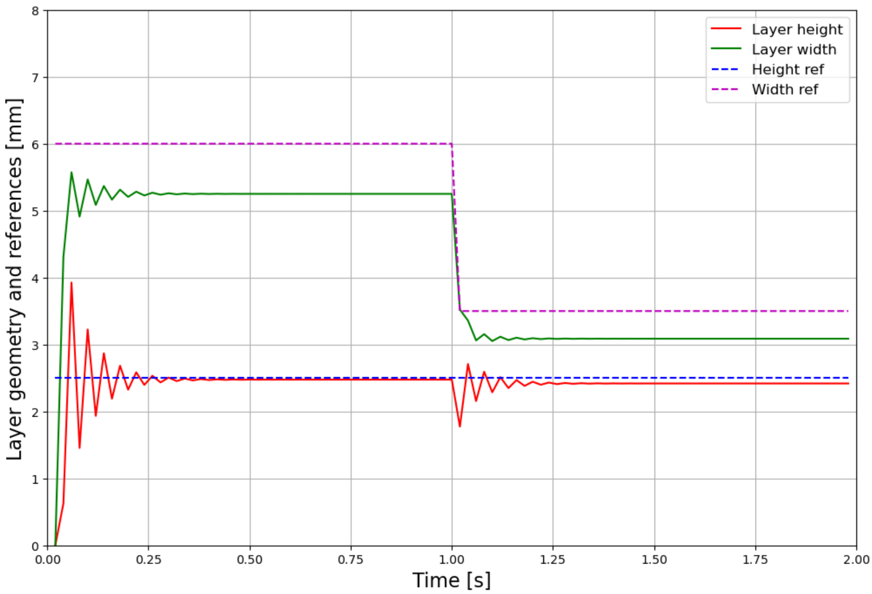

Figure 60 Results from the simulation of the linear WAAM process plant using a MIMO Linear Quadratic Regulator (LQR) controller without clipping the control variables within experimental range.

However, the optimal gain K_{LQR}, which define the control action ($u = K_{LQR}e$), is obtained without considering the control variable constraints. In **Figure 61** is reported the result obtained constraining the control variable within experiment range, by clipping with respect to the minimum and maximum values employed during experimental campaign.

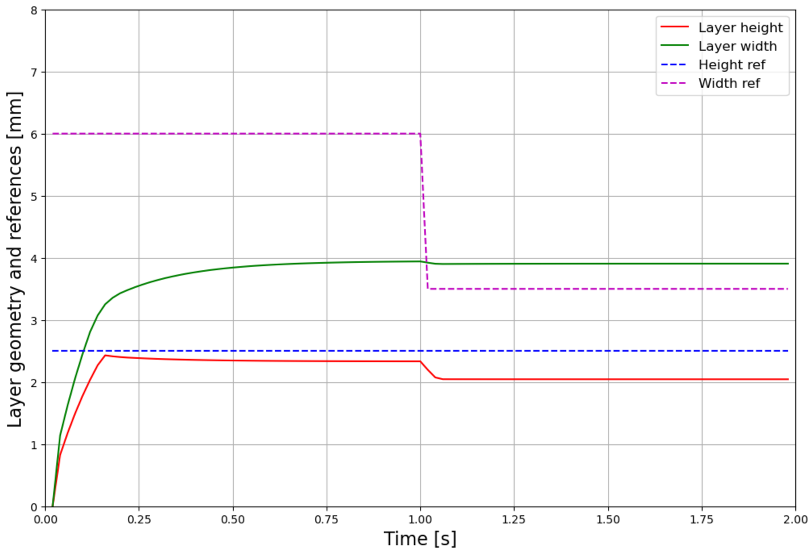

Figure 61 Results from the simulation of the linear WAAM process plant using a MIMO Linear Quadratic Regulator (LQR) controller clipping the control variables within experimental range.

To improve the performance, an MPC controller can be employed. Using the nonlinear ROM presented in the previous section, considering the constraint on the control variables within experimental range and using a Sequential Least SQuares Programming (SLSQP) optimisation method, better results are reached. The results illustrated in **Figure 62** are reached by employing $Q = [50, 50]$ and $R = [1, 1, 1, 1]$ with a Horizon of 30 steps. Although the results can be acceptable, the average computational time required for the optimal solution is of 2 seconds. This means that the applicability in effective control of the process should be better analysed, considering the faster dynamics of the WAAM system. The results of RL agent are shown in **Figure 63**. In this case, the average computational time is of 3 milliseconds, which can be effectively used for the proposed system, given a control time lower than system time constant. However, all the presented results are obtained in simulation, therefore future analysis needs to be carried out to study the effective results on the real system.

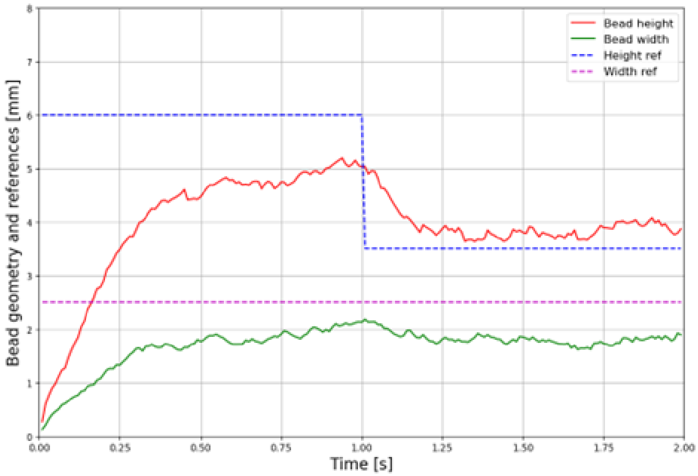

Figure 62 Results from the simulation of the nonlinear WAAM process plant using a MIMO Model Predictive Control (MPC) controller.

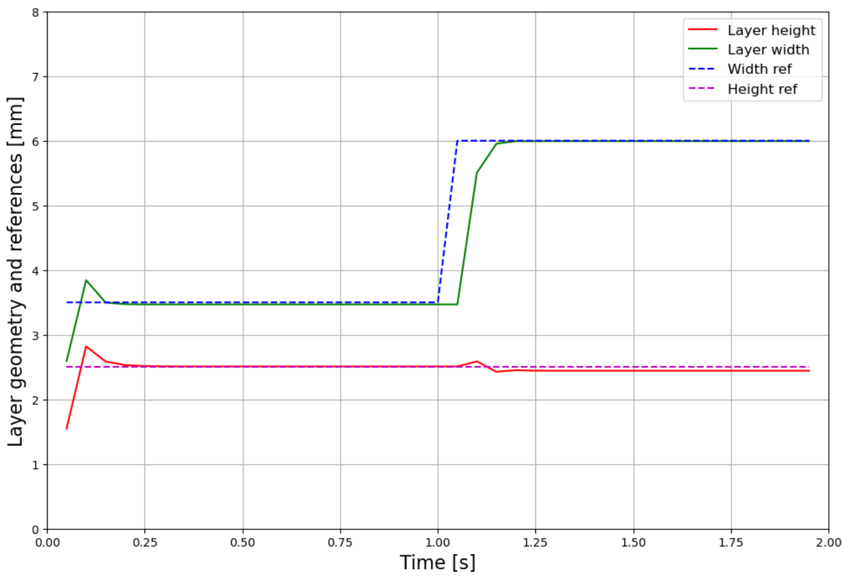

Figure 63 Results from the simulation of the nonlinear WAAM process plant using a MIMO Deep Deterministic Policy Gradient (DDPG) controller.

The final comparison of the results reached in terms of MAE during the episode and the average computational time for each policy generator is reported in **Table 4-2**.

Method	*Average computational time*	*MAE step w [mm]*	*MAE step [mm]*
LQR	< 0.001 s	1.09 mm	1.28 mm
MPC	2 s	0.93 mm	1.1 mm
DDPG	0.003 s	0.09 mm	0.29 mm

Table 4-2. Comparison of the results

4.4. Summary of Reinforcement learning for process control

In this chapter the main challenges in controlling fabrication processes like WAAM have been discussed and a novel RL-based approach is proposed for feedback control of MIMO non-linear constrained systems, a technique well-explored in robotics but new to fabrication processes like WAAM.

The developed methodology and workflow, which is general for all fabrication processes, includes developing reduced-order models, reward and control policy architectures design. A new reward has been proposed and the methodology is applied for WAAM layer geometry control. Simulation results show improved performance in employing the proposed reward with respect to traditional set-point rewards in RL, however several further explorations are mandatory to drive the application of RL within WAAM field.

In fact, although the computational time and the performance are better in simulation with respect to alternative controllers like LQR and MPC, the proposed controller is specialised for designing the component of the proposed case study, which means that RL agent needs to be trained longer in simulation to reach better generalizability in control task. Furthermore, the results presented in a simulation environment need to be validated on the real system. In fact, the influence of overfitting of WAAM ROM is not explored, which is related to the number of steps needed for the following fine-tuning in real-world applications. Although fewer optimisation steps should needed due to the close alignment between simulation and reality (low MSE of the model on test dataset), this effective number of steps for the fine tuning is not addressed in the current work and remains an area of ongoing research.

Moreover, several crucial points have not been explored, representing additional goal for future research. For example, RL allows to integrate the output of monitoring applications within reward computation, maximising the benefits of the proposed reward function. However, the part quality and energy consumption are not taken into account in this work this topic is not covered. Therefore, a future goal is to integrate in the simulation environment the energy consumption and quality estimation aiming to further enhance control performance.

However, the proposed approach allows for the direct control of a non-linear and stochastic MIMO system, which represent a crucial point of innovation in the field of GMAW and WAAM processes.

In addition to future developments in this field, several challenges concerning the seamless integration of RL in manufacturing are present, reducing the possibility to fine-tuning of the optimal policy in the real world scenario. The most important is the absence of robust frameworks like ROS (Robot Operating System) that are specifically designed for industrial machinery, such as welding machine. This lack, combined with the absence of integration with standard industrial protocols like Profinet, limits the implementation of RL in industrial environments. These limitations create obstacles to the seamless adoption of RL in manufacturing, underscoring an ongoing challenge in the broader application of RL within the industrial sector. Developing solutions that bridge these gaps is crucial for advancing the use of RL in industrial settings.

Chapter 5 : Genetic Algorithm for WAAM process optimisation

Inspired by the United Nations Sustainable Development Goals Report 2023, there has been a growing focus on research related to sustainable design and production, especially in AM [183]. Specifically, studies by Dias et al. [184] and Priarone et al. [185] have demonstrated that the WAAM process is highly efficient and has a relatively low environmental impact compared to other technologies. Moreover, cost analyses conducted by Campatelli et al. [186] and Kokare et al. [187] indicate that WAAM offers potential cost savings when compared to traditional manufacturing methods.

Optimising the WAAM process from a sustainable perspective involves depositing different layers with varying parameters and selecting the combination that minimizes power consumption, the surface roughness and the buy to fly ratio, which is influenced by layer geometry. However, it is important to note that other combinations of process parameters, beyond those explored in the experimental campaign, may yield even better results. In this case, AI tools can be used to develop frameworks that allow to explore the process parameters space in an efficient manner, using techniques like RL or metaheuristic methods like GA. A comparison between standard optimisation procedure and AI-enabled model-based optimisation procedure is shown in **Figure 64**, in which AI-enabled optimisation procedure is highlighted as automatic and its model-based procedure allows to explore the parameters space while reducing costs compared to other standard experiment-based optimisation procedures.

As highlighted in the introduction, model-based metaheuristic optimisation represents the state-of-art of welding process optimisation. However, the literature review in **Section 2** underscores the need to explore alternative methods for optimising the process, focusing on preventing defect generation more effectively than by merely constraining parameters. In fact, this approach reduces the exploration capability of the autonomous agent employed for the optimisation. Additionally, no studies have yet addressed energy efficiency in both arc welding and WAAM, highlighting the need to design appropriate fit functions to address this gap.

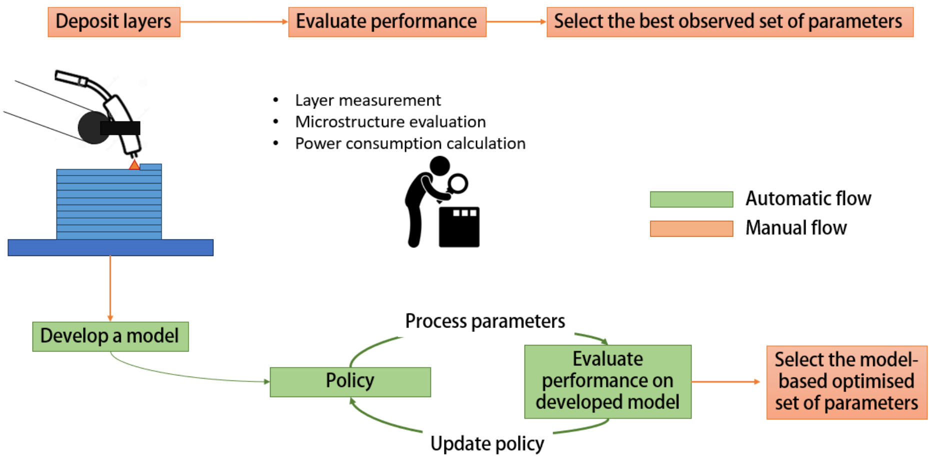

Figure 64 Comparison between experiment-based optimisation and AI-enabled model-based optimisation procedure.

In this section of the thesis, a classification capability is integrated into the WAAM ROM. The ROM includes a regression model that maps process parameters to the final layer geometry, specifically layer width and height, as well as the average power consumed during deposition. Additionally, the classification model is designed to identify and discard process parameter sets that lead to defects such as humping, spatter, and porosity. This comprehensive model, representing the WAAM process, is utilised by a continuous GA to explore the process parameter space in a continuous manner. By using a custom fit function aimed at minimising costs associated with power consumption, surface roughness, and waste from defective parts, an optimal set of process parameters is identified. These results are then validated on the real system to demonstrate the achieved performance in a real-world setting.

5.1. Experimental setup

To demonstrate the methodology, a Yasakawa AM2010 9-axis robotic station integrated with a Lincoln PowerWave 500 welding system was used to deposit 72 layers of stainless steel 316L with a 1.2mm wire, utilising a synergic Pulsed-GMAW process. The process parameters, including WFS, WS, V and the UltimArc parameter (which adjusts the welding pulse frequency in the Lincoln system), were varied according to a predetermined experimental design, reported in **Table 5-1**, while CTWD and GFR were fixed to 15mm and 20 L/min respectively. Data on welding current and welding voltage were acquired at a sample frequency of 5kHz using an NI 6003 device. To measure the layer geometry post-deposition, a ScanControl 3002 was employed, and voltage and current sensors were used to calculate the average power consumed during the deposition process, following the guidelines of Joseph et al. [188], which recommend using the average instantaneous power (PAI) as expressed in **Equation 47**, in accordance with ISO/TR 18491.

$$PAI = \frac{1}{N}\int_{t=0}^{N} V(t) \cdot I(t)dt \tag{47}$$

The layer quality has been classified by expert welder based on post-deposition surface appearance a during-deposition audio signal, classifying as anomaly layers ones subject to humping, porosity or instability during the deposition.

N Layer	UltimArc	Welding speed [mm/min]	Wire feed speed [m/min]	Welding voltage [V]	Power [W]	Layer width [mm]	Layer height [mm]	Anomaly
1	-8	552	6.5	23	0.062123	7.85	2.2	0
2	-6	552	6.5	23	0.062681	7.73	2.5	0
3	-4	552	6.5	23	0.060705	7.55	2.4	0
4	-2	552	6.5	23	0.062942	7.7	2.5	0
5	2	552	6.5	23	0.064284	8.5	3.5	0
6	4	552	6.5	23	0.059817	7.93	3	0
7	6	552	6.5	23	0.0615	7.75	2.3	0
8	8	552	6.5	23	0.060965	8	2.3	0
9	0	552	6.5	18	0.049109	6.5	2.6	1
10	0	552	6.5	20	0.053536	7.4	2	1
11	0	552	6.5	28	0.08686	8.2	2.4	0
12	4	552	6.5	28	0.063275	8	2	0
13	4	552	6.5	20	0.05219	8	2.1	0
14	4	552	6.5	18	0.052075	9.9	2.1	1
15	-4	552	6.5	18	0.045678	6.6	2.7	1
16	-4	552	6.5	28	0.048742	6.9	2.6	0
17	-4	552	6.5	20	0.085092	8	2.2	0
18	8	552	6.5	20	0.051465	6.7	2.6	0
19	8	552	6.5	28	0.083395	8.4	2.1	0
20	8	552	6.5	18	0.046251	6.4	2.5	1
21	-8	552	6.5	18	0.04927	8.4	2.4	1
22	-8	552	6.5	28	0.088027	7.9	2.3	0
23	-8	552	6.5	20	0.053659	7.5	2.2	0
24	2	552	6.5	20	0.054355	7.5	2.4	0
25	2	552	6.5	28	0.087824	8.8	2.4	0
26	2	552	6.5	18	0.050788	6.7	3	1
27	-2	552	6.5	18	0.049118	6.8	2.4	1
28	-2	552	6.5	28	0.089239	8.1	2	0
29	-2	552	6.5	20	0.056149	7.8	2.7	0
30	0	552	4.5	23	0.045558	6.8	1.6	0
31	4	552	4.5	23	0.042442	6.6	1.8	0
32	-4	552	4.5	20	0.042839	6.4	1.9	0

33	-4	552	4.5	23	0.049852	6.3	2	0
34	4	552	4.5	20	0.03968	6.2	2.1	0
35	0	552	4.5	20	0.041256	6.5	2.1	0
36	0	552	4.5	18	0.03675	5.5	2.1	0
37	-4	552	4.5	18	0.036072	5.8	2.2	0
38	4	552	4.5	18	0.036298	5.7	2.2	0
39	0	552	4.5	23	0.047775	6.1	1.9	0
40	4	552	4.5	23	0.048201	6.3	2	0
41	4	552	4.5	20	0.040508	6.6	2	0
42	0	552	4.5	20	0.040564	6.6	2.2	0
43	0	552	4.5	18	0.03655	5.6	1.9	0
44	4	552	4.5	18	0.036823	5.6	2.2	0
45	4	750	6.5	25.2	0.085719	7.2	2	0
46	4	750	4.5	21	0.053162	5.8	1.8	0
47	-4	750	6.5	25.2	0.088246	7.4	1.9	0
48	-4	750	4.5	21	0.054622	6.3	1.9	0
49	8	750	4.5	21	0.050105	6.7	1.8	0
50	8	750	6.5	25.2	0.085371	7.1	1.8	0
51	-8	750	6.5	25.2	0.089823	7.4	2	0
52	-8	750	4.5	21	0.052786	5.5	2	0
53	0	750	3	16	0.03181	4.2	1.8	0
54	10	750	3	16	0.031692	4.8	1.7	0
55	-10	750	3	16	0.031687	3.2	1.7	0
56	0	750	2	14.7	0.02036	3.2	1.6	1
57	10	750	2	14.7	0.021752	3.4	1.2	1
58	-10	750	2	14.7	0.021256	3.8	1.2	1
59	-10	550	2	14.7	0.01687	3.2	1.1	1
60	0	550	2	14.7	0.017297	3.5	1.4	1
61	10	550	2	14.7	0.017879	3.3	1.4	1
62	10	550	3	16	0.026043	4.4	1.6	0
63	-10	550	3	16	0.026254	4.6	1.3	0
64	0	550	2	16	0.001276	3.8	1.5	1
65	0	750	2	16	0.001624	3.4	1.3	1
66	-10	550	2	16	0.001479	3.7	1.4	1
67	10	550	2	16	0.016502	3.9	1.5	1
68	4	750	2	16	0.028796	3.4	1.3	1
69	-4	750	2	16	0.01675	3.4	1.3	1
70	-10	750	2	16	0.016255	3.3	1.3	1
71	10	750	2	16	0.028697	3.5	1.4	1
72	4	550	2	16	0.028895	3.8	1.5	1

Table 5-1 Comparison between experiment-based optimisation and AI-enabled model-based optimisation procedure.

5.2. Proposed methodology

Historically, optimisation procedures relied on experimental evidence, where researchers iteratively adjusted parameters based on empirical observations and personal expertise to enhance performance according to subjective metrics. While this approach has been somewhat effective and is still in use, as mentioned in the introduction of this section, it has inherent limitations in fully exploring the solution space and identifying new optimal configurations. This means that certain solutions are often ignored because they do not appear promising based on initial experimental data. For instance, the proposed experimental campaign suggests that welding voltage should not be set below 14.7 V, as it consistently results in low-quality layers. However, there is no information on whether increasing the WFS to 3 m/min might prevent defects while improving power consumption by enhancing the current. This counterintuitive solution could potentially be beneficial, but the current experimental approach limits the exploration of such possibilities, restricting the study of potential new solutions. Moreover, the numerous potential combinations of process parameters, make the exploitative process impractical, since every process parameter is a continuous variable.

The proposed AI-based approach offers an opportunity to surpass traditional optimisation methods. By using data-driven models to map process parameters to outcomes, such as layer geometry and power consumption, it enables a more effective exploration of parameter combinations within a simulation environment. Additionally, metaheuristic optimisation algorithms, like GA, can automatically and efficiently explore potential solutions, discarding those that do not satisfy an objective mathematical fit function. This allows AI to uncover non-intuitive solutions that might not be evident through conventional experimental methods.

As mentioned in the introduction, manually constraining process parameters within predefined ranges can be influenced by the designer bias introduced by experimental evidence. To address this, a more advanced technique can be integrated into the optimisation loop, utilizing complex ML models. These models act as an additional classification tool, identifying whether the selected parameters will result in anomalies or defect-free outcomes. This enhanced approach is incorporated into the environment model, as illustrated in **Figure 65**. Therefore, the proposed framework combines regression and classification analyses to estimate outcomes, namely layer geometry and PAI, based on process parameters. The goodness of these parameters is evaluated by a fit function which depends by the associated outcomes. These values guide an intelligent agent in making informed decisions with added insights. A Gaussian Process Regression (GPR) model predicts system outcomes, while a Random Forest Classifier (RFC) provides additional quality estimates. Despite the good performance reached by proposed models, other regression and classification models can be used within this framework.

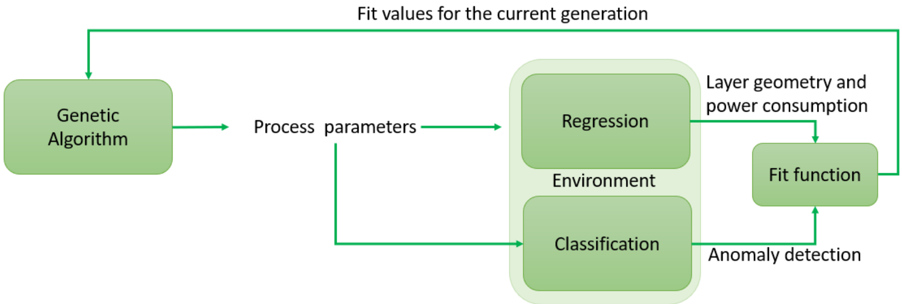

Figure 65 Proposed optimisation framework consisting of an environment which contain both regression and classification model to predict layer geometry, power consumption and anomaly generated during the deposition and of a Genetic Algorithm as Metaheuristic optimisation technique.

5.3. GA agent and fit function design

5.3.1. Continuous Genetic Algortihm

This study proposes a continuous GA as the metaheuristic optimisation agent. However, since GA is traditionally designed for discrete variable optimisation, modifications to the traditional algorithm were made.

First, all parameters were normalised based on observed minimum and maximum values. The initial population (N) of the first generation follows a standard distribution with zero mean and a variance of 1, where 0 corresponds to the minimum value of control actions and 1 to the maximum value, namely WFS, WS, V and UltimArc. Crossover is performed by sampling two random indices within the parameter range (from 0 to 3), and their values are exchanged. Mutation introduces white noise with a fixed standard deviation (mutation gain), generating a noise vector that follows the distribution but results in different mutations for each parameter.

To gradually shift from exploration to exploitation during the optimisation process, the impact of crossover and mutation is linearly decreased until reaching minimum fixed values. This approach reduces the exploration of new solutions over time.

The best candidate of each generation is then scaled using the **Equation 48** where *p* are the parameters, *o* are the actions generated by the GA agent and UB and LB the upper bound and lower bound vectors.

$$p = \frac{o-1}{2}(UB - LB) + UB \tag{48}$$

The scaling process is mandatory for fitness function computation which employs the GPR and RFC models to evaluate the specific power consumption, the bead geometry, and the anomaly detection output. In Table 5-2 are reported the hyperparameters.

Parameter	**Population size**	**Generations**	**Ini. Crossover rate**	**Ini. Mutation rate**	**Ini. Mutation gain**
Value	50	100	0.6	0.6	0.05

Table 5-2 Hyperparameters employed in the proposed continuous Genetic Algorithm and values.

5.3.2. Fit function

The objective function in the sustainable WAAM optimisation procedure aims to minimise power consumption while also reducing the buy-to-fly ratio by lowering surface roughness and avoiding the generation of defective parts. As discussed, parameters like WFS, V and UltimArc are directly linked to instantaneous power consumption and layer geometry, which influence surface roughness. However, other parameters, such as WS, impact layer quality—higher WS can lead to defects like humping, even though the reduced deposition time might benefit power consumption.

While reducing both WFS and V is clearly beneficial for lowering power consumption, the impact on surface roughness is more complex. As discussed by Xia et al. [122], increasing WS can potentially reduce surface roughness by promoting smoother layer deposition. However, it also raises the risk of humping defects. Conversely, increasing WFS tends to increase surface roughness, whereas reducing it can lead to a smoother finish. The optimisation task is complex since it is difficult to find the trade-off between increasing WS and reducing WFS for smoother layers while minimising power consumption. Although increasing WS is recommended to shorten printing time and reduce overall power consumption, it may result in geometric defects. Additionally, if welding voltage and WFS are not adjusted together properly, poor feeding can cause defects such as arc instability and porosity.

Considering all the mentioned factors, a multi-objective fitness function is proposed and expressed in **Equation 49**. In particular, if the process parameters are related to a deposition without any anomaly, the fit function needs to be designed so to increase when lower power consumption. At the same time, the agent should encourage to use of higher WS, reducing the deposition time and the surface roughness, and the same time use a lower WFS. However, the lowest fit function value has to be obtained if an anomaly is present. To avoid giving more emphasis in fit function computation to the variables of different scale, like WS, all the input of the fit function are scaled with respect to the maximum values obtained during the experimental campaign.

$$f(p, WFS, WS) = \begin{cases} -\beta \cdot \frac{p}{p_{max}} - \frac{\beta}{2} \cdot \left(\frac{WFS}{WFS_{max}} - \frac{WS}{WS_{max}}\right) - \frac{\beta}{4} \cdot \frac{w}{w_{max}} \cdot \frac{h}{h_{max}}, & \lambda = 0 \\ -4\beta & \lambda = 1 \end{cases} \quad (49)$$

In the proposed fit function, λ is the output of anomaly detection output, that is 0 for normal deposition and 1 for an anomalous deposition. p is the PAI measured in kW, the WS is the welding speed, WFS is the wire feed speed and w and h are the layer width and height respectively. The β value is used to modify the amplitude of the fit function and is equal to 2 for the specific case.

5.4. Results and discussion

The GPR and RFC models which composed the environment of the WAAM optimisation procedure were trained on 90% of the dataset in **Table 5-1** and tested on the remaining 10%, consisting of 8 samples reported in **Table 5-3**. The evaluation metrics for regression included Mean Absolute Error (MAE) and Standard Deviation of Absolute Errors (SdAE), while classification metrics included Precision, Recall, Accuracy, and F2-score. In particular, the GPR model demonstrated strong performance in predicting power consumption and layer geometry, with MAE and SdAE for power consumption of 2.2 kW and 2.3 kW, respectively. Layer width and height predictions also showed good performance was observed with a MAE of 0.29 and SdAE of 0.27 for layer width estimation, and a MAE of 0.13 and an SdAE of 0.168 for layer height estimation. The RFC model effectively detected anomalies with Precision, Recall, and F2-score all at 1.0, indicating excellent performance in identifying defects. The results are summarised in **Table 5-3**.

Layer	Target PAI	Estimated PAI	Target width	Estimated width	Target height	Estimated height	Target class	Pred Class
1	88.0	77.8	7.9	8.1	2.3	2.3	0	0
2	50.05	49.1	7.4	6.5	2.6	2.4	1	1
3	60.9	63.0	8	7.8	2.3	2.4	0	0
4	50.7	49.9	6.7	7.4	3	2.4	1	1
5	62.7	64.0	7.7	7.7	2.5	2.3	0	0
6	29.0	28.0	3.3	3.3	1.3	1.3	1	1
7	42.8	43.2	6.4	6.0	1.9	1.9	0	0
8	54.3	55.3	7.5	7.6	2.4	2.4	0	0

Table 5-3 Results obtained on the 8 samples of the test dataset used to evaluate the performance metrics

To highlight the improvements introduced by the proposed methodology, results from different approaches are presented. The results obtained from traditional optimisation based on experimental evidence are referred to as Optimisation Method 1 (OM1). Optimisation Method 2 (OM2) refers to results achieved using machine learning techniques without employing a classification algorithm for anomaly detection. Optimisation Method 3 (OM3) denotes the proposed methodology. In addition to fit value of the best process parameters combination obtained by the proposed 3 methods, the Specific Energy Consumption (SEC) index expressed in J/mm, multiplying the effective kW for the WS (see **Equation 50**), is considered as additional metrics.

$$SEC\left[\frac{J}{mm}\right] = \frac{PAI}{WS}\left[\frac{\frac{J}{mm \cdot s}}{s}\right] \tag{50}$$

Using OM1, the parameters for layer 54 were suggested, resulting in a real-system fit value of -0.28 and a SEC of 2528 J/mm. In contrast, OM2 achieved a simulation fit function value of +0.12. Although OM2 resulted in a lower SEC of 1696 J/mm on the real system, it encountered a humping defect (see

Figure 66), leading to a real fit value of -8. Despite a 32.9% reduction in power consumption, surface defects occurred. Finally, the proposed approach (OM3) achieved a fit function value of +0.024. It reduced power consumption to 2286 J/mm and minimised defects (see **Figure 67**), resulting in a 9.5% decrease in power consumption compared to the traditional approach. OM3 demonstrated the best balance between reduced power consumption and minimal defects, validating the effectiveness of integrating classification models into the optimisation process.

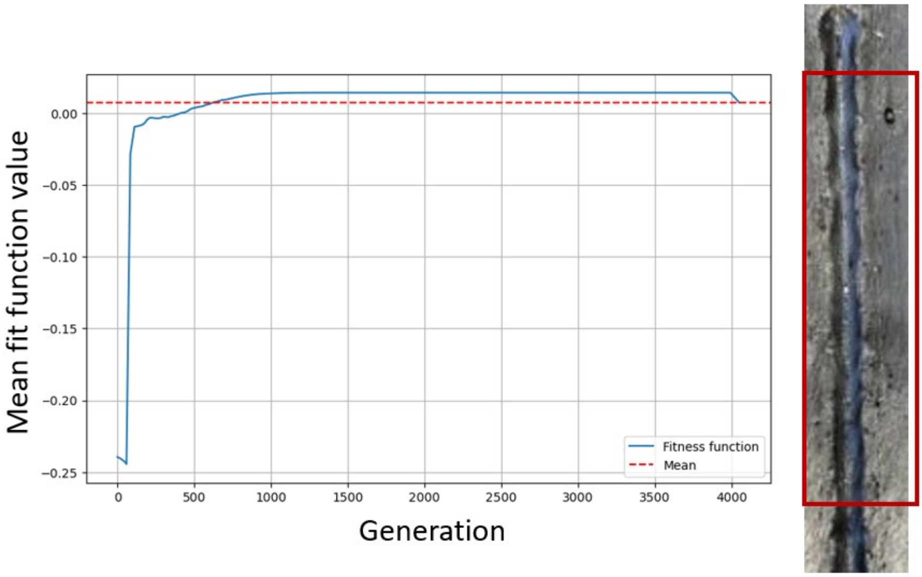

Figure 66 Behaviour of fit function along generation without using the Random Forest Classifier during the optimisation. The maximum value is reached in less iteration than the proposed case, and the process parameters lead to an anomaly.

.

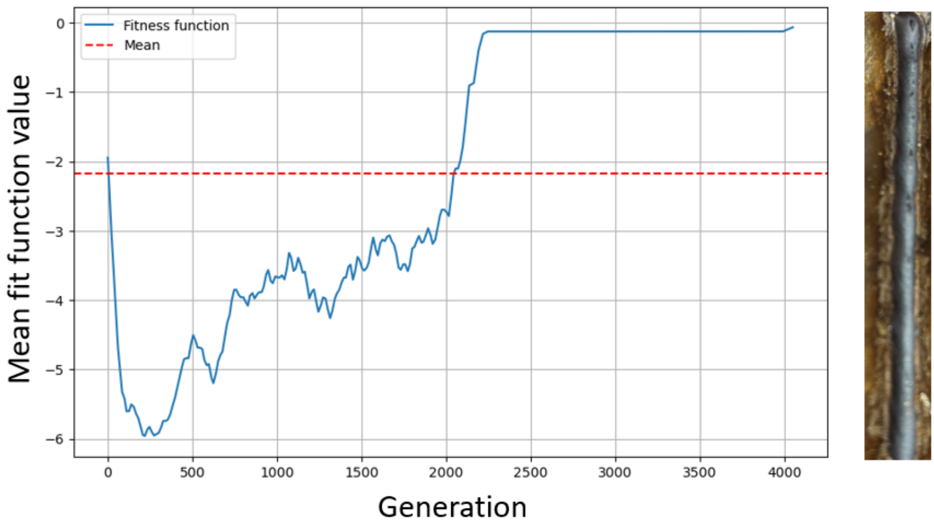

Figure 67 Behaviour of fit function along generation. Once the best process parameters are reached, the fit function is fixed to the maximum value

5.5. Summary of Genetic Algorithm approach for WAAM process optimisation

This chapter presents a novel AI-based metaheuristic optimisation approach designed to enhance the sustainability of WAAM processes, aiming to surpass traditional experimental methods for selecting optimal process parameters. The methodology integrates regression and classification ML techniques within a framework, where an agent leverages evolutionary theory to produce and assess solutions based on a designed fit function. In particular, the proposed agent uses a continuous GA to explore new parameter combinations, with a fitness function designed to evaluate the quality of solutions based on both energy saving and quality perspective. This approach resulted in smoother layers with higher deposition speeds, reducing deposition time and power consumption by 9.5% compared to traditional methods.

While the results are promising, future research should focus on defining acceptable defect limits and evaluating additional factors such as surface roughness and mechanical properties. Future studies should also consider printing wall structures rather than single layers, to account for potential defects during the building process. Despite these potential developments, this chapter demonstrates the significant impact of integrating data-driven optimisation techniques, highlighting the effectiveness of the proposed approach in real-world applications.

Chapter 6 : Summary and limitations of the thesis

6.1. Summary of the thesis

The literature review presented in *Chapter 2* of this thesis highlighted that, although research into AI applications in WAAM has been growing exponentially over the last five years, several knowledge gaps remain in both the monitoring and control of the WAAM process. Consequently, the following chapters addresses some of the identified issues.

Chapter 3 discusses the gap in knowledge regarding the use of unsupervised learning approaches for online anomaly detection and monitoring. Specifically, this thesis focuses on the application of unsupervised learning to analyse small datasets collected during the certification process. Since the data on welding current and welding voltage are crucial for certifying wire arc additively manufactured parts, these signals can be used during fabrication to assess product quality through online inspection. This is particularly important for quality assessment when transitioning to full-scale production. Anomaly detection not only helps identify NDE targets but also serves as the first step in a two-stage monitoring module. Monitoring, in turn, provides insights for more informed decision-support systems or advanced cognitive feedback controllers.

Despite the potential applications of unsupervised learning, this chapter highlights that the global feature representation in the time domain is the main reason for the poor performance of these algorithms, making them unsuitable for real industrial applications. However, it has been demonstrated that by leveraging the highly informative data contained in the frequency domain of these signals, it is possible to achieve performance comparable to that of supervised learning applications, but without the need to collect large datasets or introduce defects into components.

Chapter 4 discusses the challenges associated with developing feedback controllers for WAAM and presents an innovative optimal data-driven feedback controller based on RL. The chapter proposes a novel workflow for integrating RL as a feedback controller for industrial processes, involving reduced-order models and the design of reward and control policy architectures. This workflow is then applied to WAAM within a custom-developed simulation environment. Simulation results demonstrate improved performance compared to other controllers, such as MPC and LQR.

In addition to feedback control, the literature review emphasised the potential role of AI in offline process optimisation. *Chapter 5* provides an overview of how AI can be utilised for this purpose, particularly through the combination of GA and ML data-driven modelling techniques. This chapter presents a combination of regression and classification models as the environment model, while a GA, with a newly designed fitness function, is used to enhance the energy efficiency of the WAAM process without compromising component quality by producing non-compliant layers. The results demonstrate improved efficiency with AI-selected parameters compared to those chosen by a skilled human operator.

6.2. Discussion of the limitations

Despite the innovations proposed in this thesis, several challenges remain, which form the basis of ongoing research works.

In relation to bead modelling task, in this thesis the effect of interpass temperature, heat accumulation and component distortion on the effective values of layer width and layer height has not been addressed as well as the impact of overlapping in multi-bead components. Although preliminary experimental campaign assesses the presence of this phenomena, this effect should be considered for both proposed RL feedback controllers and optimisation modules.

Furthermore, the proposed monitoring methodologies are tailored to specific materials and welding waveforms. While they may work with other waveforms and materials, their applicability cannot be considered universal for both WAAM and GMAW processes. Although the results achieved in this thesis are comparable to those obtained through supervised learning in other studies, direct performance comparisons using the same datasets and sensors are necessary to validate these findings and benchmark the approach effectively.

Finally, this thesis highlights unsupervised ML as a powerful tool for improving quality inspection procedures by integrating anomaly detection during deposition and identifying targeted NDE areas for final assessment. Unlike current inspection methods, which rely on random sampling or costly and complex analyses, ML offers a more efficient approach by directing targeted NDE to problematic areas or preventively rejecting defective components. However, further studies involving destructive testing are required to assess component quality more thoroughly. Both the findings of this thesis and those of related research focus primarily on anomaly detection through visual inspection, without fully addressing the metallurgical and mechanical implications for real components. It remains unclear when an anomaly results in a critical defect (a "flaw") that renders a part non-compliant or when it has no significant impact on component quality based on requirements. Additionally, as with all AI applications, legal and ethical considerations must be carefully addressed to ensure the practical implementation of these techniques in industrial environments for both feedback control and quality assurance.

Chapter 7 : Conclusions and future works

This thesis highlights the transformative potential of AI in addressing key challenges in the WAAM process through contributions to process monitoring, feedback control, and offline optimisation. Unsupervised learning was leveraged to enhance online process monitoring by utilising frequency-domain features, achieving performance comparable to what achievable with supervised learning without requiring large and balanced datasets. Designed for practical industrial implementation, this approach uses data collected during certification procedure to develop effective component-based monitoring and anomaly detection modules. For feedback control, an RL-based controller was introduced to manage process nonlinearity and process parameters constraints, demonstrating superior performance in layer geometry control compared to traditional MIMO controller such as MPC and LQR. Lastly, AI-driven optimisation, combining GA and ML models, demonstrated how it is possible improve energy efficiency while preserving quality, showcasing the key role of AI in advancing WAAM technologies.

The limitations of the proposed methodologies have been discussed, highlighting the need for more in depth investigations in the field of AI-enabled WAAM. Some of the discussed limitations are going to be studied during the ongoing research projects. An extensive experimental campaign is currently being conducted on INVAR36 alloy, using the system in **Figure 67**. This study aims to investigate the effects on layer geometry of process parameters in a multi-layer multi-bead deposition, aiming to integrate it in the developed RL controller and GA optimisation techniques. In terms of monitoring applications, following the results of this thesis, there is a solid understanding of various feature extraction techniques and the methodologies for processing them using both supervised and unsupervised machine learning techniques. However, there is still a gap in knowledge regarding the employment of multi-sensor monitoring systems, like the one shown in **Figure 68**, for both anomaly detection and defect classification. This is a crucial aspect, particularly for future DSS and in relation to proposed RL-based control system, which could use this information to suggest actions to expert users or make autonomous decisions, aligning with the goals of a modern SME. The proposed experimental campaign possesses an additional occasion to assess the multi-sensor system capability, since the collected data may be carefully categorised and employed for further analysis.

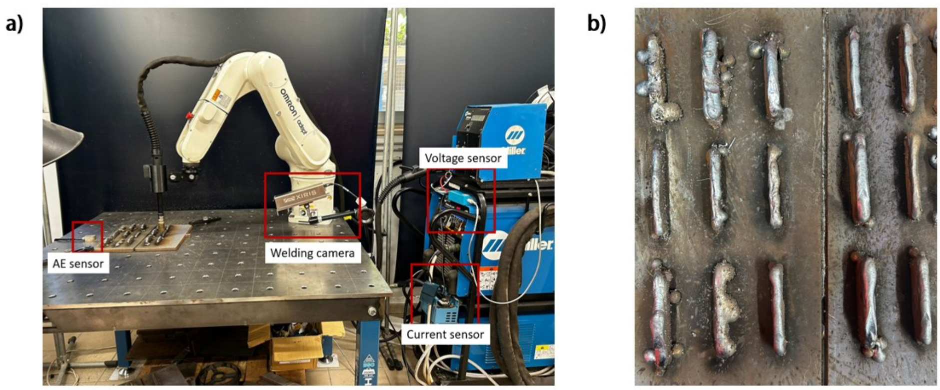

Figure 68 a) The multi-sensor monitoring system integrated within UNINA WAAM system b) the preliminary experimental campaign currently being conducted on INVAR36 alloy.

Finally, the literature review revealed that while various applications have been proposed, there is a significant knowledge gap regarding the integration of these solutions within a CPS framework. Recent work by Mu et al. [189] focused on DT technology, which represents one aspect of the broader CPS framework. Therefore, ongoing research projects are trying to develop a framework for WAAM around this crucial area of science, with a preliminary framework illustrated in **Figure 69**. Once defined the architecture, the primary goal is to integrate all the presented technology within the architecture, aiming to develop a physical demonstrator of a Cyber Physical System-based Smart Manufacturing Entity for Wire Arc Additive Manufacturing process.

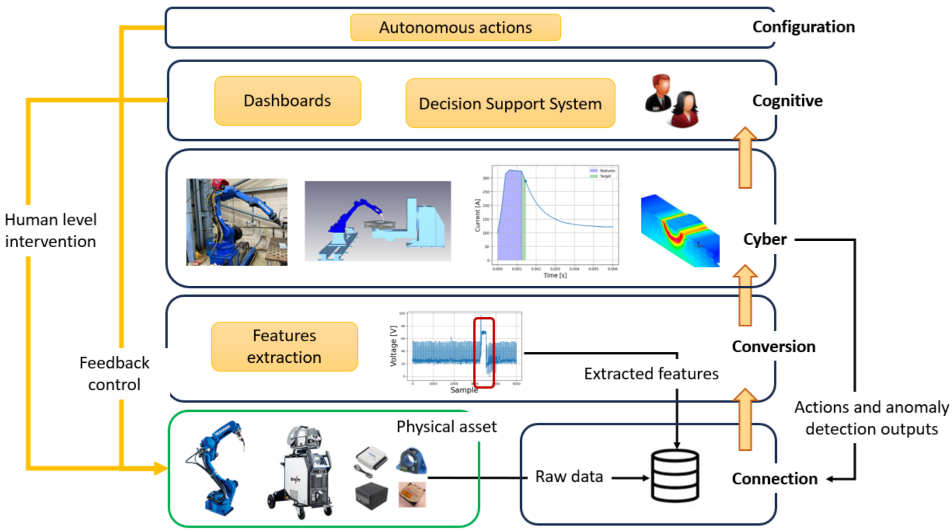

Figure 69 A General WAAM-CPS architecture inspired by 5C architecture proposed by Lee et al. [16].

References

[1] J. D. Spencer, P. M. Dickens, and C. M. Wykes, "Rapid prototyping of metal parts by three-dimensional welding," *Proc Inst Mech Eng B J Eng Manuf*, vol. 212, no. 3, pp. 175–182, Mar. 1998, doi: 10.1243/0954405981515590.

[2] A. F. Ribeiro and J. Norrish, "Rapid Prototyping Process Using Meral Directly," 1996.

[3] J. Norrish, "Evolution of advanced process control in GMAW: Innovations, implications, and application," *Weld. J.*, vol. 103, no. 06, pp. 161–175, Jun. 2024.

[4] C. Nota, G. Rückert, J. L. Heuzé, L. Carlino, J. M. Quenez, and L. Courregelongue, "A first feedback on manufacturing and in-service behaviour of a WAAM-made propeller for naval application," *Welding in the World*, Feb. 2023, doi: 10.1007/s40194-023-01475-w.

[5] T. Feucht, B. Waldschmitt, J. Lange, and M. Erven, "Additive manufacturing of a bridge in situ," *Steel Construction*, vol. 15, no. 2, pp. 100–110, May 2022, doi: 10.1002/stco.202100045.

[6] Z. Pan, D. Ding, B. Wu, D. Cuiuri, H. Li, and J. Norrish, "Arc Welding Processes for Additive Manufacturing: A Review," 2018, pp. 3–24. doi: 10.1007/978-981-10-5355-9_1.

[7] J. Norrish, J. Polden, and I. Richardson, "A review of wire arc additive manufacturing: development, principles, process physics, implementation and current status," *J Phys D Appl Phys*, vol. 54, no. 47, p. 473001, Nov. 2021, doi: 10.1088/1361-6463/ac1e4a.

[8] A. R. Doodman Tipi, N. Pariz, and others, "Improving the dynamic metal transfer model of gas metal arc welding (GMAW) process," *The International Journal of Advanced Manufacturing Technology*, vol. 76, no. 1, pp. 657–668, 2015.

[9] S. Zhao, X. Qiu, I. Burnett, M. Rigby, and A. Lele, "A lumped-parameter model for sound generation in gas metal arc welding," *Mech Syst Signal Process*, vol. 147, p. 107085, 2021.

[10] D. Ding, F. He, L. Yuan, Z. Pan, L. Wang, and M. Ros, "The first step towards intelligent wire arc additive manufacturing: An automatic bead modelling system using machine learning through industrial information integration," *J Ind Inf Integr*, vol. 23, p. 100218, Sep. 2021, doi: 10.1016/j.jii.2021.100218.

[11] B. Wu *et al.*, "A review of the wire arc additive manufacturing of metals: properties, defects and quality improvement," *J Manuf Process*, vol. 35, pp. 127–139, 2018.

[12] J. Norrish, *Advanced welding processes*. Cambridge, England: Woodhead Publishing, 2006.

[13] M. Bruce and D. Deruntz, "Assessing the Benefits of Surface Tension Transfer® Welding to Industry Manufacturing Materials & Processes Metals Production Welding," *Journal of Industrial Technology* •, vol. 19, no. 4, 2003. [Online]. Available: www.nait.org

[14] P. N. Bellamkonda, M. Dwivedy, and R. Addanki, "Cold metal transfer technology - A review of recent research developments," *Results in Engineering*, vol. 23, p. 102423, Sep. 2024, doi: 10.1016/j.rineng.2024.102423.

[15] J. N. Pires, A. Loureiro, T. Godinho, P. Ferreira, B. Fernando, and J. Morgado, "Welding robots," *IEEE Robot Autom Mag*, vol. 10, no. 2, pp. 45–55, Jun. 2003, doi: 10.1109/MRA.2003.1213616.

[16] J. Lee, B. Bagheri, and H.-A. Kao, "A Cyber-Physical Systems architecture for Industry 4.0-based manufacturing systems," *Manuf Lett*, vol. 3, pp. 18–23, Jan. 2015, doi: 10.1016/j.mfglet.2014.12.001.

[17] A. Kusiak, "Smart manufacturing," *Int J Prod Res*, vol. 56, no. 1–2, pp. 508–517, Jan. 2018, doi: 10.1080/00207543.2017.1351644.

[18] L. Monostori *et al.*, "Cyber-physical systems in manufacturing," *CIRP Annals*, vol. 65, no. 2, pp. 621–641, 2016, doi: 10.1016/j.cirp.2016.06.005.

[19] D. Powell, M. C. Magnanini, M. Colledani, and O. Myklebust, "Advancing zero defect manufacturing: A state-of-the-art perspective and future research directions," *Comput Ind*, vol. 136, p. 103596, Apr. 2022, doi: 10.1016/j.compind.2021.103596.

[20] F. He *et al.*, "Research and application of artificial intelligence techniques for wire arc additive manufacturing: a state-of-the-art review," *Robot Comput Integr Manuf*, vol. 82, p. 102525, Aug. 2023, doi: 10.1016/j.rcim.2023.102525.

[21] B. Ogunbiyi and J. Norrish, "Monitoring indices for metal transfer in the GMAW process," *Science and Technology of Welding and Joining*, vol. 2, no. 1, pp. 33–35, Feb. 1997, doi: 10.1179/stw.1997.2.1.33.

[22] S. C. Absi Alfaro, G. C. Carvalho, and F. R. da Cunha, "A statistical approach for monitoring stochastic welding processes," *J Mater Process Technol*, vol. 175, no. 1, pp. 4–14, 2006, doi: https://doi.org/10.1016/j.jmatprotec.2005.04.049.

[23] S. Feng, H. Terasaki, Y. Komizo, S. Hu, D. Chen, and Z. Ma, "Development of evaluation technique of GMAW welding quality based on statistical analysis," *Chinese Journal of Mechanical Engineering*, vol. 27, no. 6, pp. 1257–1263, Nov. 2014, doi: 10.3901/CJME.2014.0718.120.

[24] D. Ding, Z. Pan, D. Cuiuri, H. Li, S. van Duin, and N. Larkin, "Bead modelling and implementation of adaptive MAT path in wire and arc additive manufacturing," *Robot Comput Integr Manuf*, vol. 39, pp. 32–42, Jun. 2016, doi: 10.1016/j.rcim.2015.12.004.

[25] D. Ding, Z. Pan, D. Cuiuri, and H. Li, "A multi-bead overlapping model for robotic wire and arc additive manufacturing (WAAM)," *Robot Comput Integr Manuf*, vol. 31, pp. 101–110, 2015.

[26] N. A. Surovi and G. S. Soh, "Process map generation of geometrically uniform beads using support vector machine," *Mater Today Proc*, vol. 70, pp. 113–118, 2022, doi: 10.1016/j.matpr.2022.08.557.

[27] S. Tang, G. Wang, H. Song, R. Li, and H. Zhang, "A novel method of bead modeling and control for wire and arc additive manufacturing," *Rapid Prototyp J*, vol. 27, no. 2, pp. 311–320, Mar. 2021, doi: 10.1108/RPJ-05-2020-0097.

[28] H. Li, X. Shi, B. Wu, D. R. Corradi, Z. Pan, and H. Li, "Wire arc additive manufacturing: A review on digital twinning and visualization process," *J Manuf Process*, vol. 116, pp. 293–305, 2024.

[29] H. Mu, F. He, L. Yuan, P. Commins, D. Ding, and Z. Pan, "A digital shadow approach for enhancing process monitoring in wire arc additive manufacturing using sensor fusion," *J Ind Inf Integr*, vol. 40, p. 100609, Jul. 2024, doi: 10.1016/j.jii.2024.100609.

[30] C. Xia *et al.*, "A review on wire arc additive manufacturing: Monitoring, control and a framework of automated system," *J Manuf Syst*, vol. 57, pp. 31–45, 2020.

[31] X. Ying, "An Overview of Overfitting and its Solutions," *J Phys Conf Ser*, vol. 1168, p. 022022, Feb. 2019, doi: 10.1088/1742-6596/1168/2/022022.

[32] Y. Lang, A. Malacina, L. T. Biegler, S. Munteanu, J. I. Madsen, and S. E. Zitney, "Reduced order model based on principal component analysis for process simulation and optimization," *Energy & Fuels*, vol. 23, no. 3, pp. 1695–1706, 2009.

[33] J. Xiao, N. Liu, J. Lua, C. Saathoff, and W. p Seneviratne, "Data-driven and reduced-order modeling of composite drilling," in *AIAA Scitech 2020 forum*, 2020, p. 1859.

[34] H. Mu, J. Polden, Y. Li, F. He, C. Xia, and Z. Pan, "Layer-by-layer model-based adaptive control for wire arc additive manufacturing of thin-wall structures," *J Intell Manuf*, vol. 33, no. 4, pp. 1165–1180, 2022.

[35] G. Mattera, J. Polden, A. Caggiano, L. Nele, Z. Pan, and J. Norrish, "Semi-supervised Learning for Real-Time Anomaly Detection in Pulsed Transfer Wire Arc Additive Manufacturing," *J Manuf Process*, 2024.

[36] G. MATTERA, J. POLDEN, and L. NELE, "Monitoring Wire Arc Additive Manufacturing process of Inconel 718 thin-walled structure using wavelet decomposition and clustering analysis of welding signal," *Journal of Advanced Manufacturing Science and Technology*, vol. 0, no. 0, pp. 2025006–0, 2024, doi: 10.51393/j.jamst.2025006.

[37] G. Mattera, A. Caggiano, and L. Nele, "Optimal data-driven control of manufacturing processes using reinforcement learning: an application to wire arc additive manufacturing," *J Intell Manuf*, pp. 1–20, 2024.

[38] D. P. Kingma and J. Ba, "Adam: A Method for Stochastic Optimization," 2014, *arXiv*. doi: 10.48550/ARXIV.1412.6980.

[39] M. Giacalone, D. Panarello, and R. Mattera, "Multicollinearity in regression: an efficiency comparison between Lp-norm and least squares estimators," *Qual Quant*, vol. 52, no. 4, pp. 1831–1859, Jul. 2018, doi: 10.1007/s11135-017-0571-y.

[40] W. Loh, "Classification and regression trees," *WIREs Data Mining and Knowledge Discovery*, vol. 1, no. 1, pp. 14–23, Jan. 2011, doi: 10.1002/widm.8.

[41] L. Breiman, "Bagging predictors," *Mach Learn*, vol. 24, no. 2, pp. 123–140, Aug. 1996, doi: 10.1007/BF00058655.

[42] G. Biau and E. Scornet, "A random forest guided tour," *TEST*, vol. 25, no. 2, pp. 197–227, Jun. 2016, doi: 10.1007/s11749-016-0481-7.

[43] C. Bentéjac, A. Csörgő, and G. Martínez-Muñoz, "A comparative analysis of gradient boosting algorithms," *Artif Intell Rev*, vol. 54, no. 3, pp. 1937–1967, Mar. 2021, doi: 10.1007/s10462-020-09896-5.

[44] A. Caggiano, "Tool wear prediction in Ti-6Al-4V machining through multiple sensor monitoring and PCA features pattern recognition," *Sensors*, vol. 18, no. 3, p. 823, 2018.

[45] G. Mattera, J. Polden, A. Caggiano, P. Commins, L. Nele, and Z. Pan, "Anomaly detection of Wire Arc Additively Manufactured parts via Surface Tension Transfer through unsupervised machine learning techniques," *Procedia CIRP*, 2024.

[46] Y.-C. Yao, Y.-H. Chen, C.-H. Liu, and W.-P. Shih, "Real-time chatter detection and automatic suppression for intelligent spindles based on wavelet packet energy entropy and local outlier factor algorithm," *The International Journal of Advanced Manufacturing Technology*, vol. 103, no. 1–4, pp. 297–309, Jul. 2019, doi: 10.1007/s00170-019-03551-2.

[47] J. Liu, D. Cai, and X. He, "Gaussian Mixture Model with Local Consistency," *Proceedings of the AAAI Conference on Artificial Intelligence*, vol. 24, no. 1, pp. 512–517, Jul. 2010, doi: 10.1609/aaai.v24i1.7659.

[48] K. Weiss, T. M. Khoshgoftaar, and D. Wang, "A survey of transfer learning," *J Big Data*, vol. 3, no. 1, p. 9, Dec. 2016, doi: 10.1186/s40537-016-0043-6.

[49] G. Cybenko, "Approximation by superpositions of a sigmoidal function," *Mathematics of control, signals and systems*, vol. 2, no. 4, pp. 303–314, 1989.

[50] Y. LeCun *et al.*, "Backpropagation Applied to Handwritten Zip Code Recognition," *Neural Comput*, vol. 1, no. 4, pp. 541–551, Dec. 1989, doi: 10.1162/neco.1989.1.4.541.

[51] D. Pedamonti, "Comparison of non-linear activation functions for deep neural networks on MNIST classification task," Apr. 2018, [Online]. Available: http://arxiv.org/abs/1804.02763

[52] G. Pang, C. Shen, L. Cao, and A. Van Den Hengel, "Deep Learning for Anomaly Detection," *ACM Comput Surv*, vol. 54, no. 2, pp. 1–38, Mar. 2022, doi: 10.1145/3439950.

[53] Y. Bengio, P. Simard, and P. Frasconi, "Learning long-term dependencies with gradient descent is difficult," *IEEE Trans Neural Netw*, vol. 5, no. 2, pp. 157–166, Mar. 1994, doi: 10.1109/72.279181.

[54] S. Hochreiter and J. Schmidhuber, "Long Short-Term Memory," *Neural Comput*, vol. 9, no. 8, 1997, doi: 10.1162/neco.1997.9.8.1735.

[55] J. Chung, C. Gulcehre, K. Cho, and Y. Bengio, "Gated feedback recurrent neural networks," in *32nd International Conference on Machine Learning, ICML 2015*, 2015.

[56] Yu Wang, "A new concept using LSTM Neural Networks for dynamic system identification," in *2017 American Control Conference (ACC)*, IEEE, May 2017, pp. 5324–5329. doi: 10.23919/ACC.2017.7963782.

[57] M. Jung, P. R. da Costa Mendes, M. Önnheim, and E. Gustavsson, "Model Predictive Control when utilizing LSTM as dynamic models," *Eng Appl Artif Intell*, vol. 123, p. 106226, Aug. 2023, doi: 10.1016/j.engappai.2023.106226.

[58] Y. Tan, C. Hu, K. Zhang, K. Zheng, E. A. Davis, and J. S. Park, "LSTM-Based Anomaly Detection for Non-Linear Dynamical System," *IEEE Access*, vol. 8, pp. 103301–103308, 2020, doi: 10.1109/ACCESS.2020.2999065.

[59] Y. Lecun, Y. Bengio, and G. Hinton, "Deep learning," May 27, 2015, *Nature Publishing Group*. doi: 10.1038/nature14539.

[60] S. Bianco, R. Cadene, L. Celona, and P. Napoletano, "Benchmark Analysis of Representative Deep Neural Network Architectures," *IEEE Access*, vol. 6, pp. 64270–64277, 2018, doi: 10.1109/ACCESS.2018.2877890.

[61] D. Kijdech and S. Vongbunyong, "Pick-and-place application using a dual arm collaborative robot and an RGB-D camera with YOLOv5," *IAES International Journal of Robotics and Automation (IJRA)*, vol. 12, no. 2, p. 197, Jun. 2023, doi: 10.11591/ijra.v12i2.pp197-210.

[62] A. Caggiano, J. Zhang, V. Alfieri, F. Caiazzo, R. Gao, and R. Teti, "Machine learning-based image processing for on-line defect recognition in additive manufacturing," *CIRP annals*, vol. 68, no. 1, pp. 451–454, 2019.

[63] J. Kershaw, R. Yu, Y. Zhang, and P. Wang, "Hybrid machine learning-enabled adaptive welding speed control," *J Manuf Process*, vol. 71, pp. 374–383, Nov. 2021, doi: 10.1016/j.jmapro.2021.09.023.

[64] R. Bellman, "Dynamic programming," *Science (1979)*, vol. 153, no. 3731, pp. 34–37, 1966.

[65] R. S. Sutton and A. Barto, *Reinforcement learning*, Second edition. in Adaptive computation and machine learning. Cambridge, Massachusetts: The MIT Press, 2018.

[66] M. R. K. Mes and A. P. Rivera, “Approximate dynamic programming by practical examples,” in *Markov decision processes in practice*, Springer, 2017, pp. 63–101.

[67] S. Amari, “Backpropagation and stochastic gradient descent method,” *Neurocomputing*, vol. 5, no. 4–5, pp. 185–196, 1993.

[68] Y.-H. Wang, T.-H. S. Li, and C.-J. Lin, “Backward Q-learning: The combination of Sarsa algorithm and Q-learning,” *Eng Appl Artif Intell*, vol. 26, no. 9, pp. 2184–2193, 2013.

[69] V. Mnih *et al.*, “Human-level control through deep reinforcement learning,” *Nature*, vol. 518, no. 7540, pp. 529–533, 2015.

[70] H. Van Hasselt, A. Guez, and D. Silver, “Deep reinforcement learning with double q-learning,” in *Proceedings of the AAAI conference on artificial intelligence*, 2016.

[71] R. J. Williams, “Simple statistical gradient-following algorithms for connectionist reinforcement learning,” *Mach Learn*, vol. 8, no. 3, pp. 229–256, 1992.

[72] S. Kakade and J. Langford, “Approximately optimal approximate reinforcement learning,” in *In Proc. 19th International Conference on Machine Learning*, 2002.

[73] D. Silver, G. Lever, N. Heess, T. Degris, D. Wierstra, and M. Riedmiller, “Deterministic policy gradient algorithms,” in *International conference on machine learning*, 2014, pp. 387–395.

[74] J. Schulman, S. Levine, P. Abbeel, M. Jordan, and P. Moritz, “Trust region policy optimization,” in *International conference on machine learning*, 2015, pp. 1889–1897.

[75] J. Schulman, F. Wolski, P. Dhariwal, A. Radford, and O. Klimov, “Proximal policy optimization algorithms,” *arXiv preprint arXiv:1707.06347*, 2017.

[76] T. P. Lillicrap *et al.*, “Continuous control with deep reinforcement learning,” *arXiv preprint arXiv:1509.02971*, 2015.

[77] J. H. Holland, “Genetic Algorithms,” *Sci Am*, vol. 267, no. 1, pp. 66–72, Jul. 1992, doi: 10.1038/scientificamerican0792-66.

[78] Y. Guo, Y. Zhang, Z. Pan, and W. Zhou, “Recent progress of sensing and machine learning technologies for process monitoring and defects detection in wire arc additive manufacturing,” *J Manuf Process*, vol. 125, pp. 489–511, Sep. 2024, doi: 10.1016/j.jmapro.2024.07.060.

[79] J. Johnson, “Process control of GMAW: sensing of metal transfer mode,” *Weld J*, vol. 70, 1991.

[80] A. Sumesh, K. Rameshkumar, A. Raja, K. Mohandas, A. Santhakumari, and R. Shyambabu, "Establishing Correlation Between Current and Voltage Signatures of the Arc and Weld Defects in GMAW Process," *Arab J Sci Eng*, vol. 42, no. 11, pp. 4649–4665, Nov. 2017, doi: 10.1007/s13369-017-2609-9.

[81] E. Wei, D. Farson, R. Richardson, and H. Ludewig, "Detection of Weld Surface Porosity by Statistical Analysis of Arc Current in Gas Metal Arc Welding," *J Manuf Process*, vol. 3, no. 1, pp. 50–59, Jan. 2001, doi: 10.1016/S1526-6125(01)70033-3.

[82] S. Shin, C. Jin, J. Yu, and S. Rhee, "Real-Time Detection of Weld Defects for Automated Welding Process Base on Deep Neural Network," *Metals (Basel)*, vol. 10, no. 3, p. 389, Mar. 2020, doi: 10.3390/met10030389.

[83] Y. Li *et al.*, "A defect detection system for wire arc additive manufacturing using incremental learning," *J Ind Inf Integr*, vol. 27, p. 100291, May 2022, doi: 10.1016/j.jii.2021.100291.

[84] T. Zhang, C. Xu, J. Cheng, Z. Chen, L. Wang, and K. Wang, "Research of surface oxidation defects in copper alloy wire arc additive manufacturing based on time-frequency analysis and deep learning method," *Journal of Materials Research and Technology*, vol. 25, pp. 511–521, Jul. 2023, doi: 10.1016/j.jmrt.2023.05.227.

[85] Y. Arata, K. Inoue, M. Futamata, and T. Toh, "Investigation on welding arc sound (Report I): effect of welding method and welding condition of welding arc sound (welding physics, processes & instruments)," *Transactions of JWRI*, vol. 8, no. 1, pp. 25–31, 1979.

[86] J. Horvat, J. Prezelj, I. Polajnar, and M. Čudina, "Monitoring gas metal arc welding process by using audible sound signal," *Strojniški vestnik-Journal of Mechanical Engineering*, vol. 57, no. 3, pp. 267–278, 2011.

[87] F. Erdmann-Jesnitzer, E. Feustel, and D. Rehfeldt, "Akustische Untersuchungen am Schweislichtbogen," *Schw. und Schn*, vol. 19, no. 3, pp. 95–100, 1967.

[88] Y. Cheng, R. Yu, Q. Zhou, H. Chen, W. Yuan, and Y. Zhang, "Real-time sensing of gas metal arc welding process – A literature review and analysis," *J Manuf Process*, vol. 70, pp. 452–469, Oct. 2021, doi: 10.1016/j.jmapro.2021.08.058.

[89] K. Pal, S. Bhattacharya, and S. K. Pal, "Investigation on arc sound and metal transfer modes for on-line monitoring in pulsed gas metal arc welding," *J Mater Process Technol*, vol. 210, no. 10, pp. 1397–1410, 2010.

[90] A. S. Roca, H. C. Fals, J. B. Fernández, E. J. Mac\'\ias, and M. P. De La Parte, "Artificial neural networks and acoustic emission applied to stability analysis in gas metal arc welding," *Science and Technology of Welding and Joining*, vol. 14, no. 2, pp. 117–124, 2009.

[91] M. A. Rahman, S. Jamal, M. V. Cruz, B. Silwal, and H. Taheri, “In situ process monitoring of multi-layer deposition in wire arc additive manufacturing (WAAM) process with acoustic data analysis and machine learning,” *The International Journal of Advanced Manufacturing Technology*, Apr. 2024, doi: 10.1007/s00170-024-13641-5.

[92] A. Rajesh, W. Ya, and M. Hermans, “Anomaly Detection in WAAM Deposition of Nickel Alloys—Single-Material and Cross-Material Analysis,” *Metals (Basel)*, vol. 13, no. 11, p. 1820, Oct. 2023, doi: 10.3390/met13111820.

[93] M. F. M. Yusof, M. A. Kamaruzaman, M. Ishak, and M. F. Ghazali, “Porosity detection by analyzing arc sound signal acquired during the welding process of gas pipeline steel,” *The International Journal of Advanced Manufacturing Technology*, vol. 89, no. 9, pp. 3661–3670, 2017.

[94] N. A. Surovi and G. S. Soh, “Acoustic feature based geometric defect identification in wire arc additive manufacturing,” *Virtual Phys Prototyp*, vol. 18, no. 1, Dec. 2023, doi: 10.1080/17452759.2023.2210553.

[95] J. Y. I. Alcaraz, W. Foqué, A. Sharma, and T. Tjahjowidodo, “Indirect porosity detection and root-cause identification in WAAM,” *J Intell Manuf*, Apr. 2023, doi: 10.1007/s10845-023-02128-x.

[96] M. Rohe, B. N. Stoll, J. Hildebrand, J. Reimann, and J. P. Bergmann, “Detecting Process Anomalies in the GMAW Process by Acoustic Sensing with a Convolutional Neural Network (CNN) for Classification,” *Journal of Manufacturing and Materials Processing*, vol. 5, no. 4, p. 135, Dec. 2021, doi: 10.3390/jmmp5040135.

[97] C. Xia, Z. Pan, Y. Li, J. Chen, and H. Li, “Vision-based melt pool monitoring for wire-arc additive manufacturing using deep learning method,” *The International Journal of Advanced Manufacturing Technology*, vol. 120, no. 1, pp. 551–562, 2022.

[98] C. Xia, Z. Pan, Z. Fei, S. Zhang, and H. Li, “Vision based defects detection for Keyhole TIG welding using deep learning with visual explanation,” *J Manuf Process*, vol. 56, pp. 845–855, 2020.

[99] H.-W. Cho, S.-J. Shin, G.-J. Seo, D. B. Kim, and D.-H. Lee, “Real-time anomaly detection using convolutional neural network in wire arc additive manufacturing: Molybdenum material,” *J Mater Process Technol*, vol. 302, p. 117495, 2022.

[100] C. Lee, G. Seo, D. B. Kim, M. Kim, and J.-H. Shin, “Development of Defect Detection AI Model for Wire + Arc Additive Manufacturing Using High Dynamic Range Images,” *Applied Sciences*, vol. 11, no. 16, p. 7541, Aug. 2021, doi: 10.3390/app11167541.

[101] J. Redmon and A. Farhadi, “Yolov3: An incremental improvement,” *arXiv preprint arXiv:1804.02767*, 2018.

[102] Y. Li *et al.*, "Towards intelligent monitoring system in wire arc additive manufacturing: a surface anomaly detector on a small dataset," *The International Journal of Advanced Manufacturing Technology*, vol. 120, no. 7–8, pp. 5225–5242, Jun. 2022, doi: 10.1007/s00170-022-09076-5.

[103] P. Zheng, S. Han, D. Xue, L. Fu, and B. Jiang, "Deep learning assisted fabrication of metallic components using the robotic wire arc additive manufacturing," *Rapid Prototyp J*, vol. 30, no. 4, pp. 733–744, 2024.

[104] J. Wu, C. Huang, Z. Li, R. Li, G. Wang, and H. Zhang, "An *in situ* surface defect detection method based on improved you only look once algorithm for wire and arc additive manufacturing," *Rapid Prototyp J*, vol. 29, no. 5, pp. 910–920, May 2023, doi: 10.1108/RPJ-06-2022-0211.

[105] X. Zhou *et al.*, "Improved YOLOv5-based pore defect detection algorithm for wire arc additive manufacturing," *Mater Today Commun*, vol. 39, p. 108710, Jun. 2024, doi: 10.1016/j.mtcomm.2024.108710.

[106] M. Chandra, S. Rajak, and V. K.E.K, "Deep learning-based framework for the observation of real-time melt pool and detection of anomaly in wire-arc additive manufacturing," *Materials and Manufacturing Processes*, vol. 39, no. 6, pp. 761–777, Apr. 2024, doi: 10.1080/10426914.2023.2254386.

[107] W. Li *et al.*, "Deep learning based online metallic surface defect detection method for wire and arc additive manufacturing," *Robot Comput Integr Manuf*, vol. 80, p. 102470, Apr. 2023, doi: 10.1016/j.rcim.2022.102470.

[108] H. Song, C. Li, Y. Fu, R. Li, H. Zhang, and G. Wang, "A two-stage unsupervised approach for surface anomaly detection in wire and arc additive manufacturing," *Comput Ind*, vol. 151, p. 103994, Oct. 2023, doi: 10.1016/j.compind.2023.103994.

[109] B. Wu, Z. Pan, S. van Duin, and H. Li, "Thermal behavior in wire arc additive manufacturing: characteristics, effects and control," in *Transactions on intelligent welding manufacturing*, Springer, 2019, pp. 3–18.

[110] F. M. Scotti, F. R. Teixeira, L. J. da Silva, D. B. de Araújo, R. P. Reis, and A. Scotti, "Thermal management in WAAM through the CMT Advanced process and an active cooling technique," *J Manuf Process*, vol. 57, pp. 23–35, Sep. 2020, doi: 10.1016/j.jmapro.2020.06.007.

[111] B. Wu *et al.*, "Mitigation of thermal distortion in wire arc additively manufactured Ti6Al4V part using active interpass cooling," *Science and Technology of Welding and Joining*, vol. 24, no. 5, pp. 484–494, Jul. 2019, doi: 10.1080/13621718.2019.1580439.

[112] V. T. Le *et al.*, "Influences of the process parameter and thermal cycles on the quality of 308L stainless steel walls produced by additive manufacturing utilizing an arc

welding source," *Welding in the World*, vol. 66, no. 8, pp. 1565–1580, Aug. 2022, doi: 10.1007/s40194-022-01330-4.

[113] S. C. A. Alfaro, J. A. R. Vargas, G. C. de Carvalho, and G. G. de Souza, "Characterization of 'Humping' in the GTA welding process using infrared images," *J Mater Process Technol*, vol. 223, pp. 216–224, Sep. 2015, doi: 10.1016/j.jmatprotec.2015.03.052.

[114] X. Chen, H. Zhang, J. Hu, and Y. Xiao, "A passive on-line defect detection method for wire and arc additive manufacturing based on infrared thermography," 2019.

[115] M. Mozaffar *et al.*, "Data-driven prediction of the high-dimensional thermal history in directed energy deposition processes via recurrent neural networks," *Manuf Lett*, vol. 18, pp. 35–39, 2018.

[116] A. Fernández, Á. Souto, C. González, and R. Méndez-Rial, "Embedded vision system for monitoring arc welding with thermal imaging and deep learning," in *2020 International Conference on Omni-layer Intelligent Systems (COINS)*, 2020, pp. 1–6.

[117] D. Ding, Z. Pan, D. Cuiuri, and H. Li, "A practical path planning methodology for wire and arc additive manufacturing of thin-walled structures," *Robot Comput Integr Manuf*, vol. 34, pp. 8–19, Aug. 2015, doi: 10.1016/j.rcim.2015.01.003.

[118] D. Ding, Z. Pan, D. Cuiuri, and H. Li, "A multi-bead overlapping model for robotic wire and arc additive manufacturing (WAAM)," *Robot Comput Integr Manuf*, vol. 31, pp. 101–110, 2015.

[119] J. P. Ganjigatti, D. K. Pratihar, and A. RoyChoudhury, "Modeling of the MIG welding process using statistical approaches," *The International Journal of Advanced Manufacturing Technology*, vol. 35, no. 11–12, pp. 1166–1190, Feb. 2008, doi: 10.1007/s00170-006-0798-6.

[120] P. S. Sivasakthivel and R. Sudhakaran, "Modelling and optimisation of welding parameters for multiple objectives in pre-heated gas metal arc welding process using nature instigated algorithms," *Australian Journal of Mechanical Engineering*, 2018.

[121] N. P. Kumar, S. A. Vendan, and N. S. Shanmugam, "Investigations on the parametric effects of cold metal transfer process on the microstructural aspects in AA6061," *J Alloys Compd*, vol. 658, pp. 255–264, 2016.

[122] C. Xia, Z. Pan, J. Polden, H. Li, Y. Xu, and S. Chen, "Modelling and prediction of surface roughness in wire arc additive manufacturing using machine learning," *J Intell Manuf*, vol. 33, no. 5, pp. 1467–1482, 2022.

[123] J. Xiong, G. Zhang, J. Hu, and L. Wu, "Bead geometry prediction for robotic GMAW-based rapid manufacturing through a neural network and a second-order regression analysis," *J Intell Manuf*, vol. 25, no. 1, pp. 157–163, 2014.

[124] G. Mattera, A. Caggiano, and L. Nele, “Reinforcement learning as data-driven optimization technique for GMAW process,” *Welding in the World*, 2023, doi: 10.1007/s40194-023-01641-0.

[125] M. M. Tafarroj, M. A. Moghaddam, H. Dalir, and F. Kolahan, “Using hybrid artificial neural network and particle swarm optimization algorithm for modeling and optimization of welding process,” *Journal of Advanced Manufacturing Systems*, vol. 20, no. 04, pp. 783–799, 2021.

[126] S. B. Chen, D. B. Zhao, L. Wu, and Y. J. Lou, “Intelligent methodology for sensing, modeling and control of pulsed GTAW: Part 2–Butt joint welding,” *Welding Journal(USA)*, vol. 79, no. 6, p. 164, 2000.

[127] L. Yin, J. Wang, H. Hu, S. Han, and Y. Zhang, “Prediction of weld formation in 5083 aluminum alloy by twin-wire CMT welding based on deep learning,” *Welding in the World*, vol. 63, no. 4, pp. 947–955, Jun. 2019, doi: 10.1007/s40194-019-00726-z.

[128] C. Jin, S. Shin, J. Yu, and S. Rhee, “Prediction Model for Back-Bead Monitoring During Gas Metal Arc Welding Using Supervised Deep Learning,” *IEEE Access*, vol. 8, pp. 224044–224058, 2020, doi: 10.1109/ACCESS.2020.3041274.

[129] N. Lv, Y. Xu, S. Li, X. Yu, and S. Chen, “Automated control of welding penetration based on audio sensing technology,” *J Mater Process Technol*, vol. 250, pp. 81–98, 2017.

[130] A. Chabot, M. Rauch, and J.-Y. Hascoët, “Novel control model of Contact-Tip-to-Work Distance (CTWD) for sound monitoring of arc-based DED processes based on spectral analysis,” *The International Journal of Advanced Manufacturing Technology*, vol. 116, no. 11–12, pp. 3463–3472, Oct. 2021, doi: 10.1007/s00170-021-07621-2.

[131] B. Chen, J. Wang, and S. Chen, “A study on application of multi‐sensor information fusion in pulsed GTAW,” *Industrial Robot: An International Journal*, vol. 37, no. 2, pp. 168–176, Jan. 2010, doi: 10.1108/01439911011018948.

[132] J. E. Pinto-Lopera, J. M. ST Motta, and S. C. Absi Alfaro, “Real-time measurement of width and height of weld beads in GMAW processes,” *Sensors*, vol. 16, no. 9, p. 1500, 2016.

[133] C. Xia, Z. Pan, S. Zhang, H. Li, Y. Xu, and S. Chen, “Model-free adaptive iterative learning control of melt pool width in wire arc additive manufacturing,” *The International Journal of Advanced Manufacturing Technology*, vol. 110, no. 7, pp. 2131–2142, 2020.

[134] M. Menaka, M. Vasudevan, B. Venkatraman, and B. Raj, “Estimating bead width and depth of penetration during welding by infrared thermal imaging,” *Insight-Non-Destructive Testing and Condition Monitoring*, vol. 47, no. 9, pp. 564–568, 2005.

[135] S. Chokkalingham, M. Vasudevan, S. Sudarsan, and N. Chandrasekhar, "Predicting weld bead width and depth of penetration from infrared thermal image of weld pool using artificial neural network," *Insight-Non-Destructive Testing and Condition Monitoring*, vol. 54, no. 5, pp. 272–277, 2012.

[136] P. Ghanty *et al.*, "Artificial neural network approach for estimating weld bead width and depth of penetration from infrared thermal image of weld pool," *Science and Technology of Welding and Joining*, vol. 13, no. 4, pp. 395–401, 2008.

[137] R. Yu, J. Han, L. Bai, and Z. Zhao, "Identification of butt welded joint penetration based on infrared thermal imaging," *Journal of Materials Research and Technology*, vol. 12, pp. 1486–1495, 2021.

[138] Y. Wang, C. Zhang, J. Lu, L. Bai, Z. Zhao, and J. Han, "Weld Reinforcement Analysis Based on Long-Term Prediction of Molten Pool Image in Additive Manufacturing," *IEEE Access*, vol. 8, pp. 69908–69918, 2020, doi: 10.1109/ACCESS.2020.2986130.

[139] L. B. A. Caio, A. M. A. Silva, G. A. Bestard, L. S. Vieira, G. C. de Carvalho, and S. C. A. Alfaro, "Mild Steel GMA Welds Microstructural Analysis and Estimation Using Sensor Fusion and Neural Network Modeling," *Sensors*, vol. 21, no. 16, p. 5459, 2021.

[140] J. G. Cruz, E. M. Torres, and S. C. Absi Alfaro, "A methodology for modeling and control of weld bead width in the GMAW process," *Journal of the Brazilian Society of Mechanical Sciences and Engineering*, vol. 37, no. 5, pp. 1529–1541, 2015.

[141] S. B. Chen, Y. Zhang, T. Qiu, and T. Lin, "Robotic Welding Systems with Vision-Sensing and Self-learning Neuron Control of Arc Welding Dynamic Process," *J Intell Robot Syst*, vol. 36, no. 2, pp. 191–208, 2003, doi: 10.1023/A:1022652706683.

[142] J. A. Goldak and M. Akhlaghi, *Computational welding mechanics*. Springer Science & Business Media, 2005.

[143] J. Kershaw, R. Yu, Y. Zhang, and P. Wang, "Hybrid machine learning-enabled adaptive welding speed control," *J Manuf Process*, vol. 71, pp. 374–383, 2021.

[144] C. Xia *et al.*, "Model predictive control of layer width in wire arc additive manufacturing," *J Manuf Process*, vol. 58, pp. 179–186, 2020.

[145] N. Nievas, A. Pagès-Bernaus, F. Bonada, L. Echeverria, and X. Domingo, "Reinforcement Learning for Autonomous Process Control in Industry 4.0: Advantages and Challenges," *Applied Artificial Intelligence*, vol. 38, no. 1, Dec. 2024, doi: 10.1080/08839514.2024.2383101.

[146] A. S. Polydoros and L. Nalpantidis, "Survey of model-based reinforcement learning: Applications on robotics," *J Intell Robot Syst*, vol. 86, no. 2, pp. 153–173, 2017.

[147] Q. Li, G. Li, X. Wang, and M. Wei, "Diffusion welding furnace temperature controller based on actor-critic," in *2019 Chinese Control Conference (CCC)*, 2019, pp. 2484–2487.

[148] F. Ogoke and A. B. Farimani, "Thermal control of laser powder bed fusion using deep reinforcement learning," *Addit Manuf*, vol. 46, p. 102033, 2021.

[149] Z. Jin, H. Li, and H. Gao, "An intelligent weld control strategy based on reinforcement learning approach," *The International Journal of Advanced Manufacturing Technology*, vol. 100, no. 9, pp. 2163–2175, 2019.

[150] I. do V. Tomaz, F. H. G. Colaço, S. Sarfraz, D. Yu. Pimenov, M. K. Gupta, and G. Pintaude, "Investigations on quality characteristics in gas tungsten arc welding process using artificial neural network integrated with genetic algorithm," *The International Journal of Advanced Manufacturing Technology*, vol. 113, no. 11–12, pp. 3569–3583, Apr. 2021, doi: 10.1007/s00170-021-06846-5.

[151] D. Katherasan, J. V. Elias, P. Sathiya, and A. N. Haq, "Simulation and parameter optimization of flux cored arc welding using artificial neural network and particle swarm optimization algorithm," *J Intell Manuf*, vol. 25, no. 1, pp. 67–76, Feb. 2014, doi: 10.1007/s10845-012-0675-0.

[152] A. Kumar and K. Maji, "Selection of Process Parameters for Near-Net Shape Deposition in Wire Arc Additive Manufacturing by Genetic Algorithm," *J Mater Eng Perform*, vol. 29, no. 5, pp. 3334–3352, May 2020, doi: 10.1007/s11665-020-04847-1.

[153] V. Gulia and A. Nargundkar, "Application of Evolutionary Algorithms for Optimizing Wire and Arc Additive Manufacturing Process," 2024, pp. 671–683. doi: 10.1007/978-981-99-5180-2_52.

[154] "EN ISO 15614-1:2017 Specification and Qualification of Welding Procedures for Metallic Materials—Welding Procedure Test—Part 1: Arc and Gas Welding of Steels and Arc Welding of Nickel and Nickel Alloys; ISO: Geneva, Switzerland, 2017."

[155] " NI662 additive manufacturing - guidelines for certification of product made using wire arc additive manufacturing (waam) process, Bureau Veritas."

[156] "ISO/ASTM 52943-2:2024 Additive manufacturing for aerospace — Process characteristics and performance Part 2: Directed energy deposition using wire and arc," 2024.

[157] S. C. Absi Alfaro, K. S. Chawla, and J. Norrish, "Computer based data acquisition for welding research and production," *J Mater Process Technol*, vol. 53, no. 1–2, pp. 1–13, Aug. 1995, doi: 10.1016/0924-0136(95)01956-F.

[158] Y. Li *et al.*, "A defect detection system for wire arc additive manufacturing using incremental learning," *J Ind Inf Integr*, vol. 27, p. 100291, 2022.

[159] R. X. Gao and R. Yan, *Wavelets: Theory and applications for manufacturing*. Springer Science & Business Media, 2010.

[160] M. Monemian, M. Irajpour, and H. Rabbani, "A review on texture-based methods for anomaly detection in retinal optical coherence tomography images," *Optik (Stuttg)*, vol. 288, p. 171165, Oct. 2023, doi: 10.1016/j.ijleo.2023.171165.

[161] W. Li, K. Mao, H. Zhang, and T. Chai, "Selection of Gabor filters for improved texture feature extraction," in *2010 IEEE International Conference on Image Processing*, IEEE, Sep. 2010, pp. 361–364. doi: 10.1109/ICIP.2010.5653278.

[162] J. LIN and L. QU, "FEATURE EXTRACTION BASED ON MORLET WAVELET AND ITS APPLICATION FOR MECHANICAL FAULT DIAGNOSIS," *J Sound Vib*, vol. 234, no. 1, pp. 135–148, Jun. 2000, doi: 10.1006/jsvi.2000.2864.

[163] I. Deeva, A. Bubnova, and A. V. Kalyuzhnaya, "Advanced Approach for Distributions Parameters Learning in Bayesian Networks with Gaussian Mixture Models and Discriminative Models," *Mathematics*, vol. 11, no. 2, p. 343, Jan. 2023, doi: 10.3390/math11020343.

[164] A. A. Pol, V. Berger, C. Germain, G. Cerminara, and M. Pierini, "Anomaly Detection with Conditional Variational Autoencoders," in *2019 18th IEEE International Conference On Machine Learning And Applications (ICMLA)*, IEEE, Dec. 2019, pp. 1651–1657. doi: 10.1109/ICMLA.2019.00270.

[165] C. Zhou and R. C. Paffenroth, "Anomaly detection with robust deep autoencoders," in *Proceedings of the 23rd ACM SIGKDD international conference on knowledge discovery and data mining*, 2017, pp. 665–674.

[166] J. Fan, W. Wang, and H. Zhang, "AutoEncoder based high-dimensional data fault detection system," in *Proceedings - 2017 IEEE 15th International Conference on Industrial Informatics, INDIN 2017*, 2017. doi: 10.1109/INDIN.2017.8104910.

[167] M. A. Henson and D. E. Seborg, "Input-output linearization of general nonlinear processes," *AIChE Journal*, vol. 36, no. 11, pp. 1753–1757, 1990.

[168] B. Sereni, E. Assunção, and M. Carvalho Minhoto Teixeira, "New gain-scheduled static output feedback controller design strategy for stability and transient performance of LPV systems," *IET Control Theory & Applications*, vol. 14, no. 5, pp. 717–725, 2020.

[169] S. Y. Xu and T. W. Chen, "Robust H-infinity control for uncertain stochastic systems with state delay," *IEEE Trans Automat Contr*, vol. 47, no. 12, pp. 2089–2094, 2002.

[170] M. Athans, "The role and use of the stochastic linear-quadratic-Gaussian problem in control system design," *IEEE Trans Automat Contr*, vol. 16, no. 6, pp. 529–552, 1971.

[171] D. E. Rivera, M. Morari, and S. Skogestad, "Internal model control: PID controller design," *Industrial & engineering chemistry process design and development*, vol. 25, no. 1, pp. 252–265, 1986.

[172] L. Liu, S. Tian, D. Xue, T. Zhang, and Y. Chen, "Industrial feedforward control technology: a review," *J Intell Manuf*, vol. 30, no. 8, pp. 2819–2833, 2019.

[173] N. Nicola\"\i, I. Nopens, M. Verstraeten, and T. De Beer, "Process control levels for continuous pharmaceutical tablet manufacturing," *Chemical engineering in the pharmaceutical industry: drug product design, development, and modeling*, pp. 561–584, 2019.

[174] S. J. Qin and T. A. Badgwell, "An overview of industrial model predictive control technology," in *AIche symposium series*, 1997, pp. 232–256.

[175] P. K. Juneja, A. Sharma, A. Sharma, R. R. Mishra, and F. S. Gill, "A Review on Model Order Reduction Techniques for Reducing Order of Industrial Process Transfer Function Model," in *2020 International Conference on Advances in Computing, Communication & Materials (ICACCM)*, 2020, pp. 346–350.

[176] L. Matignon, G. J. Laurent, and N. Le Fort-Piat, "Reward function and initial values: Better choices for accelerated goal-directed reinforcement learning," in *International Conference on Artificial Neural Networks*, 2006, pp. 840–849.

[177] S. P. K. Spielberg, R. B. Gopaluni, and P. D. Loewen, "Deep reinforcement learning approaches for process control," in *2017 6th International Symposium on Advanced Control of Industrial Processes (AdCONIP)*, IEEE, May 2017, pp. 201–206. doi: 10.1109/ADCONIP.2017.7983780.

[178] J. Sola and J. Sevilla, "Importance of input data normalization for the application of neural networks to complex industrial problems," *IEEE Trans Nucl Sci*, vol. 44, no. 3, pp. 1464–1468, 1997.

[179] I. Osband, B. Van Roy, D. J. Russo, Z. Wen, and others, "Deep Exploration via Randomized Value Functions.," *J. Mach. Learn. Res.*, vol. 20, no. 124, pp. 1–62, 2019.

[180] C. Dann, Y. Mansour, M. Mohri, A. Sekhari, and K. Sridharan, "Guarantees for Epsilon-Greedy Reinforcement Learning with Function Approximation," in *International Conference on Machine Learning*, 2022, pp. 4666–4689.

[181] S. Fujimoto, H. van Hoof, and D. Meger, "Addressing Function Approximation Error in Actor-Critic Methods," 2018. [Online]. Available: https://arxiv.org/abs/1802.09477

[182] Z. Li, Z. Hou, Z. Pan, D. Wu, and J. Xu, "A Non-autoregressive Dynamic Model based Welding Parameter Planning Method for Varying Geometry Beads in WAAM," *IEEE Transactions on Industrial Electronics*, 2022.

[183] H. Hegab, N. Khanna, N. Monib, and A. Salem, "Design for sustainable additive manufacturing: A review," *Sustainable Materials and Technologies*, vol. 35, p. e00576, Apr. 2023, doi: 10.1016/j.susmat.2023.e00576.

[184] M. Dias, J. P. M. Pragana, B. Ferreira, I. Ribeiro, and C. M. A. Silva, "Economic and Environmental Potential of Wire-Arc Additive Manufacturing," *Sustainability*, vol. 14, no. 9, p. 5197, Apr. 2022, doi: 10.3390/su14095197.

[185] P. C. Priarone, E. Pagone, F. Martina, A. R. Catalano, and L. Settineri, "Multi-criteria environmental and economic impact assessment of wire arc additive manufacturing," *CIRP Annals*, vol. 69, no. 1, pp. 37–40, 2020.

[186] G. Campatelli, F. Montevecchi, G. Venturini, G. Ingarao, and P. C. Priarone, "Integrated WAAM-Subtractive Versus Pure Subtractive Manufacturing Approaches: An Energy Efficiency Comparison," *International Journal of Precision Engineering and Manufacturing-Green Technology*, vol. 7, no. 1, pp. 1–11, Jan. 2020, doi: 10.1007/s40684-019-00071-y.

[187] S. Kokare *et al.*, "Wire arc additive manufacturing of a high-strength low-alloy steel part: environmental impacts, costs, and mechanical properties," *The International Journal of Advanced Manufacturing Technology*, Jul. 2024, doi: 10.1007/s00170-024-14144-z.

[188] A. Joseph, D. Harwig, D. F. Farson, and R. Richardson, "Measurement and calculation of arc power and heat transfer efficiency in pulsed gas metal arc welding," *Science and Technology of Welding and Joining*, vol. 8, no. 6, pp. 400–406, Dec. 2003, doi: 10.1179/136217103225005642.

[189] H. Mu, F. He, L. Yuan, P. Commins, H. Wang, and Z. Pan, "Toward a smart wire arc additive manufacturing system: A review on current developments and a framework of digital twin," *J Manuf Syst*, vol. 67, pp. 174–189, 2023.